Quatitative variation in *Drosophila melanogaster* wing shape and size

Quantitative variation in *Drosophila melanogaster* wing shape and size within and between popualtions

By Katie Pelletier, MSc

A Thesis Submitted to the School of Graduate Studies in the Partial Fulfillment of the Requirements for the Degree Doctor of Philosophy

McMaster University
Doctor of Philosophy (2023)
Hamilton, Ontario (Department of Biology)

TITLE: Quantitative variation in *Drosophila melanogaster* wing shape and size within and between popualtions
AUTHOR: Katie Pelletier (McMaster University)
SUPERVISOR: Dr. Ian Dworkin
NUMBER OF PAGES: xiii, 150

Abstract

Several studies examining the genetics of adaptation have identified single alleles, of large phenotypic effect, contributing to divergence between populations. This empirical finding is consistent with predictions made by the geometric model of adaptation, where a small number of alleles of large effect and many alleles of small effect are fixed as the population adapts. However, these examples of single genes of large effect may represent a biased sample of the alleles of adaptation with polygenic allele shifts having a greater contribution than currently understood. Increasing power to detect smaller effect variants, due to falling sequencing costs and improved statistical methods, has made the contribution of small allele frequency shifts at many loci, or polygenic adaptation, more apparent. In contrast to models predicting single genes of large effect with large allele frequency changes, polygenic adaptation allows for small allele frequency changes across many alleles of small effect to contribute to phenotypic change. Using artificial selection, I demonstrate the alignment of genetic effects contributing to wing shape variation within a developmental pathway but a lack of replication of these same genetic effects in other wild-caught populations. Secondly, using advanced intercross QTL mapping between altitudinally diverged populations, I demonstrate a polygenic basis for wing shape and size variation. Finally, using comparative developmental biology I investigate how change to cell size and number in the wing may contribute to divergence between high and low altitude populations. Together, this work provides evidence for many alleles of small effect rather than alleles of large effect contributing to adaptive divergence of wing shape and size and provides context for identified alleles through replication in other populations and comparative developmental biology.

Acknowledgements

None of the work in this thesis would have been possible without the excellent community and support systems that I have had throughout my degree. Most of all, I need to thank all the undergraduates and collaborators who spent countless hours on creating many of the data sets used in this work.

I also need to thank Ian, who has been an excellent mentor and friend though this whole process. His guidance has made me a much better and more confident scientist over the last five years. Thank you to the rest of my committee: Ben, Ben and Marie who challenged me to become a better communicator, asked difficult questions and gave helpful suggestions throughout my degree.

Thank you to the Dworkin lab, where I have always been able to find a friend to ask a stupid question of or who will join me for a beer after a particularly long day. The biology graduate community has also been a tremendous support throughout my degree, I am lucky to have such supportive friends around me who truly made Hamilton feel like home. I don't think I could have made it through the final push to finish up without the TEAM2023 writing group, who were always there to make sure I wrote, even when I didn't want to. My family have also been my greatest cheerleaders thought out this process.

None of this would have been possible without David's support.

Contents

List of Figures

List of Tables

Declaration of Authorship

Much of the work of this thesis was collaborative in experimental design and data collection, with specific details below. Data analysis and manuscript preparations were all done by myself and Ian Dworkin.

Chapter 2: Collection and phenotyping and design of wild population experiments were done by Will Pitchers, Anna Mammel, Emma Northrop-Albrecht and Ian Dworkin. Artificial selection experiment and creation of ds, emc and neur effect vectors was done by Eladio Marquez, Rosa Moscarella and David Houle. Sequencing of samples was done by Will Pitchers. Yun Bo Xi did the Sanger sequencing experiment, supervised by me.

Chapter 3: Creation of F20 intercross populations was done by Yuheng Huang and John Pool. Fly husbandry for the deletion mapping and RNAi experiments was done by myself. Numerous undergraduate students contributed to the dissection, imaging and image processing of wing shape data: Isabella DiLanio, Daniel Simeions, Meghan Bilodeau, Yun Bo Xi, Cindy Vo, Stephanie Wang, Francessco Russo.

Chapter 4: Design of experiments was done by Katie Pelletier and Ian Dworkin. I created the synthetic outbred population and did all immunochemistry experiments. Ian Dworkin assisted with the fine dissection of wing discs. Many undergraduate volunteers contributed to the collection of cell count data in adult wing discs including: Johnston Ku, Humphry Erizo, Archana Thurairajah, Cindy Vo and Stephanie Wang.

Chapter 1

Introduction

1.1 Introduction

1.1.1 Genetic Architecture of quantitative traits

Complex traits have a complex genetic basis

Human height, crop yield, cardiovascular disease, insecticide resistance in crop pests and brood size in fish are all examples of complex traits. The expression, or observable phenotype, of these traits is mediated both by many loci in the genome and by their interactions with environmental factors. From even this short representative list, it is clear that these traits are of great importance to human health, plant and animal breeders as well as evolutionary biologists. Although these are important traits, understanding the genetic variation underlying phenotypic variation, or the genetic architecture, is difficult. In the case of human height, the proportion of trait variance that can be explained by inheritance, is estimated to be about 80% (Visscher et al. 2017). However, a genome wide association study (GWAS) with over 5.4 million individuals' genomes was able to identify over 11000 variants, encompassing about 20% of the genome. Yet, that explained only about 40% of height variation in European populations (Yengo et al. 2022). This is an excellent illustration of how difficult identifying the genetic architecture of traits can be even with enormous sample sizes; it is impossible to identify all the alleles contributing to phenotypic variation.

This problem becomes even more complex when replicating findings in other populations as there different segregating alleles, changes to minor allele frequencies and different environmental conditions that make replication difficult. The same SNPs that explained 40% of human height variation in European populations, explained up to 15%

of phenotypic variation in non-European populations (Yengo et al. 2022). What explains these differences? In the cited example, differences in allele frequencies as well as a loss of linkage disequilibrium (LD) between different populations likely explains why less variation is explained in other populations. The reduction in LD means that the effect of actual causal SNPs and "marker" SNPs in LD with them can alter the apparent contributions. The differences in allele frequencies influence additive genetic variation (V_g), as, at a given site the contribution to $V_g = 2pqa^2$ (p and q are allele frequencies at the bi-allelic site, a is the additive effect for the variant) so that co-variation at linked sites can inflate effect size estimates. However, other, often less considered issues are also likely contributing. Typically, there is a non-linear genotype-phenotype relationship that can make replication of genetic effects difficult. Trait expression can vary for the same mutant allele in different genetic backgrounds (Chandler et al. 2013) and between different environments (Chen et al. 2023).

This makes understanding the genetic architecture of traits particularly difficult. However, human height, as with many traits, an obvious yet often ignored aspect, is that what is measured for height is a composite made up of several traits such leg length, torso length, and skull length. These in turn reflect the composite effects of the individual bones, and so on. While all these jointly contributing traits are generally correlated to some degree, the genetic variants modulating trait expression of each are partially independent (Pearson and Davin 1924) Thus, considering those individuals who are above average in height we may be in fact examining sub-populations of "long-leg" and "long torso" individuals. By lumping these two groups together, we ingore the possiblity for unique effects within the subgroups, resulting in something analogous to a Wahlund effect (Wahlund 1928), but for phenotypes. Moving forward to understand the genetic architecture of complex traits, as well as their developmental underpinnings, will require us to focus more on dis-aggregating complex phenotypes into component parts. In my thesis, I explored the genetics of *Drosophila melanogaster* wing shape and size, to better understand the number and types of alleles that contribute to phenotypic variation within and between populations. Furthermore, as two jointly regulated complex traits, themselves the sum of individual phenotypic components, I also explored the relative contribution of local patterns (across the wing) of cell size and number on variation for these traits.

How many genes contribute to variation of complex traits?

Quantitative traits, where traits values have a continuous distribution, are rarely controlled by a single Mendelian locus (and if they were, it would require an enormous

environmental component of variation). However, the upper limit of the number of loci we can expect to contribute to trait variation is harder to understand. As the number of genes influencing trait variation grows, the individual effects of each contributing gene become smaller such that for traits with large numbers of loci contributing, mutational effect sizes become very small (Fisher 1930). With this prediction, the results of the human height GWAS discussed above are unsurprising. With such a large portion of the genome contributing to a trait, effect sizes of individual alleles are predicted to be small, requiring very large sample sizes to detect individual contributions. In addition to the observation that complex traits tend to have many alleles of small effect contributing to variation, many contributing variants are in non-coding, regulatory regions (Stern and Orgogozo 2008). Because genes do not exist in isolation and are part of larger regulatory networks, expression changes to many genes will be 'funneled' through key regulatory pathways. The combination of Fisher's infinitesimal model with this idea of variation being concentrated in regulatory pathways results in the omnigenic model of variation. In this model, every site in the genome has a non-zero effect on trait variation; however, the expression of core genes will be more affected as many small changes will accumulate at these 'hubs' (Boyle et al. 2017). This leaves predictions for the upper limit of the number of genes that can influence trait variation somewhere between two and every gene in the genome, which is not a particularly useful estimate.

The problem of identifying the alleles contributing to trait variation is particularly well exemplified in the example of *Drosophila* wing shape, one of the traits my thesis focuses on. Mutation accumulation experiments and genetic screens have implicated between 15 and 85% of the *Drosophila* genome influencing trait expression of wing shape, a substantial mutational target size (Houle and Fierst 2013; Weber et al. 2005). Early mapping studies in wild populations identified alleles in *epidermal growth factor receptor* (*egfr*) contributing to shape variation. These effects could be replicated in most, but not all populations studied (Dworkin et al. 2005; Palsson and Gibson 2004; Palsson et al. 2005). A GWAS for variants influencing wing shape in a North American population identified SNPs in about 500 genes, less than 1% of the *Drosophila* genome (Pitchers et al. 2019). This number is an under representation of the total number of alleles contributing to phenotypic variation in this population, as the 5% significance threshold used and the lack of power to detect variants of very small effect could not be detected with enough confidence to pass the threshold. In both the cases of the *egfr* SNP and GWAS identified SNPs, the variants generally individually explained no more than 1%, and typically far less, of total phenotypic variation. This ability to detect only a portion of total polymorphisms contributing to phenotypic variation within populations may be

the best that is possible without creating gigantic data sets, which is unlikely outside of human studies.

Despite not being able to identify many of the loci contributing to phenotypic variation within populations, patterns in identified loci can indicate pathways that are particularly important. For example, in the GWAS of *Drosophila* wing shape variation, there is an enrichment for variants in the hippo signaling pathway (Pitchers et al. 2019). Hippo signaling is best characterized for its roles in regulating size of tissues across many phyla (Zhao et al. 2011), but also is known to affect wing shape though regulation of cell polarity (Baena-López et al. 2005). This observation is in line with predictions by the omnigenic model, with some core pathways (in this case, hippo) having a greater influence on trait variation. What is not clear is why there is a bias for some pathways and not others. The influence of pleiotropy, developmental and mutational constraints, and the history of selection in a population are all important for influencing what alleles segregate and contribute to phenotypic variation.

1.1.2 The loci of evolution for polygenic traits

One gene or many?

Mutation creates the genetic variation upon which natural selection acts. When considering alleles contributing to phenotypic variation within populations, many traits will be under balancing or purifying selection (Barton and Keightley 2002). As such mutation-drift-selection balance likely dominates, influencing the segregating alleles in the population. When we consider divergence between populations, we do not necessarily expect the same models to explain patterns of variation as selective pressures will change (become directional). This process requires *de novo* mutations to occur or segregating variants at a high enough frequency in the population on which selection can act. Although most mutations are thought to be nearly neutral as larger effect sizes would be deleterious due to pleiotropy and selected against and smaller effect size alleles would not confer enough of a selective advantage to overcome drift (Kimura 1968), larger effect beneficial mutations can confer fitness advantage as populations adapt to a new optimum (Orr 1998). For polygenic traits where many alleles contribute to phenotypic variation within populations, do a small number of large effect alleles or many small effect alleles contribute to divergence between populations?

Many examples in the literature identify single alleles of large effect contributing to adaptive divergence between populations. One well-cited example is the body armor of sticklebacks, where there is a lot of variation in the number and size of lateral body

armor plates between salt and freshwater populations (Colosimo et al. 2005). Because armored plates are energetically expensive to make in freshwater environments, and there are fewer predators, there is a fitness advantage to reducing the number of plates in freshwater populations (Schluter et al. 2021). Mapping studies identified one large effect quantitative trait locus (QTL) explaining variation between populations with a polymorphism in the *eda* gene being fixed in freshwater populations (Colosimo et al. 2005; O'Brown et al. 2015). The same pattern is found for many other traits, including mouse coat colour (Steiner et al. 2007), colouration in butterflies (Martin and Reed 2014), and beak size in Galapagos finches (Lamichhaney et al. 2016), among others. These large effect alleles are relatively easy to detect using QTL mapping approaches with small sample sizes and single representative genetic backgrounds from parental populations. For example, the mapping of the *eda* locus used only about 500 individuals and 2 parental lines to detect the QTL (Colosimo et al. 2005).

As whole genome sequencing has advanced, many of the technical constraints on mapping studies have been removed. As we sequence more individuals and genotype individuals at more genomic sites, it has become clear that single alleles of large effect alone do not explain adaptive divergence between populations in most cases. In the case of stickleback armored plates, subsequent mapping studies have identified over 100 alleles contributing to adaptive divergence between populations, with many alleles of small effect and a small number of alleles of large effect contributing (Miller et al. 2014). This is in line with the predictions made with Orr's revision of the geometric model, where as a population moves to a new phenotypic optima, the effect sizes of subsequent substitutions will be smaller as the population approaches the optimum since large effect alleles will 'overshoot' the optimum (Orr 2005; Orr 1998).

Chromosomal inversions can also create conditions where a single gene, or a small number of genes held together in linkage, sweep to fixation. Local suppression of recombination can create large blocks of genetic differentiation between populations, making these regions easier to map (to the level of the inversion). One example of the contribution of polymorphisms found on chromosomal inversions to divergence is that of *Drosophila* wing size adaptation along latitudinal clines. Wing size in *Drosophila* has a large mutational target size, with about 15% of the genome contributing to trait variation (Carreira et al. 2009). In natural populations, wing size varies along latitudinal clines, with animals closer to the equator smaller than those nearer to the poles, with the same genetic basis found across continents (Calboli et al. 2003). The observed natural variation along clines is associated with polymorphisms in the Insulin/TOR signaling

pathways (Jong and Bochdanovits 2003; Paaby et al. 2010). These pathways are associated with the regulation of both metabolism and size (Oldham and Hafen 2003). In the case of *insulin receptor* and its substrate *chico* both exist on the common *In(3R)Payne* inversion in *Drosophila* (Paaby et al. 2010). This inversion, and the mapped alleles on it, explains about 23% of altitudinal variation in wing size in both North American and Australian populations (Kennington et al. 2007).

However, such large effect allele, or linkage block of alleles that may behave like a large effect allele, contributing to divergence between populations is not identified in every case. The basis of adaptive divergence is often polygenic with small effect alleles contributing. For example, *Littorina* marine snails have evolved two ecotypes, one form inhabiting wave exposed rocks with a small globular shell adapted for sticking to rocks in the waves, while the other ecotype lives in boulder fields and has a thicker, elongated shell to prevent predation from crabs (Johannesson et al. 1993). Although this trait has a known genetic basis (Koch et al. 2021), F_{ST} between ecotypes remains low (Westram et al. 2021). Although segregating inversions between populations explain some variation among ecotypes, genetic background, or other polymorphisms in the genome were equally important in predicting phenotypic expression (Koch et al. 2022). Although this system demonstrates that many sites in the genome can contribute, it cannot indicate exactly how many sites do contribute to the adaptive divergence seen.

Allele frequency Sweeps or subtle Shifts?

Variation in many genes contributes to adaptive divergence for polygenic traits; however, there are opposing views on the number, relative effect size, and origins of the alleles that contribute. Although all alleles are created through mutation, these mutations can occur concurrently with adaptation to a new optimum, as predicted by the geometric model, or can be found in variation already segregating in a population, prior to the new selective regime. The source and effect size of the mutations contributing to divergence create different expectations for the number of alleles and genomic signatures of selection at contributing sites. As larger effect alleles should also have larger selection coefficients, these are more likely to sweep to fixation in the genome. In contrast, selection will be weaker on small effect alleles; when many alleles contribute in aggregate, small allele frequency shifts at many sites will be sufficient to dramatically change trait values (Barghi et al. 2020). Given that sweeps, particularly "hard" sweeps, are relatively simple to detect with population genetic data, small allele frequency shifts at many loci are often used to explain cases where there is a known genetic basis, but signatures of selection can't be found at any loci.

Key to the geometric model of adaption is that as benefical alleles arise in the population, they sweep to fixation. Because these mutations are *de novo*, they exist on a single haplotype and will undergo a hard sweep (Orr 1998). This is the simplest case of adaptation; however, mutation rate is not often a rate limiting step for adaptation (Karasov et al. 2010). In simulations, adaptation from true *de novo* mutation is rare except in cases of rapid evolution to distant optima; rather, the alleles contributing to divergence are more likely to come from standing variation in the population (Stetter et al. 2018). This results in 'soft sweeps', or the fixation of a polymorphism with the maintainance of genetic diversity at nearby sites because the polymorphism exists on many haplotypes. Evidence for soft sweeps from seggregating variation comes from repeated 'use' of the same alleles across populations, as the allele also segregates in the ancestor and was selected on multiple times. In three spined sticklebacks the same alleles have been found to explain armor plate loss in multiple populations as well as segregating in the ancestral marine populations at low frequency (Barrett et al. 2008; Colosimo et al. 2005)

Fixation does not have to be the fate of alleles contributing to adaptive divergence. In fact, many factors such as pleiotropy, balancing selection and frequency dependant fitness may prevent fixation at alleles. Polygenic adaptation models predict allele frequency shifts across many loci that are sufficient to alter the phenotype towards a new selective optimum (Barghi et al. 2020). This architecture is much harder to detect, not only with scans for selection but also with methods such as F_{ST} scans for allele frequency changes or GWAS, because of the co-variation in allele frequency that is shared between populations (Barghi et al. 2020). For *Drosophila*, where effective population sizes are large and for traits with high mutational target sizes, such as wing shape and size, polygenic adaptation may be a particularly good model. Rapid adaptation can be facilitated by high mutational target size as there are many 'routes' that can be taken to achieve the same change in phenotype (Barghi et al. 2019).

Although the allelic sweep and all polygenic shift models have been discussed as opposing viewpoints of how adaptation can occur, neither model will be able to explain all cases of adaptive divergence. These represent extreme cases and very few biological examples fit compleatley into these neat categories. The biological 'rules' that govern the number, type and dynamics of alleles contributing to divergence depend strongly on the population size, mutation rate and demographic history of a population as well as the specific genetic architecture of the selected trait. Even when comparing between the same populations, there is evidence that adaptive divergence can be explained by

shifts in allele frequency at many loci for some traits and sweeps of larger effect alleles for other traits.

Clunio marine midges have populations with district reproduction times linked to low tides associated with the moon cycle, one group reproducing at the new moon and one at the full moon (Kaiser et al. 2011). At least 4 QTLs exist that influence reproduction timing between ecotypes, with a polymorphism in the period gene predicted to have the largest effect and the other 3 QTL associated with neural development genes (Briševac et al. 2023). Period is important for regulating circadian clocks in insects (Tomioka and Matsumoto 2015). In this case, there is not a clear signature of a sweep of alleles contributing to differentiation, alleles are not fixed in one ecotype, likely due to continuous gene flow between populations (Kaiser et al. 2021). In addition to this variation in timing of reproduction, populations of *Clunio* from the Artic and Baltic sea have evolved a reproduction strategy that does not require low tides and is not linked to the moon cycle as is true for the European Atlantic population (Fuhrmann et al. 2023). QTL mapping of alleles associated with the loss of rhythmicity related to the moon cycle did not identify any loci significantly contributing to trait variation (Fuhrmann et al. 2023). Additional genomic scans for differentiated regions between ecotypes identified only 65 loci that were highly differentiated, and none of those were associated with the signatures of a sweep. This contrast of genetic architectures of adaptation between two arguably similar traits in the same species is interesting but the reason behind these contrasting architectures is unclear.

In Trinidadian guppies, life history traits vary extensively between high and low predation populations (Reznick and Endler 1982). In translocation experiments populations adapt rapidly, on the order of a few generations, to the new environment (Gordon et al. 2009). When life history traits were mapped between populations, two fitness traits exhibited a polygenic basis with many identified QTL throughout the genome while two traits had single QTL identified that explained the majority of variance for that trait (Whiting et al. 2022). The diffrence in archetectures between traits may reflect the contrasting genetic architecture of the traits as rapid adaptation is facilitated by many alleles of small effect segregating or beneficial alleles of large effect segregating at an intermediate frequency for different traits (Kardos and Luikart 2021), these dynamics could easily explain the observation of different genetic architectures between both examples used here.

1.1.3 Understanding the loci of evolution

Simply identifying the genes that contribute to variation in traits is only the first step in understanding the genetic variation that contributes to phenotypic variation in natural populations. Particularly for complex traits with large mutational target sizes, it is easy and even expected to identify many regions of the genome contributing to trait variation. For example, in a screen for genes contributing to *Drosophila* pupal attachment height, knock down of all the genes identified in a GWAS resulted in an phenotypic effect but and effect was also observed for three quarters of randomly selected gene knockdowns (Zhang et al. 2021). This finding is not particularly surprising in the light of the omnigenic model where most genes in the genome are predicted to influence trait variation. With so many genes and alleles contributing to variation, and so many of the alleles with effect sizes small enough that they will never be detected without enormous sample sizes, it may be less important to identify all alleles contributing to variation (Rockman 2012). The same power problem exists when detecting alleles contributing to adaptive divergence when the genetic architecture of adaptation is explained by small shifts in allele frequency at many loci. However, not all alleles are equally likely to contribute to adaptive divergence because of developmental and mutational constraints (Stern and Orgogozo 2008; Uller et al. 2018), pleiotropy (Orgogozo et al. 2015), and the history of selection in a population (Schluter 1996), will influence the available genetic diversity on which selection will act. In cases where we may not find specific alleles of adaptation, such as in the case of polygenic shifts in allele frequencies, it may be more helpful to understand the pathways affected (Bomblies and Peichel 2022), either though changes to gene expression , changes to developmental mechanisms or an analysis, such as gene ontology (GO) terms, of the genes contributing to divergence. When mutational targets are high and changes in allele frequency at individual sites are low, this approach may be useful in understanding the changes underlying phenotypic divergence.

Beyond creating lists of loci associated with a phenotype of interest, functional work and replication of genetic effects across different populations can help to better understand biological relevance of alleles. In the *D. melanogaster* wing shape GWAS discussed above, in a single gene, *dachsous* (*ds*), there were 5 identified polymorphisms (Pitchers et al. 2019). Are all these polymorphisms important for contributing to wing shape variation, or could linkage explain some of the enrichment for significantly associated sites in this gene? Using developmental genetic tools and other methods, we can ask questions about which polymorphisms really matter for trait variation, either though replication

in other populations, correlating predicted or known effects with those seen during development or testing specific effects of each polymorphism though genome engineering. My thesis contributed to identifying polymorphisms important for wing shape and size variation in *Drosophila melanogaster* using a variety of methods: first, by replication of GWAS identified effects (chapter 2), then by mapping QTL contributing to adaptive divergence (chapter 3) and assaying some of the developmental changes between populations (chapter 4).

1.1.4 Specific Thesis Goals and Summary

This goal of this thesis was to identify alleles and mechanisms that contribute to phenotypic variation in *Drosophila melanogaster* to broaden our understanding of the the number and type of alleles, and the relationsips between these, that contribute to quantitative trait variation in wild populations. For most complex traits with large mutational target sizes, only a subset of the genes that can contribute to variation are identified in mapping studies. Understanding the 'rules' that shape genetic variation within and between populations first requires an understanding of the genetic architecture of trait variation. However, this becomes much more complicated for quantitative traits where both environmental and genetic sources of variation can contribute to trait expression.

In my second chapter, I demonstrate the difficulties in understanding the genetic architecture of wing shape variation due to genetic and environmental influences. The initial goal of this work was to replicate genetic effects of SNPs identified in a previous GWAS study using both artificial selection and wild caught populations. Using artificial selection based on the shape change associated with knockdown of *dachsous* (*ds*), a gene in the hippo signaling pathway, we demonstrate allele frequency changes at not only *ds* but a number of other hippo signaling loci. This demonstrates the repeatability of the effect of the *ds* SNP on wing shape previously identified. Because the starting population for the selection experiment was designed to maximize genetic diversity at *ds*, to ensure that these variants were at a high enough frequency to be selected on, without consideration for diversity at other sites in the genome, it was surprising that we also observed allele frequency shifts at other hippo loci. This indicates the strong and correlated relationship between alleles within the same developmental pathway contributing to wing size. Additionally, although we had a response to selection at hippo signaling loci, and hippo signaling is known to be a major component of size regulation in the *Drosophila* wing, we do not observe a substantial change in wing size between selection lineages, indicating that the effect of hippo signaling on wing size and shape are genetically separate. The same experiment using the similar *emc* shape change vector

for selection, resulted in only modest allele frequency changes at *emc* itself, and much larger changes associated with hippo signaling loci, indicating that replication of genetic effects is dependent on the available genetic diversity within a population. Finally, using wild caught populations of *Drosophila* from three locations in Michigan and a bulk segregant analysis (BSA) approach, we were unable to replicate any of the genetic effects previously identified. However, phenotypic variation in the wild caught populations is largely in the same direction as the *ds* shape change vector, indicating that this is an important direction of variation in wild populations. However, our approach was likely not powerful enough to detect genetic differentiation between bulks considering additional environmental and genetic variation as well as low allele frequencies segregating in the populations. This work demonstrates the importance of genetic background, environmental effects and allele frequency in replicating genetic effects as well as the interesting finding that selection can act simultaneously on a number of alleles with aligned effects within a population.

In the third chapter, I use adaptively diverged populations from sub-Saharan Africa to map alleles contributing to wing shape and size variation between two populations. The main goal of this work was to ask how polygenic this adaptive divergence was and if we could find evidence of fixation of large effect alleles, as would be predicted by the geometric model. Using an advanced intercross between inbred lines derived from a low altitude and a high-altitude population, I took a QTL mapping approach to identify the genetic architecture contributing to the adaptative divergence in wing shape and size between populations. Using pooled DNA sequencing, I measured genetic differentiation between pools of individuals that were outliers (most extreme) along both the shape and size axes. Shape adaptation had a highly polygenic basis, in agreement with earlier mapping studies. The genetic architecture of wing shape adaptation also has a polygenic basis, but we identified one locus on chromosome 3R as a candidate QTL contributing to divergence. Although it is not likely that this allele was fixed in the high-altitude population, as this locus was not differentiated in a third cross, it is still an interesting QTL contributing to shape divergence. A semi-quantitative mapping study using a panel of lines carrying deletions in this region as well as RNAi knock down of candidate genes point to *winged eye* (*wge*) as a candidate gene in this region. However, we are not able to rule out the possibility that more than one polymorphism, in more than one gene, in this region that contributes to divergence. Additionally, I demonstrated that despite the intrinsic link between shape and size though shape-size allometry, adaption of these two traits has at least a partially distinct genetic basis and allometric relationships remain constant between different genetic backgrounds. This chapter demonstrates the

polygenic basis of adaptation to high altitude for both wing shape and size and provides support to the model that small shifts at many alleles segregating in populations may contribute more to adaptative divergence than subsequent sweeps of larger effect alleles.

In my fourth chapter, I took a comparative developmental approach to understand divergence between high and low altitude populations. Because the mapping study in chapter 3 revealed a polygenic basis of adaptation to high altitude, I wanted to compare developmental changes to provide context to what alleles may be contributing and what developmental mechanisms, if any, appear changed between populations. The omnigenic model predicts that although many (or all) loci in the genome can contribute to trait variation, core genes or pathways will show increased variation. First, using adult wings from the advanced intercrosses that were created for the mapping study in chapter 3, I investigated the relationship between cell size and wing shape and size in the adult wing. A structure can become larger either through having more cells or larger cells. Although in natural evolutionary contexts *Drosophila* wings generally become larger though the addition of more cells, previous work in our lab and others has shown that adaptation to high altitude is explained in substantial part by larger cells in the high-altitude population. I demonstrated that although there is an association between larger wings and larger cells in the intercross, there are many individuals with wings that have more cells rather than larger cells, suggesting that the two traits can be partially de-coupled genetically. This can in part explain the finding in chapter 3 as both the "larger cells" and the "more cells" genetic programs can be selected on and create more targets for selection. I also demonstrated that although variation of cell size averaged over the entire wing has little effect, local cell density variation (across the wing) does have a shared co-variation structure with wing shape. This indicates that regional differences in cell size in the wing, but not changes in the mean cell size of a wing, are associated with shape changes. Wing size and cell size also only behave as moderate predictors of wing abnormalities, with evidence that large effect alleles segregating in the populations may better explain the observed loss of robustness. Although we observe few developmental differences between populations, technical limitations of the data collection may be able to explain this result and more work is needed before conclusions are made about quantitative developmental changes in the wing disc.

Chapter 2

Complexities of recapitulating polygenic effects in natural populations: replication of genetic effects on wing shape in artificially selected and wild caught populations of *Drosophila melanogaster*

This chapter is in press at Genetics, the online version can be found here

2.1 Abstract

Identifying the genetic architecture of complex traits is important to many geneticists, including those interested in human disease, plant and animal breeding, and evolutionary genetics. Advances in sequencing technology and statistical methods for genome-wide association studies (GWAS) have allowed for the identification of more variants with smaller effect sizes, however, many of these identified polymorphisms fail to be replicated in subsequent studies. In addition to sampling variation, this failure to replicate reflects the complexities introduced by factors including environmental variation, genetic background, and differences in allele frequencies among populations. Using *Drosophila*

melanogaster wing shape, we ask if we can replicate allelic effects of polymorphisms first identified in a GWAS (Pitchers et al. 2019) in three genes: *dachsous* (*ds*), *extra-macrochaete* (*emc*) and *neuralized* (*neur*), using artificial selection in the lab, and bulk segregant mapping in natural populations. We demonstrate that multivariate wing shape changes associated with these genes are aligned with major axes of phenotypic and genetic variation in natural populations. Following seven generations of artificial selection along the *ds* shape change vector, we observe genetic differentiation of variants in *ds* and genomic regions containing other genes in the hippo signaling pathway. This suggests a shared direction of effects within a developmental network. We also performed artificial selection with the *emc* shape change vector, which is not a part of the hippo signaling network, but showed a largely shared direction of effects. The response to selection along the *emc* vector was similar to that of *ds*, suggesting that the available genetic diversity of a population, summarized by the genetic (co)variance matrix (**G**), influenced alleles captured by selection. Despite the success with artificial selection, bulk segregant analysis using natural populations did not detect these same variants, likely due to the contribution of environmental variation and low minor allele frequencies, coupled with small effect sizes of the contributing variants.

2.2 Introduction

Dissecting the genetic architecture underlying complex traits remains challenging, because of the joint contributions of many alleles of small effect, genotype-by-environment interactions, and other factors. Progress in sequencing technology in conjunction with development of GWAS statistical methodologies has enabled identification of loci contributing to numerous complex traits and diseases. However, such mapping approaches identify only a subset of loci contributing to trait variation (Visscher et al. 2017). In part, this reflects the low power to detect rare alleles, and those with small effects (Tam et al. 2019). For alleles that are relatively common in a population, replication rates between GWAS studies are high, even when effect sizes are small (Marigorta et al. 2018). However, GWAS studies have failed to replicate the effects observed in many candidate gene studies, in part due to the fact that many alleles identified in these studies are rare in populations, and require very large cohorts to detect (Fritsche et al. 2016; Ioannidis et al. 2011).

In cases where an association is replicated between studies, the magnitude of the effect can vary substantially between different cohorts or populations (CONVERGE consortium 2015; Marigorta et al. 2018). Differences can arise because of genetic background

due to epistatic gene by gene (GxG) interactions, or due to gene-by-environment (GxE) interactions. The initial estimates of effect size will be biased upwards if statistical testing in the initial cohort is used to determine which SNPs are chosen for replication studies. It is important to understand which of these causes of differences in effect size are of practical significance when we want to generalize results to different populations or environments.

In this study, we focus on the issue of replication in a multivariate context, where the joint inheritance of multiple features are simultaneously investigated. We will refer to the suite of measured features as a 'multivariate trait' for convenience. In this case, what we want to estimate is the vector of effects of each SNP on all measured features. Each SNP may have a unique combination of effects. Univariate effects vary only in magnitude, as we can only infer effects on a single feature. For a multivariate trait, estimated genetic effects vary in magnitude, the sum of effects on all traits, and also in direction, how the total effect is allocated among different features (Melo et al. 2019).The ability to study the direction along with the magnitude of genetic effects provides an additional and important way of assessing repeatability. For a univariate trait, there is a 50% chance that the replicate estimate will be in the same direction as the original estimate, even with no true effect. By contrast, the probability of a "replicated" genetic effect sharing a similar direction by chance alone decreases as the number of measured features increases (Marquez and Houle 2015; Stephens 2013).

Studying genetic effects in a multivariate context is beneficial in other ways. First, it has been demonstrated both empirically and via simulations, that genetic mapping for multivariate traits generally increases statistical power over trait by trait analyses (Fatumo et al. 2019; Pitchers et al. 2019; Porter and O'Reilly 2017; Shriner 2012). Second, some multivariate traits cannot be sensibly reduced to a single measurement. The wing shape we study is a great example of such a multivariate trait. We have good reason to believe that wing shape is important for flight (Ray et al. 2016), but we cannot yet say that any feature, such as wing length or width, is more or less important than any other. Natural selection on wing shape may affect any or all combinations of measurements.

Perhaps most importantly, traits are not inherited in isolation, but are the joint outcome of an integrated developmental process that results in extensive genetic correlations that can have important effects on evolution. The main source of such correlations are the patterns of pleiotropic effects generated by mutational effects. Multivariate studies of inheritance allow pleiotropic effects to be estimated in a rigorous and justifiable

manner (Melo et al. 2019). The multivariate breeder's equation, $\Delta z = G\beta$, enables short term prediction of evolutionary responses. Key to understanding how populations respond to selection in the short term requires an understanding of properties of the genetic (co)variance matrix (**G**), and in particular the axis of greatest genetic variation g_{max}. Studies demonstrate that the direction of g_{max}influences evolutionary trajectories (McGuigan 2006; Blows and McGuigan 2015; Schluter 1996). The degree to which genetic effects associated with particular variants align to major axes of genetic (co)variance, expressed through **G**, may provide insights into which alleles are most likely to be "captured" by selection (Pitchers et al. 2019). Due to the polygenic nature of complex traits, including multivariate ones, it is important to consider not only the direction of effect for alleles in a single gene but also correlated effects between genes contributing to the phenotype. Interestingly, initial comparisons of directions of genetic effects among induced mutations in two *Drosophila melanogaster* wing development pathways showed only partially correlated effects on wing shape within and between pathways (Dworkin 2006). However, recent work has demonstrated that despite large differences in magnitude, the direction of genetic effects of variants segregating in populations are sometimes similar to those from validation experiments using RNAi knockdown of those same genes (Pitchers et al. 2019). Additionally, Pitchers et al. (2019) demonstrated this shared direction of effect could also be shared between a SNP and RNAi knockdown of other genes in the same signaling pathway, such as those involved with hippo signaling, a key pathway involved with wing growth and morphogenesis (Pan et al. 2018).

Pitchers et al. (2019) identified over 500 polymorphisms contributing to wing shape variation in the *Drosophila* genetic resource panel (DGRP). Among these, the hippo pathway was over-represented in SNPs associated with wing shape (Pitchers et al. 2019). The degree to which identified hippo pathway variants reflect allele specific effects, differences in magnitude of genetic effects, and even the large statistical uncertainty associated with genetic effects of small magnitude are unclear. Given common dominance patterns, and the likely non-linear genotype-phenotype relationships of most genetic effects, small to moderate changes in gene function may result in modest phenotypic effects (Green et al. 2017; Melo et al. 2019; Wright 1934). Large effect mutants and many RNAi knockdown studies have moderate to large phenotypic effects that are not reflective of the magnitude of genetic effects of SNPs contributing to phenotypic variance in natural populations.

The expression of genetic effects also depends on genetic and environmental context, with gene-by-gene (GxG) and gene-by-environment (GxE) interactions contributing to

phenotypic variation. The context-dependence of genetic effects for a multivariate trait has been demonstrated for *Drosophila* wing shape. Variants in *Epidermal growth factor receptor* (*Egfr*), influencing *Drosophila* wing shape are replicable in both lab reared, and wild-caught cohorts (Dworkin et al. 2005; Palsson and Gibson 2004; Palsson et al. 2005). However, in replication studies, effect sizes of alleles were diminished in both outbred populations and wild cohorts. In the latter case the same variant explained 1/10 of the phenotypic variance explained in the initial study (Dworkin et al. 2005). Interestingly, in a series of experimental crosses among strains, the effects of the SNP were replicable for direction and magnitude in multiple experimental assays and crossing schemes. Despite this, the genetic effect on wing shape from this SNP largely disappeared in one natural population (Palsson et al. 2005). A number of reasons have been proposed for the failure to replicate genetic effects including environmental effects, differences between controlled lab and natural environments (Dworkin et al. 2005) and genetic background (Greene et al. 2009), among others. Because both environment and genetic background likely affect the genotype-phenotype map in a non-linear fashion (Wright 1934), it is important to test observed associations in other experimental contexts.

A promising approach to confirm the estimated effects of candidate genetic variants is to test whether they respond to artificial selection in the direction of the inferred effect. This approach is particularly relevant to evolutionary questions, but has rarely been used. In this study, we use artificial selection and bulk segregant analysis (BSA), to replicate and validate SNPs associated with three genes, previously identified in a GWAS of *Drosophila* wing shape (Pitchers et al. 2019); *dachsou*s (*ds*), an atypical cadherin involved with hippo signaling; the transcriptional co-repressor *extra-macrochetae* (*emc*), and the E3 ubiquitin ligase *neuralized* (*neur*), involved with Notch signaling. Using the vectors of shape change based on RNAi knockdowns of each gene, we demonstrate that the direction of shape change for these genetic effects is aligned with major axes of natural phenotypic and genetic variation. Using artificial selection based on the direction of shape change defined by RNAi knockdown, we were able to replicate the effects observed for *ds*, but not *emc*, likely due to the available genetic diversity in the population. We then asked if these effects could be replicated in a natural population using a bulk segregant approach, observing little evidence for replication in these samples. We discuss our results in the context of the replicability of genetic effects and the shared direction of genetic effects due to shared developmental processes.

2.3 Methods

2.3.1 *Drosophila* strains

Phenotype data for the *Drosophila* genetic resource panel (DGRP) was collected for 184 strains as part of a GWAS study as described in Pitchers et al (2019). Genotype data for these strains was obtained from freeze 2 of the DGRP (Huang et al. 2014). For replication using artificial selection, 30 DGRP strains were used: DGRP-149, 324, 383, 486, 563, 714, 761, 787, 796, 801, 819, 821, 822, 832, 843, 849, 850, 853, 859, 861, 879, 887, 897, 900, 907, 911, 913. These strains were selected to increase genetic variation at the *ds* locus (Figure A1.1, Table 2.1). Reciprocal pairwise crosses between the 30 selected DGRP strains were used to create heterozygotes and these 30 heterozygous genotypes were successively pooled for 4 subsequent generations, allowing for recombination. After pooling, the synthetic outbred population was maintained for approximately 47 subsequent generations (allowing for recombination) before the start of artificial selection experiments.

For the replication in wild-caught populations using BSA, individuals were collected via sweep-netting from orchards and vineyards in Michigan and after species identification, stored in 70% ethanol. In 2013 and 2014, cohorts were collected from Fenn Valley Winery (FVW13 and FVW14 respectively, GPS coordinates: 42.578919, -86.144936). Additionally in 2014, cohorts were collected from Country Mill Orchard (CMO, GPS coordinates: 42.635270, -84.796706), and Phillip's Hill Orchard (PHO, GPS coordinates: 43.117981, -84.624235). For all collected cohorts, except for the FVW14 collection, only males were used in this study given difficulties distinguishing *Drosophila melanogaster* and *D. simulans* females morphologically. For the genomic analysis of the FVW14 wild caught population (below) we utilized both males and females as the number of individuals was insufficient otherwise. For the collection where females were included in the study, there is no evidence of contamination with *D. simulans* as all dissected wings were classified as *D. melanogaster* using linear discriminant analysis (LDA). LDA was trained using male wings from the collected *D. melanogaster* data set and males from *D. simulans*. There was 100% agreement between the classification of females within each species with our phenotypic classification, indicating that it is unlikely that *D. simulans* females were included in our samples (Supplemental Figure A1.2).

2.3.2 Morphometric Data

Landmark and semi-landmark data were captured from black and white TIFF images using the pipeline described in (Houle et al. 2003). First, two landmark locations, the humeral break and alula notch, were digitized using tpsDig2 (version 2.16). Wings (Van der Linde 2004–2014 , v3.72) software was used to fit nine cubic B-splines, and manually correct errors. All shape data was subjected to Procrustes superimposition (registration), removing the effects of location, isometric scaling, and minimizing effects of rotation, via an iterative least squares approach (Rohlf and Slice 1990). Generalized Procrustes superimposition (registration) and extraction of 14 landmarks and 34 semi landmarks was done using CPR v1.11 (Marquez 2012–201)(Figure2.1). Superimposition results in the loss of 4 possible dimensions of variation while semi-landmarks are constrained to vary along one "axis", restraining these points to approximately a single dimension of variation each. This results in a total of 58 available dimensions of shape variation, that can be summarized using the first 58 Principal components (PCs). Allometry was adjusted for in the analysis by fitting a model for landmark coordinates onto centroid size, and using the residuals from this model (Klingenberg 2022). By accounting for the allometric component of shape, shape variation associated with size variation can be accounted for (Supplemental Figure A1.3). For most analyses, 'allometry corrected' shape data were used, with the exception of shape models fit using the Geomorph package in R, where Procrustes landmarks were used and centroid size was included as a predictor in the model.

2.3.3 Generation of shape vectors for artificial selection and bulk segregant analysis

A panel of shape change vectors was estimated using the progesterone-inducible Geneswitch GAL4, under the regulation of an ubiquitous tubulin driver, to drive the expression of RNAi for genes of interest (*ds, emc, neur*), as previously described in Pitchers et al., 2019. GAL4 expression was induced throughout larval development by adding mifepristone, an analog of progesterone, to the larval food. Knockdown was varied by assaying phenotypes at mifepristone concentrations of 0.3, 0.9, and 2.7 μM, plus a control without mifepristone. Wing shape change associated with knockdown of the gene of interest was estimated using multivariate regression of shape on concentration of mifepristone. Shape change vectors estimated from the RNAi experiments for *ds,emc* and *neur*, were used in this experiment (Figure 2.1B, Supplemental Figure A1.4). The magnitude ('length') of the vector measures how much shape change occurs per unit change in mifepristone. In general, vectors of greater magnitudes enable better estimate of direction of effect for

shape change. As reported in Pitchers et al., (2019), the magnitude (l^2-norm) of vectors for RNAi knockdown of these genes are 5.5 for *ds*, 2.8 for *neur*, and 0.44 for *emc*.

Shape data collected as part of a previous study (Pitchers et al. 2019) was used to assess the relationships between shape change vectors from the RNAi titration and g_{max}, the first eigenvector of the **G** matrix estimated from DGRP line means. The effects of sex, centroid size and their interaction were removed using a linear model and these residuals were used to calculate shape score by projecting the data (Supplemental Figure A1.5) onto the shape change vector estimated in each knockdown experiment. To assess major axes of genetic variation among DGRP strains, principal component analysis was performed on allometry adjusted model residuals (Supplemental Figure A1.5B). PCA was done in a similar manner for individuals from the wild caught cohorts. Correlations between the first three eigenvectors ("genetic PCs" including g_{max}), the first three PCs from the wild caught cohorts and the shape scores for *ds*, *emc* and *neur* were calculated (Figure 2.1A, Supplemental Figure A1.5). From this, *ds*, *emc* and *neur* shape change vectors were selected for further experiments given high correlation with directions of natural genetic variation (Figure 2.1A, Supplemental Figure A1.5). Note, as described below, while *ds* and *emc* were used for artificial selection, due to the similar response between them, we used *ds* and substituted *neur* (for *emc*) for the BSA.

2.3.4 Artificial selection of synthetic outbred population

The synthetic outbred population resulting from pooling DGRP lines was used as the parent population for artificial selection. Both the *ds* and *emc* artificial selection experiment were carried out with three independent replicates of each "up" and "down" selection regimes, along with unselected control lineages. Each generation, wings of live flies were imaged using the 'wingmachine' system and shape data collected (Houle et al. 2003)(Houle et al., 2003, Van der Linde 2004–2014 ,v3.72). Shape scores were calculated by projecting the data onto the *ds* or *emc* shape change vector as described above, and the 40 individuals each with highest or lowest shape scores, were selected to found the next generation (Supplemental Figure A1.5A). For the control lineages, 40 individuals were randomly selected for the next generation within each replicate lineage. Following seven generations of selection, 75 individuals from each lineage were selected for pooled sequencing, described below. The response to selection was evaluated both by computing Procrustes distance (PD) between average shape of wings between generations one and seven, and using shape scores (projections) with a linear mixed effect model allowing for the fixed effect factors of treatment and sex, continuous predictors of centroid size and generation, with third order interactions among these effects. The effect of generation

was allowed to vary by replicate lineages (lmer(ds $\sim$ (CS + Sex + line + gen0)$\hat{3}$ + (1 + gen0|line:rep)). Realized heritabilities were estimated separately for up and down selection lineages, from the slope of the regression of cumulative selection differentials on cumulative selection response, averaging over sex and with a random effect of replicate lineage.

2.3.5 Wild populations

For the BSA, wings for wild caught individuals were dissected and mounted in 70% glycerol in PBS. Images of wings were captured using an Olympus DP30B camera mounted on an Olympus BX51 microscope (Olympus software V.3,1,1208) at 20X magnification. When possible, both left and right wings were dissected, imaged and averaged to calculate an individual's mean shape. For some individuals a wing was damaged so only one wing could be used. Shape was captured as described above. The total number of individuals phenotyped from each cohort can be found in Supplemental Table A1.5.

To remove allometric effects in the data, shape was regressed onto centroid size and the model residuals were used for all subsequent morphometric analysis. Only data from males was used to compare shape in wild populations, although, including females from the FVW14 population and regressing shape onto centroid size and sex gave equivalent results (Supplemental Figure A1.6). To test for shape differences between collection cohorts, the effect of centroid size and collection cohort on shape were modeled (procD.lm(shape $\sim$ CS + pop_year)) using the procD.lm function in Geomorph v 3.1.3 (Adams and Otárola-Castillo 2013) and distances between populations were calculated using the pairwise function. To select individuals for sequencing, a 'shape score' was calculated using the method described above. Shape data was projected onto the vector of shape change defined by the *ds* or *neur* knockdowns. The *emc* projection vector was not used for BSA due to the high similarity with *ds* shape change (Figure 2.1), and the similarity of the selection response. Its inclusion would result in selection of largely the same cohorts of individuals for sequencing for both *ds* and *emc*. As an alternative, we utilized the *neur* shape vector as it was largely uncorrelated with that of *emc* and *ds*, but strongly correlated with natural variation in shape. The 75 most extreme individuals on the shape score distribution, within each wild-caught cohort, were selected for pooled sequencing. Allele frequencies within each population was estimated by sequencing 75 random individuals within each cohort. The difference vector between mean shapes of selected pools (within each population) was used to calculate Procrustes distance (PD) between pools and the correlation of this shape change vector with the selection vector used. An estimate of genetic distances between populations was calculated using allele

frequencies (mapping pipeline described below) in the pools of the 75 randomly selected individuals using Bray's distance with the vegdist() function from the vegan package (v2.6-2) in R.

2.3.6 Sequencing and Genomic Analysis

DNA extractions from pools of selected individuals was performed using a Qiagen DNeasy DNA extraction kit. Library preparation and Illumina sequencing was performed at the research technology support facility at Michigan State University. All library samples were prepared using the Rubicon ThruPLEX DNA Library Preparation kit, without a procedure for automatic size selection of samples. Paired end libraries (150bp) were sequenced using Illumina HiSeq 2500, with each sample (either one pool of 75 individuals in the BSA or one pooled replicate lineage in the artificial selection) being run on two lanes. Reads were trimmed with Trimmomatic (v0.36) to remove adapter contamination and checked for quality using FastQC prior to alignment (Bolger et al. 2014). Trimmed reads were aligned to the *Drosophila melanogaster* genome (v6.23) using BWA-MEM (v0.7.8) (Li and Durbin 2010). Sequencing replicates of the same biological samples were merged using SAMtools (v1.11). PCR duplicates were removed using Picard with the MarkDuplicates tool (v 2.10.3) and reads with a mapping quality score less than 20 were removed using SAMtools (Li et al. 2009). A local realignment around indels was performed using GATK using the IndelRealigner tool (v3.4.46). For artificial selection experiments, reads were merged for all up, down and control selection lines as replicates lineages were independent. For wild cohorts, pools were not merged between populations. mpileup files were created using SAMtools and used for subsequent genomic analysis. Highly repetitive regions of the *Drosophila* genome were identified and subsequently masked in mpileup files using RepeatMasker (v4.1.1) with default settings. INDELs and regions within 5bp of an indel were identified and masked using PoPoolation2 scripts. Population genetic statistics were calculated using PoPoolation (v1.2.2) and PoPoolation2 (v1.201) (Kofler et al. 2019a; Kofler et al. 2019b).

For the BSA in the wild-caught cohorts, a modified Cochran-Mantel-Haenszel (CMH) test was used to measure significantly differentiated sites between pools of individuals. Sampling effects were accounted for using the ACER package (v.1.0) in R, assuming $N_e = 10^6$ with 0 generations of differentiation between selected pools (Spitzer et al. 2020). (Spitzer et al., 2020). To adjust for multiple testing, the p-value was corrected using a Benjamini-Hochberg correction (Benjamini and Hochberg 1995) with an adjusted alpha of 0.05. For each significant site from the CMH test, using an adjusted p-value cut-off of 0.05, we identified the nearest gene using BEDtools (v2.19.1) (Quinlan and

Hall 2010). In addition, to account for sampling variation, we sampled genomic coverage to 75x for all samples, dropping sites that did not meet this threshold and repeating the CMH test. We confirmed that there was no association between genetic and shape differentiation between populations, and that the populations do not show strong phenotypic differentiation based on either overall shape variation, or shape scores used to identify selected individuals for BSA (Supplemental Figures A1.3 A1.7). There was some variation among populations in overall wing size (Supplemental Figure A1.8), however we (assuming common allometry) adjusted for allometric effects on shape.

For artificial selection experiments, F_{ST} was calculated in 5000bp windows. We chose this window size as it is expected that blocks of LD in the synthetic outbred population will be much larger in comparison to that of the wild caught samples (King et al. 2012a; King et al. 2012b; Marriage et al. 2014). This statistic was used to compare the "up" selected pools to the "down" selected pools to help identify regions of differentiation between selected populations.

For the artificial selection comparisons, genes in regions of high F_{ST} were identified by finding overlaps between outlier windows and annotated Drosophila genes using GenomicRanges (v1.46.1) in Bioconductor. High F_{ST} was defined as F_{ST} values greater than three standard deviations above the mean. GO terms associated with identified genes were annotated using TopGO package (v2.34.0) (Alexa et al. 2006) in Bioconductor. GO enrichment was then performed to identify those terms overrepresented in the identified list using TopGO and a Fisher's exact test. Over representation of 2 GO terms in outlier windows (hippo signaling, GO:0035329; negative regulation of hippo signaling GO:0035331) were tested using a permutation test that randomly sampled genomic windows from the total windows for which F_{ST} was calculated and the permutation was run 1000 times. The distribution of the ratio of observed to expected genes annotated with the term of interest within randomly sampled regions was compared to the number observed in the data.

2.3.7 Verification of *ds* indel in DGRP

Sanger sequencing was performed on individuals from a cross between DGRP lines predicted to have the polymorphism (DGRP 195, 28, 96, 48, 59, 801) and those without (DGRP 129, 301, 69, 385, 75, 83, 491, 34, 774) crossed to a line carrying a deletion in the region of interest (BDSC 24960) to account for potential residual heterozygosity in otherwise inbred strains. DNA was prepared by incubating flies in DNA extraction buffer (1mM EDTA, 25mM NaCl, 10 mM TrisHCl pH 7.5) for 10 minutes, followed

by storage at -20 C. PCR application of the region of interest (Forward primer: ggagtacaagttgctcgaac: Reverse Primer: cagatcgtgttccctttagc) using Taq DNA polymerase (Gene DirectX) (PCR mix: 1 μ L DNA, 1 μ L forward primer, 1 μ L reverse primer, 0.5 μ L 10mM dNTPs, 2 μ L 10x PCR Buffer, 0.1 μL taq, H20 to 20 μL). PCR conditions were as follows: 5 minutes 95°, (30 seconds 95°, 30 seconds 55°, 30 seconds 72°)x30. Reactions were checked on a gel and cleaned with the $GenepHlow^TM$ Gel/PCR Kit (Geneaid). Sanger sequencing reactions were performed by the Mobix Lab at McMaster University. All alignments were created using ClustalOmega (Madeira et al. 2022).

2.4 Results

2.4.1 *dachsous (ds)* shape change is aligned with major axes of genetic and phenotypic variation in natural populations

To assess the relationship between shape change vectors and axes of natural variation described in the the DGRP, mean shape vectors were calculated for each DGRP strain, then used in a PCA to summarize axes of variation among strains. Mean shape vectors for each strain of DGRP were projected onto shape change vectors for *ds*, *emc*, and *neur*, defined from the RNAi knockdowns (see Supplementary Figure A1.5, which visually explains the procedure), generating gene specific "shape scores". Correlations between shape scores for individual DGRP projected onto the shape change vectors (Figure 2.1, Supplemental Figure A1.5), and with PC1 generated from the DGRP ($PC1_{DGRP}$) strains was estimated ($PC1_{DGRP}$ - *ds*: r = -0.56; $PC1_{DGRP}$ - *emc*: r = -0.45; Figure 2.1). The correlation of the DGRP data, projected onto each of the *ds* and *emc* shape change vectors was also correlated (Figure 2.1, *ds-emc*: r = 0.69). This is likely due to the correlation between gene specific shape change vectors themselves (r = 0.65), based on RNAi titration experiments. Projections of the DGRP data onto the vector defining the *neur* shape change is aligned with PC1 ($PC1_{DGRP}$-*neur*: r = -0.69) and PC3 ($PC1_{DGRP}$-*neur*: r = -0.64), indicating this as an important axis of shape variation in this population (Figure 1), that is moderately similar to projections onto *ds* (*ds-neur*: r = 0.56) and very similar to *emc* (*neur-emc*: r = 0.83) shape change vectors. Interestingly, the strength of the correlation for the DGRP strains projected onto these vectors, differs from the magnitude of correlations for the RNAi titration vector of *neur* with that of *ds* (r = 0.034) or *emc* (0.3). Because of these observed correlations, and previous associations observed (Pitchers et al. 2019) *ds*, *emc* and *neur* were selected as focal genes for subsequent studies.

We also examined the relationship between direction of phenotypic effects with the wild caught cohorts. For these samples, phenotypic variance for shape is due to the joint contribution of genetic and environmental effects. To illustrate the difference in shape variance in wild populations and the DGRP, we calculated correlations between the first three eigenvectors for shape in the DGRP, the combined wild cohorts as well as the CMO cohort alone. We observed low correlations between the DGRP eigenvectors and those estimated from wild populations (Supplemental Table A1.2). As observed with the DGRP, there is a substantial correlation between projections of shapes of individuals onto the ds shape change vector and PC1 (defined by phenotypic variation among wild caught files, PC_{wild}) in most of the sampled cohorts (*ds*-$PC1_{wild}$ PHO: r = 0.78; CMO: r = 0.87; FVW13: r = -0.22; FVW14: r = 0.95, Figure 2.2, Supplemental Figure A1.5). In cohorts where the ds shape change vector was not correlated with PC1, specifically the FVW13 collection, this vector is correlated with PC2 (*ds*-$PC2_{wild}$ PHO: r = 0.12; CMO r = -0.44; FVW13: r = -0.63; FVW14: r = 0.19; Figure 2.2, Supplemental Figure A1.9). The pattern for the wing shape from wild-caught individuals projected onto the *emc* shape change vector was generally similar to that observed for *ds* (Figure 2.2). We also observe a correlation between *neur* shape change and PC1 in most cohorts (*neur*-PC_{wild} PHO: r = 0.51; CMO: r = -0.051; FVW12: r = -0.95 FVW13; FVW14: r = -0.084; Figure 2.2; Supplemental Figure A1.7). As with the *ds* shape change vector, in some cohorts such as the CMO the stronger correlation is between the *neur* shape change vector and PC2(PHO: r = 0.22; CMO: r = -0.57; FVW13: r = -0.059; FVW14: r = 0.85; Figure 2.2; Supplemental Figure A1.7). Interestingly, in the CMO cohort, the correlations between the projection of shape data onto the *ds* and *neur* shape change vectors is low (*ds*-*neur*: r = 0.11, Figure 2.2).

2.4.2 Multiple loci linked to hippo signaling - including *ds*- respond to artificial selection for *ds* and *emc* shape changes.

To examine if variants in *ds* are contributing to shape variation, and independently replicate the findings of the earlier GWAS (Pitchers et al. 2019), we performed artificial selection experiment for wing shape along the *ds* shape change vector, and examined the genomic response to selection. By the final generation of selection, we observed a substantial shape change in both the "up" (females: Procrustes Distance (PD) = 0.039, males: 0.044) and "down" directions (females: PD = 0.022, males: PD = 0.022), compared to the base population at the start of the experiment. In comparison, the shape change among unselected control lineages was much smaller (females: PD = 0.005, males: PD = 0.005, Figure 2.3, Supplemental Figure A1.10). The direction of phenotypic

shape change after seven generations of selection was in a similar direction to the *ds* shape change vector (defined by RNAi knockdown) for both the up (females: r = 0.90, males: r = 0.90) and down (females: r = -0.82, males: r = -0.77) selection lineages. Realized heritabilities, averaged over sex and replicate were moderate (Supplemental Figure A1.11 up = 0.38, 95% CI: 0.25 – 0.50; down = 0.28, 95% CI: 0.24 – 0.50). Hippo signaling, including the effects of *ds*, is often associated with changes in size (Pan 2007). However, we do not observe a significant change of wing size in our selection lineages in either sex (Supplemental Figure A1.12). It is possible that with more generations of selection we would have observed a clear change in size, as there is a trend indicating such divergence (Supplemental Figure A1.12).

Genome-wide patterns of F_{ST} were examined between up and down *ds* selection lineages. We observed strong genetic differentiation linked with the *ds* locus (Figure 2.3, Supplemental Figure A1.13),), along with several other regions in the genome. One of the SNPs in the intron of ds (2L:702560), identified in Pitchers et al. (2019) through GWAS, showed the expected pattern of response to selection, with opposing sign in up and down selection lineages, with the SNP going to high frequency in all three up selection lineages (Table 2.1). It should be noted that this SNP is near a complex polymorphism including an insertion of 18bp that may result in inaccurate genotyping at this locus (Supplemental Figure A1.14).). Gene ontology analysis for genes in regions of the genome with an FST greater than 0. 345 (three standard deviations from mean F_{ST}), show enrichment for hippo signaling loci (figure A1.3). The top 20 enriched terms are all related to cell signaling and development. Of note is the inclusion of the terms for 'negative regulation of hippo signaling' (GO:0035331), and 'hippo signaling' (GO:0035329) in this list (Supplemental Table A1.3, Supplemental Figure A1.13). Using a permutation test we confirmed these results, selecting random sets of genomic intervals equal in size to the number of observed outlier windows, and measured the ratio of genes annotated to the expected number of genes in these regions. The observed value for the terms for hippo signaling (ratio = 4.76) and negative regulation of hippo signaling (ratio = 9.23) were in the upper 99.5% percentile in comparison to the distributions under permutation (Supplemental Figure A1.15).

For the artificial selection experiment based on the *emc* shape change vector we observed phenotypic differentiation under artificial selection in both up (females: PD = 0.043, males: PD = 0.040), and down directions (females: PD = 0.021, males: PD = 0.020), with little change in control lineages (females: PD = 0.009, males: PD = 0.008, Figure 2.4). The direction of phenotypic change is correlated with the *emc* (RNAi

knockdown) shape change vector in both up (females: r = 0.75, males: r = 0.69) and down (females: r = -0.69, males: r = -0.75) directions. Realized heritabilities, averaged over sex and replicate were calculated for both up and down lineages (Supplemental Figure 16, up = 0.38, 95% CI: 0.29 – 0.47; down = 0.28, 95% CI: 0.21 – 0.35). Genetic differentiation linked to the *emc* locus was modest following selection, but we again observed striking genetic differentiation linked to *ds* (Figure 2.4, Supplemental Figures A1.13 A1.16). Notably, as seen in Supplemental Figure A1.1 the site frequency spectrum (SFS) suggests modest allelic variation at the *emc* locus in the synthetic outbred population. Using a three standard deviation cut-off for F_{ST}, we did observe enrichment for various developmental GO terms, but not of hippo signaling terms (Supplemental Table A1.4, Supplemental Figure A1.13).

2.4.3 Bulk segregant analysis in wild caught cohorts does not recapitulate effects of the GWAS or artificial selection

Having demonstrated that variants in (or linked to) *ds* respond to artificial selection for wing shape along the *ds* shape change vector, we next wanted to determine whether we could recapitulate these findings with wild caught individuals. In addition to determining whether we can replicate effects in wild cohorts, it provides the opportunity to identify causal SNPs because of low LD generally observed in wild caught *Drosophila*. Wild caught populations introduce considerably more environmental variation for shape along with a different site frequency spectrum for variants contributing to shape variation (and *ds* like shape changes specifically). In particular, it is known that several of the variants that the original GWAS detected in *ds* have low minor allele frequency (MAF) (Pitchers et al. 2019)(Table 2.2). The SNP at 2L:702560 does appear to be at intermediate frequency but it occurs both directly before and after an indel, making alignment and variant calling in this region challenging (Supplemental Figure A1.14). We have included the frequencies (Table 2.2), but these results should be interpreted with caution due to the technical complexities of mapping and variant calling close to indels.

As we sampled multiple cohorts of wild-caught flies in different locations and years in Michigan (USA), we wanted to confirm that any phenotypic differentiation among these samples was modest and would not impact genomic analysis for the BSA. We observe modest, statistically significant wing shape differences among cohorts from a Procrustes ANOVA, utilizing permutations of the residuals for the relevant "null" model (Supplemental Table A1.2; R^2= 0.16, F = 351, Z_{RRPP} = 18.3, p = 0.001)(Collyer and Adams 2018). This appears to be due to differences in wing shape between the PHO

population and other populations based on pairwise Procrustes Distances (Supplemental Tables A1.2, A1.4). In a joint PCA including all populations, there is very modest separation between populations using allometry adjusted shape (Supplemental Figure A1.3). Most relevant to the BSA approach we used, when we project all wild caught individuals onto the *ds* and *neur* vectors, there is no clear separation among sampling locales (Supplemental Figure A1.7).There is some variation in wing size between populations (Supplemental Figure A1.8), but this is unlikely to influence downstream analysis as we use size adjusted estimates.There is little evidence of genetic differentiation between populations with the two collections from Fenn Valley Winery separating more on a Principal Co-ordinate Analysis (PCoA) (Supplemental Figure A1.17) than other sampling locales. There is also no relationship between genetic and phenotypic distances between samples (Supplemental Figure A1.18). These results suggests that the multiple sampling locales should not influence downstream genomic analysis as individuals used for generating pools were compared within each population, and we observe little evidence for substantial differences among populations.

Because there is a single bout of phenotypic selection distinguishing pools for the BSA, changes in shape and allele frequencies are expected to be modest. We observe shape differences between the two pools within each population (PD = CMO: 0.033; PHO: 0.036; FVW13: 0.040; FVW14: 0.041; Supplemental Figure A1.19). Correlations of the shape difference vectors of the pools (i.e. difference between the two pools created from the extremes along the ds shape change axis), and the direction of the *ds* shape change vector used for selection, is high (CMO: 0.94, PHO: 0.79, FVW13: 0.92, FVW14: 0.90).

BSA genome scans show little evidence of genetic differentiation linked to the *ds* gene (Figure 2.5). Across the genome, 15 sites were detected as significantly differentiated between "up" and "down" selected pools based on a CMH test with FDR cut-off of 5% (Figure 2.5, Table 2.3).The genes nearest to these sites are not associated with hippo signaling pathways or implicated in the development of the *Drosophila* wing (Table 2.3). Because PHO had somewhat distinct shape variation from the other populations and had a lower correlation of the difference vector between selected pools and *ds* shape change vector, we repeated the CMH test with this population left out. We observe significant differentiation at 174 sites between "up" and "down" pools (Supplemental Table A1.6, Supplemental Figure A1.20). We identified the nearest genes to these sites and GO analysis indicated enrichment for wing development terms, in particular related to Wnt signaling, but not hippo signaling terms (Supplemental Table A1.7). Importantly,

we do not observe differentiation linked to *ds* or any other hippo loci. To ensure that the results we obtained were not due to uneven coverage between samples, we down-sampled genomic coverage to 75x for each sample, dropping sites that did not meet this threshold. Significant differences were detected at 19 sites (Supplemental Figure A1.21, Supplemental Table A1.8), but none of these overlapped with those identified using all the genomic data. Two of the significant sites are located in the *dumpy* gene, a gene known to have a role in wing morphogenesis during pupation (Etournay et al. 2015). F_{ST} between selected and random pools within each cohort are generally low (Supplemental Figure A1.22).

In addition to the BSA selection based upon the *ds* shape change, we also selected pools of individuals based on the *neur* shape change vector. We did not use *emc* shape change in this experiment due to the high similarity between the *ds* and *emc* shape change vectors (r = 0.65), and the similar response to selection reported above. We selected the *neur* shape change vector as it is not aligned with *ds*, but does align with directions of natural variation, in wild populations (Figures 2.1, 2.2, Supplemental Figure A1.9). Additionally, there is little relationship between the *ds* and *neur* shape change axis (Supplemental figure A1.7, A1.9), in the wild caught cohorts. We observe shape changes between pools of individuals (PD = CMO: 0.027; PHO: 0.028; FVW14: 0.041; FVW13: 0.038, Supplemental Figure A1.23).). There is little evidence of genetic differentiation between *neur* selected pools (Supplemental Figure A1.24). Only 4 sites were identified as being significantly differentiated between pools and none of these sites are associated with wing development (Supplemental Table A1.9). When population differentiation between pools within populations is measured using F_{ST}, genetic differentiation remains low across the genome (Supplemental Figure A1.25).

2.5 Discussion

The primary goal of this study was to determine whether we could recapitulate genetic effects initially observed through a traditional GWAS using an "inverted" approach: artificially selecting on phenotypes and observing changes in allele frequencies. We observed that shape changes associated with the *ds*, *emc* and *neur* genes were associated with major axes of genetic variation among a panel of wild type strains (DGRP) reared in the lab, and axes of phenotypic variation among wild caught individuals (Figures 2.1, 2.2). After observing a strong response to artificial selection along two shape change vectors (*ds* and *emc*), we examined patterns of genomic differentiation and observed substantial changes in allele frequency for markers linked with *ds* itself (Figure 2.3),

and markers linked to numerous genes associated with hippo signaling (Supplemental Figures A1.13, A1.14).

In contrast, our BSA experiments, using pools of wild caught individuals chosen to be phenotypically divergent on the same shape vectors, did not detect differences in the loci identified in the artificial selection experiments (Figure 2.5, Supplemental Figure A1.24). As we discuss in detail below, these seemingly contradictory results are in fact not that surprising.

Following artificial selection based on *ds* shape change we observe allele frequency changes not only at *ds* but also linked to a number of other hippo signalling loci (Figure 2.3, Supplemental Table A1.3). The previous GWAS study identified a number of loci associated with wing shape variation in the DGRP, however, this approach cannot predict which alleles are causative (Pitchers et al. 2019). In our synthetic outbred population, we maximized variation among haplotype blocks containing many of the candidate SNPs in *ds*, increasing our ability to detect frequency changes at and near the implicated variants. Although LD blocks in the outcrossing population from this study remain large, *ds* variants exist on multiple distinct haplotypes, allowing for an examination of allele frequency changes for each. Of particular interest is SNP 2L:702560, previously identified though GWAS (Pitchers et al. 2019) as influencing wing shape variation. It was driven to near fixation in each of the artificial selection lineages (Table 2.1). Although this polymorphism is annotated as a SNP, this region may contain a complex polymorphism (Supplemental Figure A1.14), making it difficult to accurately assess genotypic calls. Because of this, the predicted allele frequency in the founding population and allele frequencies in this region may be inaccurate. Previous studies demonstrate the importance of alleles at intermediate frequency in founding populations to those contributing to responses to selection over short timescales (Kelly and Hughes 2019). If this polymorphism is at a more intermediate frequency in the founding population, it would be more likely to be captured by selection during these experiments. Additionally, haplotype blocks in the initial population are large, and may contain many potential functional variants. However, based on the results of both the current and previous studies, these *ds* variants associated with 2L:702560 are good candidates for functional validation in future work. When selecting on the *emc* shape change vector, which is similar to that of the *ds* shape change, we observe only a modest allele frequency change at *emc*, and a more robust response at *ds* (Figure 2.4). In hindsight, this is not particularly surprising and there are multiple contributing factors. Given the increased genetic diversity at *ds* compared to *emc* in the founding population, alleles in *ds* may have provided a more accessible

genetic target, as selection can only act upon the diversity available in the population. Additionally, if our estimated direction of effects and selection for *emc* (based on RNAi knockdown) was not well aligned with the actual direction of *emc* SNP effects, this could result in weaker selection on variants at the *emc* locus. It is worthwhile pointing out the small magnitude of the *emc* shape change vector (0.44) relative to *ds* (5.5). However, previous work has indicated that there is a relationship between this estimated *emc* shape change vector (from RNAi) and the effect of SNPs in *emc* on shape change (Pitchers et al. 2019).

In addition to a response on allele frequency associated with *ds*, our results suggest a response on segregating variation at other hippo signaling loci in the *ds* artificial selection experiment. Earlier work has suggested that the direction of effects within signaling pathways are inconsistent for alleles of small effect (Dworkin 2006). However, allelic effect sizes in the 2006 study were heterogeneous and may result in direction and magnitude being confounded. In contrast, in both the current and the Pitchers et al. (2019) studies, we estimated the direction of genetic effects by titrating gene knockdown. The strength of this approach is highlighted in the result that segregating variation at multiple hippo loci was selected on (Supplemental Figures A1.13, A1.15). Our finding is consistent with models for the architecture of complex traits that predict that many alleles of small effect will contribute to trait variation with many genes within developmental pathways (Boyle et al. 2017; Wray et al. 2018). This pathway response has also been demonstrated in human adaptation to pathogen resistance (Daub et al. 2013) and high altitude (Gouy et al. 2017). These results are consistent with the expectation that polymorphisms in the same developmental pathway would show correlated phenotypic effects and therefore correlated genomic responses to selection. However, this may not be reflective of all wild caught populations. In this study, we generated a population that had high diversity at *ds*, while these variants are at much lower frequency in natural populations (Table 2.2). The amount of selectable variation a variant provides, depends on both effect size, a, and variant frequencies, p, as $V_A = 2p(1-p)a^2$. When allele frequencies are near 0 or 1, even variants with large effects will have only a small contribution to short term selection response. Therefore, the outcrossed population we created here is an ideal situation to validate the existence of the measured effects. It is unlikely to be typical of natural populations where functional variants may be rare.

Given the clear and robust response observed in the artificial selection experiment, it may seem surprising that we do not observe allele frequency changes in the BSA using the wild cohorts. Indeed, previous work has demonstrated that variants in *Egfr*, could

be replicated in wild caught samples (Dworkin et al. 2005; Palsson et al. 2005) and were also found in genome wide associations (Pitchers et al. 2019). However, there are many explanations for why we may not have been able to detect these allele frequency changes in our experiment. First, the addition of environmental variation to the system introduces additional complications. In the aforementioned example with *Egfr*, the genetic effect of the SNP in wild-caught cohorts was 10% of the magnitude estimated in lab-reared flies. As discussed previously, the *ds* variants implicated in the previous GWAS study are at low frequency in the natural cohorts (Table 2.2). Given that natural populations of Drosophila are generally large and wing shape is likely under weak selection (Gilchrist and Partridge 2001), mutation-drift-selection balance may maintain most variation, resulting in low minor allele frequencies at these sites. Because allelic contribution to wing shape are expected to be both rare in wild populations and of small phenotypic effect, we do not expect large allele frequency changes given only one "generation" of selection. Using the approach of ACER (Spitzer et al. 2020) to account for sampling effects, we observe few differentiated sites, and none in the *ds* gene, indicating that BSA may not be well-suited to identify modest allele frequency changes, thus, not particularly effective for polygenic traits. Although our approach was tailored to look for variants that had consistent direction of frequency changes across the four collection cohorts, it is possible that different loci were contributing variation within each cohort. We attempted to address this question by examining allele frequency changes between selected pools within each cohort (Supplemental Figures A1.22, A1.25) but could not identify specific loci contributing to differences within any one population. Previous successful BSA studies identified smaller numbers of contributing loci with few polymorphisms contributing to the trait of interest. For example, in *Drosophila*, a number of melanin synthesis genes contributing to variance in pigmentation between populations were identified using a BSA (Bastide et al. 2013). Pigmentation may represent a relatively 'simpler' genetic architecture (fewer variants of individually larger genetic effect, smaller impact of environmental variation, smaller mutational target size) and if so, this may have enabled the success of the BSA approach with such systems. In the case of wing shape, we know that many alleles of small effect contribute to variation in the trait (Pitchers et al. 2019).

Our approach for the BSA was to perform the same phenotypic selection within each of four distinct "populations". It is important to recognize that there was heterogeneity among our populations, not only in allele frequencies, but in environmental variance and potentially GxE, even though all were caught in locales in lower Michigan. We detected small degrees of phenotypic and genetic differences between cohorts, however

these effects are neither correlated with one another, nor related to the ds and neur shape scores used for selecting individuals (Supplemental Figures A1.3, A1.7, A1.17).). The population from the Phillips Orchard (PHO) was phenotypically distinct from the other populations. When we performed the BSA without this population, we observed a larger set of variants associated with shape (Supplemental Figure A1.20), albeit still not showing any effects at *ds* or *neur* genes themselves. One possibility is that the increased number of sites when the PHO sample is removed from analysis represents an unknown statistical artefact we have not identified. However, a more likely explanation is that there are some large unknown environmental influences (E), or that the genetic effects show a degree of GxE (with a specific environment in PHO) that contributed to shape variation along the *ds* direction in this population. Such obfuscating effects have been observed before with the previously discussed *Egfr* example, where the SNP effect identified and validated in multiple contexts (Dworkin et al. 2005; Palsson et al. 2005; Palsson and Gibson 2004) could not be detected in one natural population, despite being at intermediate frequencies in each sample (Palsson et al. 2005). Importantly, we did detect differentiation at sites associated with developmental processes in the wild cohorts, suggesting that the failure to detect variation linked to *ds* or other hippo signaling loci (Table 2.3, Supplemental Table A1.6, A1.7) is not due simply to a lack of power.

The response to selection at *ds* and other hippo signaling loci in the artificial selection experiment based on *ds* shape change indicates that this is an important axis of variation for wing shape. Coupled with the alignment of phenotypic effects of perturbations in genes in this pathway with directions of **G** and **P**, this finding may seem to suggest a developmental bias in available variation. However, we caution against such interpretations based solely on the findings in this study. The structure of the **G** matrix strongly influenced our findings as we artificially created a population to maximize genetic diversity at *ds*. When another effect is aligned with *ds* shape change, as in the case of *emc* shape change, we observed the same response at the hippo signaling loci and not at *emc*. Only the genetic diversity in the starting population was available to be selected on so this influenced selection towards the "spiked in" *ds* variants, even if the inferred phenotypic effects of *emc* variants are very similar. Alternatively, the inferred *emc* direction of effects (via RNAi knockdown) may be sufficiently "distant" from true effects of *emc* variants. If this was the case, we were ineffectively selecting for *emc* shape changes. In other cases where single genes are implicated in divergence between multiple populations, such as *mc1r* in mice (Steiner et al. 2007) or *pitx1* in stickleback (Chan et al. 2010), other factors such as low pleiotropy, developmental and mutational constraints and history of selection in the population are used to explain why these genes

are so often implicated in evolutionary change (Gompel and Prud'homme 2009; Martin and Orgogozo 2013; Stern and Orgogozo 2008). In our case, it is not *ds* itself that is special but rather the orientation of the **G** matrix to align $g_{max}$with the direction of effect for *ds* that shapes our results. Selection acts on variants aligned with the vector of selection (Reddiex and Chenoweth 2021). By varying the orientation of g_{max}in the parental population, we would be able to address questions about the repeatability of hippo overrepresentation and if this can be explained by more than just the orientation of **G**.

Despite the need for skepticism about the potential for developmental bias influencing directions of variation, the correlated response of sites linked to multiple other hippo signaling genes is intriguing. Coupling of more traditional mapping approaches like GWAS with short term artificial selection provides an additional route to validation and replication of genetic effects. It also suggests that using multivariate data to address the distribution of genetic effects will pay long-term dividends to our understanding of both inheritance and the evolution of multivariate traits.

2.6 Figures and Tables

TABLE 2.1: Variants from Pitchers et al. (2019) in *ds* artificial selection experiment. Estimated effect sizes for SNPs are estimated from a GWAS in the DGRP using LASSO regularized coefficients. Average frequency is given with replicate lineage frequencies in brackets. Estimated effect is the l^2-norm of shape differences associated with the variant. MAF = minor allele frequency.

Variant	Estimated Effect	DGRP MAF	Estimated MAF in synthetic outcross	Average allele frequency "up" selection	Average allele frequency "down" selection	Average allele frequency "control" selection
2L:655894	0.072	0.44	0.067	0(0, 0, 0)	0(0, 0, 0)	0.003(0, 0, 0.0105)
2L:702560*	**0.159**	**0.056**	**0.06**	**0.995(1, 0.98, 1)**	**0.446(0.32, 0.35, 0.67)**	**0.705(0.69, 0.56, 0.87)**
2L:702798	0.101	0.089	0.1	0.007(0, 0.0217, 0)	0(0, 0, 0)	0.005(0, 0, 0.139)
2L:718623	0.225	0.033	0	0(0, 0, 0)	0(0, 0, 0)	0(0, 0, 0)
2L:718627	0.11	0.033	0	0(0, 0, 0)	0(0, 0, 0)	0(0, 0, 0)

* This is a complex polymorphism with linked SNPs and INDELs, in Pitchers et al (2019) a SNP in this region was found to be linked. However, the variant calling pipeline used in this work recognized an INDEL in this region which was used for counting.

Table 2.2: *ds* Variants from Pitchers et al. (2019) in wild-caught cohorts used in the present study. Estimated effect sizes for SNPs are estimated from the DGRP GWAS with LASSO regularized coefficients. MAF in wild cohorts was estimated from sequenced pools of 75 random individuals.

Variant	Estimated Effect	DGRP MAF	Estimated MAF CMO	Estimated MAF FVW13	Estimated MAF FVW14	Estimated MAF PHO
2L:655894	0.072	0.445	0	0	0	0
2L:702560*	0.159	0.056	0.375	0.473	0.485	0.336
2L:702798	0.101	0.089	0.077	0.101	0.044	0.034
2L:718623	0.225	0.033	0.051	0.021	0.044	0.100
2L:718627	0.11	0.033	0.055	0.020	0.046	0.099

* This is a complex polymorphism with linked SNPs and INDELs, in Pitchers et al (2019) a SNP in this region was found to be linked. However, the variant calling pipeline used in this work recognized an INDEL in this region which was used for counting.

Table 2.3: Significantly differentiated variants for *ds* shape change from the wild-caught cohorts (BSA).

Location	CMH p-value (FDR corrected)	Gene	FlyBase ID	Distance from ORF (bp)
2R:17491270	0.026	*NT5E-2*	FBgn0050104	0
2R17498059	0.034	CG30103	FBgn0050103	2061
2R:17515133	0.022	CG4853	FBgn0034230	0
2R: 20537878	0.013	CG13423	FBgn0034513	0
2R:23601278	0.005	CG10332	FBgn0260455	0
2R:23601278	0.005	*IM18*	FBgn0067903	0
2R:23613785	0.013	*Eglp4*	FBgn0034885	0
2R:23613785	0.013	*Eglp2*	FBgn0034883	0
2R: 23646252	0.016	*retn*	FBgn0004795	0
3L:12831924	0.005	CG10960	FBgn0036316	0
3L: 20999119	0.022	*skd*	FBgn0003415	0
3R: 21523866	0.013	CG7956	FBgn0038890	0
3R: 2559549	0.011	*Pzl*	FBgn0267430	0
X: 14891220	0.013	*Flo2*	FBgn0264078	0
X: 14891220	0.013	CG9514	FBgn0030592	0
X:16039731	0.017	*Muc14a*	FBgn0052580	0
X: 793052	0.011	CG16989	FBgn0025621	95
X: 9448676	0.034	*mgl*	FBgn0261260	0

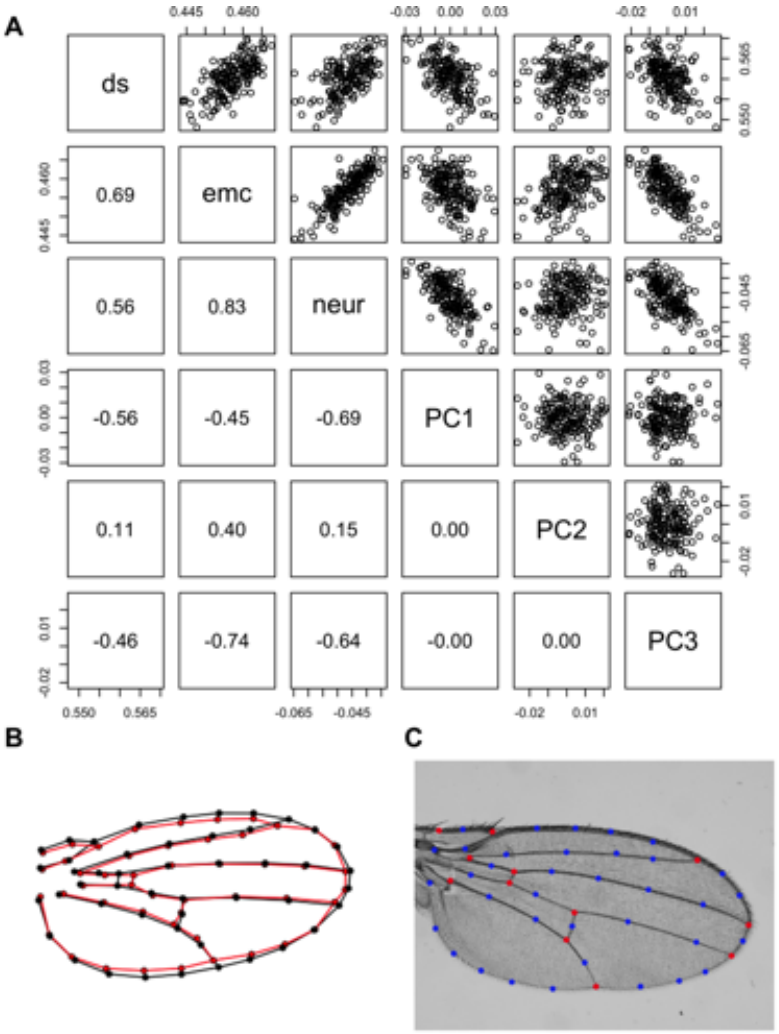

Figure 2.1: Projections of data onto RNAi shape change vectors are correlated with major axes of shape variation among DGRP strains. (A) Shape change vectors from RNAi titration experiments for *ds*, *emc* and *neur* were used, and DGRP line means were projected onto these vectors to calculate shape scores. Eigenvectors for the PCA were estimated based on the same DGRP line means. Vector correlations between shape change vectors from RNAi knockdown: *ds* - *emc*: 0.65, *ds* - *neur*: 0.03, *emc* - *neur*: 0.30. (B) Effect of *ds* shape change estimated from RNAi knockdown, effects not magnified. (C) Landmarks (red) and semi-landmarks (blue) used in geomorphic morphometric analysis on a *Drosophila* wing. PCs 1-3 account for 22%, 20% and 9% of the overall, among DGRP shape variance.

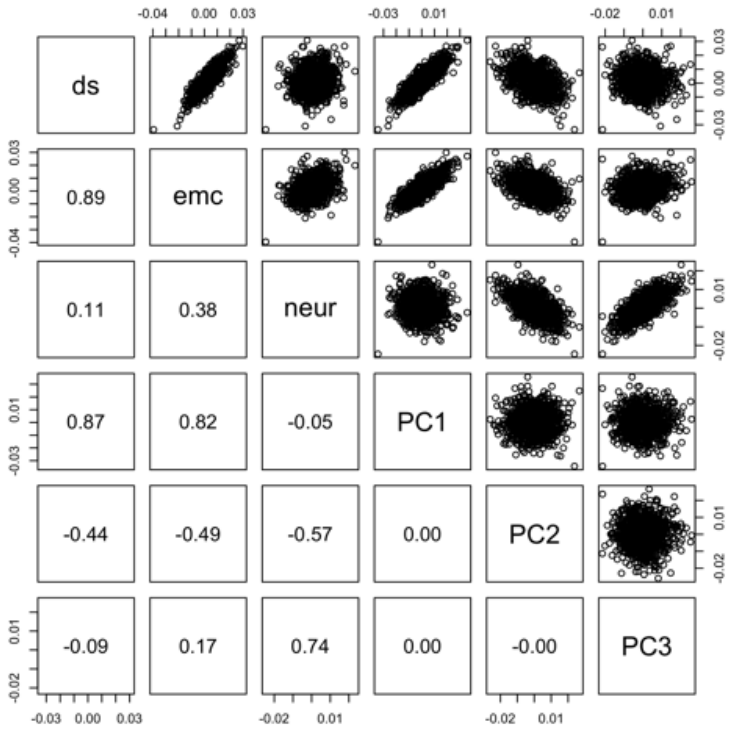

Figure 2.2: Projections of data onto RNAi shape change vectors are correlated with major axes of shape variation in wild-caught *Drosophila*. Correlations between projection of shape data from CMO population onto *ds*, *emc* and *neur* RNAi shape change vectors, and the first three eigenvectors from the PCA, calculated from shape data from all samples in the CMO population. PCs 1-3 account for 24%, 18% and 9% of overall shape variance in the CMO population.

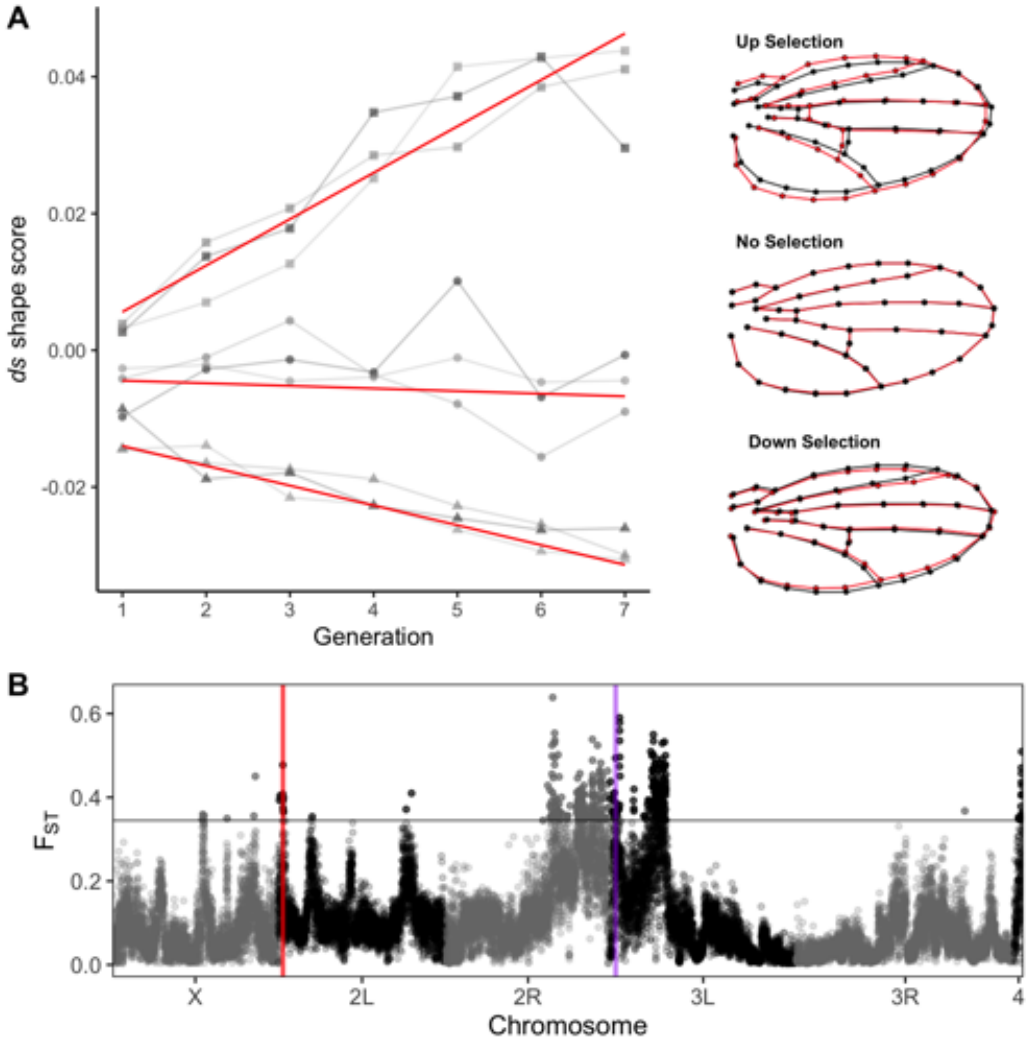

Figure 2.3: Artificial selection along *ds* shape change vector influences allele frequencies of variants at *ds*. (A) Phenotypic response to selection based on *ds* shape change vector. Only data from females is plotted for ease of visualization. Each replicate of up (squares), control (dots) and down (triangles) selection lineages are plotted (greys). Estimated response to selection shown along red lines. Wing plots represent the effect of selection on shape change between generation one and seven (red, effects not magnified). (B) Genomic differentiation (F_{ST}) between up and down selection treatments measured in 5000bp windows. Red line represents the location of the *ds* locus. Grey line represents 3 standard deviations from genome wide mean F_{ST}.

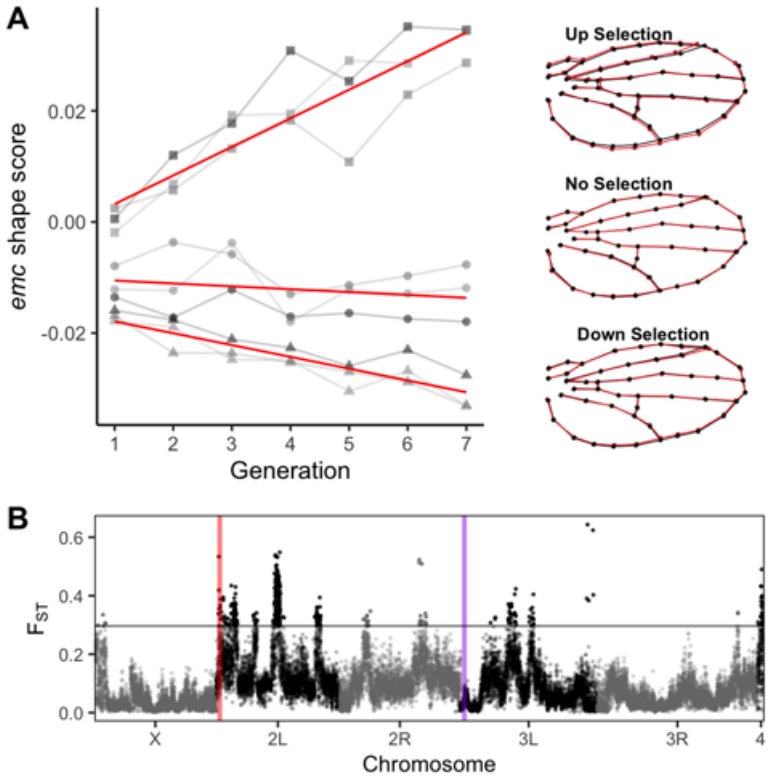

FIGURE 2.4: Artificial selection along *emc* shape change vector has modest influence on allele frequencies at *emc*, but a greater impact at the *ds* locus. (A) Phenotypic response to selection based on the *emc* shape change vector. Only data from females is plotted for ease of visualization. Each replicate of up (squares), control (dots) and down (triangles) selection lineages are plotted in greys. Estimated response to selection shown along red lines. Shape change between generation 1 and 7 is indicated on the right. Shape effects have been magnified 5x. (B) Genomic differentiation between up and down selection lineages (F_{ST}) measured in 5000bp sliding windows. Red and purple vertical lines represent genomic locations of *ds* and *emc* respectively. Grey line represents 3 standard deviations from genome wide mean F_{ST}.

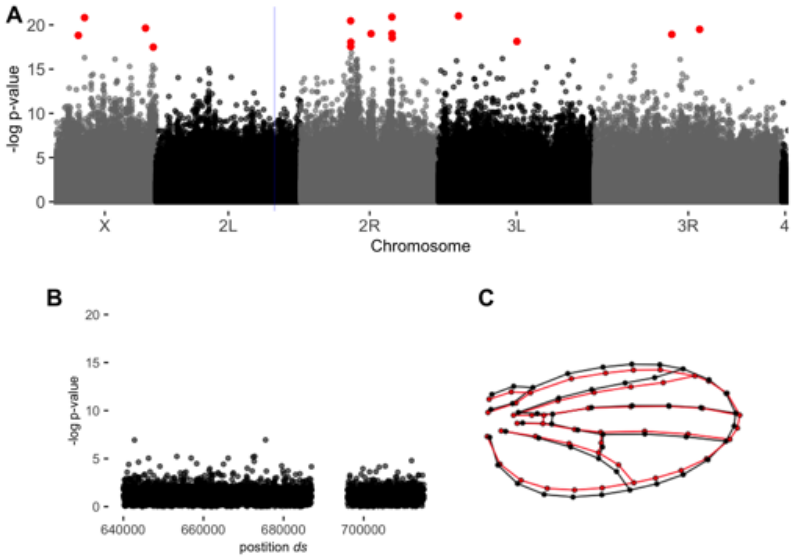

FIGURE 2.5: Genetic differentiation between pools selected based on *ds* shape change among the wild-caught cohorts. (A) Genome-wide scan for differentiated loci between pools selected based on *ds* shape change vector using the CMH test implemented in ACER. Points in red indicate sites with significant differentiation. Position of *ds* gene in blue (B) Genomic differentiation at *ds* between pools selected based on *ds* shape change vector. No sites are significantly differentiated in *ds*. The large gap in sites is due to a masked region in the genome due to repetitive sequence and poor (syntenic) mapping scores. (C) Shape difference between selected pools of individuals from one representative (CMO) population, with the mean shape of pools represented in black and red.

Chapter 3

Polygenic architecture of adaptation of *Drosophila melanogaster* wing shape and size to a high-altitude environment.

3.1 Abstract

Populations of *Drosophila melanogaster* from high altitude environments have larger wings and a different wing shape than populations living at lower altitudes. Because the colonization of high altitude environments is thought to be relatively recent (2000-3000 years ago), this is an interesting system to study alleles contributing to adaptive divergence on short time scales. Increasingly, models predict that genetic variants already present in a population are more likely to contribute to adaptation on short time scales, particularly when populations are large and genetically diverse as is the case for *Drosophila*. Selected isogenic lines derived from a lowland (500m) and highland (3000m) population were crossed together for 20 non-overlapping generations to allow for recombination. F20 offspring were phenotype for wing shape and size and the most phenotypically extreme individuals for each trait were sequenced. Measuring genetic differentiation between the phenotypically extreme pools of individuals revealed a polygenic architecture of adaptive divergence for both size and shape as is predicted by many simulation models. Despite the polygenic nature of adaptation, we identify one QTL that is a particularly interesting candidate contributing to shape variation in the same direction as the adaptive divergence, however it is not replicated in all mapping crosses,

indicating the allele is not fixed in high altitude populations. Additionally, we demonstrate the independence of wing shape and size, despite the intrinsic links between the two traits. Overall, this work demonstrates that many alleles, distributed throughout the genome rather than single large effect alleles contribute to adaption in *Drosophila* wing shape and size which adds to the growing body of evidence for the importance of polygenic adaption.

3.2 Introduction

Polygenicity of complex traits is common, and even traits with seemingly monogenic effect often have many genes of small effects contributing. The genetic architecture of changes in trait mean in response to selection is a broadly studied question. Classic studies that have mapped alleles contributing to trait variation identify one or a small number of alleles contributing to phenotypic divergence, such as *mc1r* influencing coat colour in mice (Hoekstra 2006; Hubbard et al. 2010), *eda* influencing stickleback armor plate variation (Barrett et al. 2008; Colosimo et al. 2004; Hubbard et al. 2010), among other systems. Large effect variants are often *de novo* mutations that occurred concurrently with selection or were very rare in the ancestral population (Dittmar et al. 2016). These examples may represent a very biased sample of the genetic architecture of complex traits as identifying these single loci of large effect requires smaller sample sizes and a smaller number of unique genotypes to identify alleles. With the falling cost of genomic sequencing and more widespread whole genome mapping in much larger populations, it has become apparent that adaptive changes in trait values generally involve contributions from many loci (Pritchard and Di Rienzo 2010). These small effect variants usually include a substantial fraction of alleles segregating in ancestral populations at non-negligible frequency, as opposed to *de novo* mutations or very rare variants. The relative contribution of large and small effect alleles matters, as they will affect relative contribution of (hard) genetic sweeps at a few genomic loci at one end of the spectrum, to subtle shifts in allele frequencies across many loci with no fixation of alleles on the other. The former case is much easier to detect in population genetics data than the latter, as hard sweeps leave clear genomic footprints of low diversity. As such, where on the spectrum of the alleleic distribution the alleles contributing to adapation occur is an open but essential question in understanding the mechanisms of adaptation for complex traits (Barghi et al. 2020).

Hard sweeps from single alleles of large effect, subtle shifts in allele frequencies and all the points on the spectrum in between allow for rapid adaptation with contribution

from multiple loci, but the relative effect sizes of contributing alleles and contribution of mutation and segregating variation varies amung them. The theory of an adaptive walk predicts subsequent fixation of alleles (Orr 1998; Orr 2005). This sweep can be either "hard", with *de novo* mutations contributing, or soft, with contributions from alleles segregating in the population (Coop and Ralph 2012). For alleles to be selected on, they must be beneficial enough to escape the selection-drift boundary and segregate at a high enough frequency in the population. Thus, mutational patterns are likely to drive the alleles available for selection in populations under this model.

When genetic diversity in a population is high and with a large effective population size, selection at individual variants of large effect will be "weakened" in favor of polygenic adaptation or allele shifts at many loci (Chevin and Hospital 2008). As predicted by Fisher's infinitesimal model and subsequent extensions, the effect of many mutations are predicted to be small as pleiotropy for genes is high and large effect alleles are likley to be deleterious for one or more of the affected traits (Boyle et al. 2017; Fisher 1930). Small shifts in allele frequency across many loci in response to directional selection, followed by a period of stabilizing selection, can result in phenotypic divergence, without the fixation of alleles in the diverged population (Hayward and Sella 2019). Because of the small shifts predicted by this model, identification of particular alleles can be difficult, as F_{ST} scans to identify differentiated alleles cannot detect these shifts (Yeaman 2015). Thus, mapping approaches may be better suited to identify the alleles contributing to divergence as these small effect alleles can still be identified.

Drosophila melanogaster populations are particularly tractable systems for mapping alleles contributing to divergence due to short generation times, ease of culture and the extensive genetic tools available. A number of traits vary between high and low altitude populations of *D. melanogaster* in Sub-Saharan Africa, including body size, pigmentation, wing shape and size (Bastide et al. 2016; Pitchers et al. 2013; Fabian et al. 2015; Pool et al. 2016; Groth et al. 2018; Lack et al. 2016b). As is typical of small insects (Dillon 2006), high altitude *D. melanogaster* have a larger wing size and increased wing loading as compared to lowland populations (Pitchers et al. 2013). Using nearly isogenic lines isolated from highland populations (Fiche, Ethiopia >3000 m) and lowland populations representing the ancestor (Siavonga, Zambia 500 m)(Lack et al. 2015), many mapping studies have been conducted to identify the genetic basis of this adaptive divergence. In the case of pigmentation, a small number of polymorphisms have been identified that explain the darker pigmentation in highland populations (Bastide et al. 2014). In contrast, mapping studies that have examined differences in both body and

wing size identified a polygenic basis with little evidence of selective sweeps at single loci (Sprengelmeyer et al. 2022). The differences in the genetic architecture of these traits could help to explain the differences in the two patterns discovered. Pigmentation has a 'simpler' genetic basis with a smaller mutational target size (Dembeck et al. 2015; Wittkopp et al. 2003) than wing size, about 15% of the genome (Carreira et al. 2009; Carreira et al. 2013). The previous wing size mapping study used four Zambian and four Ethiopian inbred lines to identify alleles and likely did not fully capture the complete genetic architecture. By adding mapping studies with more genetic backgrounds, we can begin to understand the degree of polygenicity in wing size adaptation.

The genetic basis in wing shape variation between these two populations has not been investigated although there is a documented wing shape change between highland and lowland populations (Pitchers et al. 2013). Like wing size, wing shape has a large mutational target size (Carreira et al. 2011; Houle et al. 2017) but differs from wing size in its multivariate nature. In contrast to a univariate trait, such as size, that can only vary in a single direction (larger or smaller), where directions of effects can be aligned by chance 50% of the time, wing shape varies in many directions; as the number of available dimensions of variation increases, the likelihood of effects being aligned by chance decreases. Both simulations and empirical studies have demonstrated the power of such an approach to understanding the genetic architecture of traits (Pitchers et al. 2013; Porter and O'Reilly 2017). The increased number of directions in which effects can vary allows for the analysis of shared directions of variation. The major axes of shape variation between Drosophild species are more aligned with mutational variation rather than standing genetic variation within *D. melanogaster* (Houle et al. 2017). This example is on a longer time scale than the relatively recent adaption to high altitude observed between highland and lowland populations (<3000 years) (Sprengelmeyer et al. 2020) but creates an interesting model with which to understand the genetic architecture of divergence on short and long time scales.

Allometry is a major component of shape variation in many systems, including *Drosophila* wings (Klingenberg 2016). Although it is possible to separate the allometric component of shape (Klingenberg 2022) and there is evidence for a change in the non-allometric component of shape between highland and lowland populations (Pitchers et al. 2013), it is not clear if the change is a consequence of selection on shape itself or due to selection for larger wings though allometry. The adaptive benefit of larger wings at high altitudes is explained by the increased surface area of the wing creating lift at lower air pressures (Dillon 2006). However, the adaptive benefit of a wing shape change

is not as obvious, and the fitness benefits of subtle wing shape changes are difficult to test. By asking if non-allometric wing shape change and wing size change have unique genetic architectures, we can test there is an adaptive advantage to wing shape change that is genetically separable from selection on wing size.

Using highland and lowland populations of *D. melanogaster*, we investigated the genetic architecture of two complex traits, wing shape and size divergence. We demonstrate a polygenic architecture of adaptation for both wing size and wing shape with no QTL shared between different crosses, supporting the hypothesis that contributing alleles are not fixed in the derived high-altitude population. Despite the unique genetic basis of adaptation, a common allometric size-shape relationship and similar structure of shape variation was observed between different F20 intercrosses, even when the parental inbred lines the the crosses were derived from have unique allometries and shape variation structures themselves. This is what we would expect in a situation where many alleles of small effect, rahter than a few alleles of large effect, contribute to shape. We also demonstrate the unique genetic basis of wing shape and size adaptation, even through the two traits are intrinsically linked thought the size-shape allometric relationship. Overall, we provide support for the model of polygenic adaptation due to small shifts in allele frequency rather than subsequent fixations of alleles.

3.3 Methods

3.3.1 Creation of F20 advanced intercross

To map the genetic basis of shape and size adaptation between low altitude (Siavonga, Zambia, "ZI," 16.54 S, 28.72 E, alt. 530 m) and high altitude (from Fiche, Ethiopia, "EF," 9.81 N, 38.63 E, alt. 3,070 m) populations of *Drosophila*, 3 highland lines and 3 lowland lines were selected for creation of pairwise F20 advance intercrosses. The Zambian (ZI192, ZI251, ZI418) and Ethiopian (EF43, EF81, EF96) lines were selected from wild-caught isofemale lines that were inbred for 8 generations (Lack et al., 2015)(Figure 3.1). Lines were selected to be free of the most common, known chromosomal inversions: *In(1)A, In(1)Be, In(2L)t, In(2R)NS, In(3L)OK, In(3L)P, In(3R)K, In(3R)Mo*, and *In(3R)P* in previous analysis (Lack et al. 2016b; Lack et al. 2015). All crosses were done at 20°C in the lab of John Pool (University of Wisconsin), using the lab's standard recipe (see supplementary file 1 for all fly media recipes). Each pairwise cross was done in a single 28cm x 14cm x 15cm cage. In the first generation, 8 parents from the appropriate highland and lowland lines were crossed in a reciprocal manner to ensure equal

contributions of X chromosomes from high and low-land populations. 125 F1 individuals of each sex from this cross were selected to start the cage cross population. In cages, flies were provided with 14 vials of food and allowed to lay for 1 week before food was changed. For each non-overlapping generation 1200 progeny from the previous generation were used to lay for the next generation. No selection was used in choosing which individuals contributed to the next generation. After 20 generations of crossing, adult flies were collected and stored in 70% ethanol and shipped to McMaster University for wing dissection and mounting as well as DNA extraction and sequencing.

3.3.2 Collection of Morphometric Data

The right wing from individual flies were dissected and mounted in 70% glycerol in PBS and bodies were stored in 95% ethanol in wells of a 96 well plate until genomic extraction. Wings were imaged using a using an Olympus DP30B camera mounted on an Olympus X51 microscope (Olympus software version 3.1.1208) using a 4X objective (total 40X magnification) and images were taken using cellSens Standard (version 1.14).

Shape data were collected using two methods, with the second method used to increase the speed of data collection and largely captured a similar shape change (Figure A2.1). The first method (referred to as the WINGMACHINE method) used extracted positional information for 14 landmarks and 34 semi landmarks, allowing for 58 available dimensions of variation (explained below). In this method, shape data was collected using the WINGMACHINE pipeline outlined in (Houle et al. 2003). First, two landmarks were placed at the humeral break and alula notch using tpsDIG2 (version 2.16). Wings (Van der Linde 2004–2014, v4) software was used to fit nine cubic B-splines and correct errors. All shape data was subjected to full Procrustes superimposition to scale images to the same size, translocate to the same location and rotate to minimize distance between points (Rohlf and Slice 1990), and landmark and semi-landmark information was extracted using the program CPR (version 1.11). Superimposition results in the loss of 4 possible dimensions of variation while semi-landmark variation is constrained to a single axis (dimension), resulting in 58 available dimensions of variation.

The second method (referred to as the 15 landmark method) extracted positional information for 15 landmarks, resulting in 26 available dimensions of variation (2 available dimensions for each landmark 4 dimensions due to superimposition). Landmarks were identified using a Fiji (v4.0.3) plug in designed to capture wing shape in this way. In this case, Procrustes superimposition was done with the gpapagen() function in the

geomorph (v 4.0.3) package (Adams and Otárola-Castillo 2013). The shape change captured using both methods is similar, as demonstrated by the similar variance structures and shape changes between the two methods (Figures A2.1, A2.2). In both cases, the methods used for downstream analysis of shape were the same.

Males and females were considered separately for downstream analyses due to sexual dimorphism for both wing shape and size. To remove allometric components on shape in the data, and to ensure that the size and shape axes of variation were independent, a PCA that included the shape residuals along with the natural log transform of centroid size was used. Using this method, size variation, including the allometric component of shape, is captured by PC1 (Klingenberg 2022)(Figure A2.3). The remaining PCs (PC2 – 58) for the WINGMACHINE method or PC2 – PC26 for the 15 point method) were then used for the subsequent steps of the analysis. The vector of shape change between the high and low altitude parental populations was calculated from the difference between the mean shape for the three highland and three lowland lines used as the parents in F20 crosses. Shape data (represented by the PCs) from individual wings was projected onto this difference vector to create the 'shape score'.

3.3.3 Genomic analysis and QTL mapping

For a given cross, the 50 most extreme individuals, within each sex, in the distribution of shape (measured as a shape score, described below) and size (measured as centroid size) were selected. Those individuals with the 50 highest and 50 lowest shape scores were selected for sequencing while size pools were created from the 50 largest and 50 smallest individuals. In cases where an individual was an outlier for both size and shape, these individuals were included in both pools (details below, Figure 3.2).

Genomic DNA extractions were performed using a Quiagen DNeasy kit on a maximum of 25 individuals in each sample. To create pools for sequencing, samples were combined such that each fly contributed an equimolar amount of DNA to the sequenced pool, using concentrations measured with the DeNovix dsDNA Broad Range Kit. The number of flies in extraction sample and the amount of DNA added to the final pool can be found in supplemental file 1. Library prep using the NEB Ultra II kit for library preparation and 150bp paired end sequencing using illumina NovaSeq6000 by Genome Quebec (Montreal, QC).

Reads were trimmed with Trimmomatic (v0.36) to remove adapter contamination and checked for quality using FastQC prior to alignment (Bolger et al. 2014). Trimmed reads were aligned to the *Drosophila melanogaster* genome (v6.23) using BWA-MEM

(v0.7.8) (Li and Durbin 2010). Sequencing replicates of the same biological samples were merged using SAMtools (v1.11). PCR duplicates were removed using Picard with the MarkDuplicates tool (v 2.10.3) and reads with a mapping quality score less than 20 were removed using SAMtools (Li et al. 2009). A local realignment around indels was performed using GATK using the IndelRealigner tool (v3.4.46). Highly repetitive regions of the *Drosophila* genome were identified and subsequently masked in mpileup files using RepeatMasker with default settings (v4.1.1) with default settings. INDELs and regions within 5bp of an indel were identified and masked using PoPoolation2 scripts. F_{ST} was calculated in 5000bp windows using PoPoolation (v1.2.2) and PoPoolation2 (v1.201) (Kofler et al. 2019a; Kofler et al. 2019b)

3.3.4 RNAi of candidate regions on chromosome 3R

To estimate the effects of candidate gene knockdown on shape change, we expressed an RNAi construct for the gene of interest in the developing wing disc. RNAi experiments were done using fly media with the Dworkin lab recipe (see supplementary file 1). A *nubbin-Gal-4* line (BDSC:25754) was crossed to RNAi lines of the gene of interest (UAS-GOI RNAi) and progeny were allowed to develop at low larval density. All but one RNAi line were derived from the *Drosophila* transgenic RNAi project (TRiP) panel (Perkins et al. 2015) and a common background with the TRiP control (BDSC:36303). The RNAi lines used in the experiment were: *locomotion defects* (*loco*), *winged-eye* (*wge*), *button* (*btn*), *wake*, *eukaryotic translation elongation factor alpha 2a* (*ef6a*) and *TGF-β activated kinase 1-like2* (*takl2*)(Table A2.1. The *loco* RNAi line also carries a *scute* allele, known to have effects on wing shape. To account for this effect, *loco* RNAi flies were also crossed to a *white* mutant. The *wge* RNAi line did not have a known genetic background so we crossed this line to a *w-* mutant as well as a control for this construct. Each cross was done in two replicate vials to account for environmental variance. Adult F1 flies were collected 24-48 hours following eclosion to allow for wing hardening and stored in 70% EtOH until dissected and imaged for morphometrics using the same methods as above. Shape data were collected using the 15-landmark method.

The effect of RNAi knockdown on shape was estimated by fitting a model with the procD.lm function (geomorph package) with terms for log centroid size, genotype of the cross and the interaction of the two as well as a term for the replicate vial as predictors. Males and females were considered separately in this analysis, as the altitudinal effect vectors were also calculated separately. Least squared means for each cross genotype were estimated and contrasts between RNAi crosses and the appropriate control (Table A2.1) were calculated to get the effect vector for RNAi knock down for plotting shape

changes. Bootstrapped distributions of vector correlations were calculated between the altitude and effect vector and RNAi knockdown effect vector by first estimating the effect of population on size from a model with terms for size, population and their interaction. Then the RNAi effect vector was calculated for each RNAi knockdown and the appropriate control from the same model as was used in the geomorph analysis (the effects of centroid size, genotype and their interaction plus the effect of replicate vial within genotype). Observations were sampled with replacement in a non-stratified manner, because sample sizes between groups were approximately equal, for 1000 iterations.

3.3.5 Mapping of candidates on chromosome 3R

A genomic deletion series from both the *Drosophila* Deletion (DrosDel) (Ryder et al. 2007) and Exelixis (Parks et al. 2004) genomic deletion panels, spanning the region of differentiation on chromosome 3R (22580970..22733819) in the Zi192 x Ef 96 and Zi192 x Ef 81 crosses were used for quantitative complementation mapping of the contributing allele. A full list of the deletion lines used, and the genes predicted to be included in deleted regions, is included in supplementary file 2. In addition to the lines used in mapping crosses, we included a number of other high and low altitude lines: EF 43, 81, 96 and 119 ; ZI 192, 251, 360, 357, to test for effects at the population level. Virgin females from African lines were crossed to deletion line males and allowed to lay eggs for 2 days on Dworkin lab fly media (Supplemental file 1). Each cross was done in two replicate vials. F1 heterozygotes were selected based on loss of the balancer chromosome phenotype and preserved in 70% ethanol until males were dissected and imaged following the standard protocol outlined above. Shape data were collected using the 15-point landmark method. Each deletion panel was considered separately (as they were generated in different isogenic wild type strains) for statistical analysis, but using the same methods. A mixed model for the effect of size, deletion line, and African population, all two-way interactions between these terms plus a random effect for the replicate vial within cross and for genetic lines within background (`shapescore ~ (CS+delLine+background)^2 + (1 | delLine:background:rep)`) was used to test associations with shape change. The response variable was the shape score calculated by projecting superimposed shape data onto the vector based on the differences between high and low altitude populations.

3.3.6 Analysis of wing shape and size variation

For all morphometric analyses, male wing shape data from three high altitude (EF43, EF81, EF96) strains, three low altitude (ZI192, ZI251, ZI418) strains, and 3 crosses

(ZI192 x EF43, ZI192 x EF81, ZI192 x EF96) was used. Each distinct group, whether an inbred line or F20 intercross is referred to as a 'genotype' throughout the analysis for convenience. All data for these analyses were collected using the 15 landmark method and jointly superimposed.

We examined changes to the allometric (shape-size) relationship between different genotypes, within and between populations. Allometric effect vectors were estimated at the level of line using a model regressing wing size, genotype, and the interaction on shape. The projection of wing shape onto the estimated allometry vectors (shape score) and predicted shape values (PC1 of fitted shape residuals), was calculated with the plotAllometry function from the geomorph package. Using the pairwise() function within RRPP/geomoph, vector correlations for allometric effects were calculated at the strain level. Additionally, to understand group level changes (high altitude lines, low altitude lines and F20 crosses), the effect vectors within group were estimated from a linear model regressing the effect of wing size, population, and the interaction of the two on shape. Confidence intervals for both statistics were estimated using non-parametric bootstrapping of observations (not residuals).

To compare shape variation between groups, we calculated several statistics based on the variance-covariance (VCV) matrix of allometry corrected shape residuals using the EvolQG package in R (v0.3-2) (Melo et al. 2016). To describe the shape of the variation within each group, we calculated the integration (proportion of total variance in the direction of greatest variance), eccentricity (standard deviation of the eigenvectors, normalized by the mean of all eigenvectors) and total variance (sum of all eigenvectors) for each group. The first two statistics measure how "spherical" the variance structure is, with lower values indicating a more "ball shaped" structure and higher values indicating a more elliptical or "pencil shaped" structure. 95% CI for all estimates were calculated using bootstrapping. Pairwise correlations of VCV matrices were calculated using the PCAsimilarity() function, which calculates the correlation in principal components (subspace occupied by each group), weighted by the magnitude of variance in that direction. These estimates were corrected by the replicability of each group's VCV matrix, which was measured using the BootstrapRep() function, which samples data within group and measures the shared substance between samples and the observed data. Mean correlations based on the type of pairwise comparison (for example: comparisons within populations or between), were estimated. Finally, the effect of population on shape score, calculated based on the effect vector between high and low altitude populations was estimated using a model with main effects for wing size, group and their interaction

and a random effect of genotypes within group.

To compare the selection vector used in this experiment with the direction of shape variation in the population, mean line shape from 10 additional Zambian and 11 additional Ethiopian lines was obtained from (Pesevski and Dworkin 2021) One line was shared between studies to allow for the estimation of effects between the two data sets. An approximate **G** matrix could then be calculated using a PCA of the line means of the 6 lines used in this study plus the additional lines. Shape change vectors were calculated by finding the difference between mean shape vectors for the Zambian and Ethiopian populations. The effect of lab rearing conditions and shape data collection from different people (known to have a significant effect on shape) and size were accounted for by fitting a linear model with terms for size and experimental source.

3.4 Results

3.4.1 Size and shape adaptation have a polygenic basis

QTLs contributing to wing size variation were mapped by measuring genetic differentiation between large and small pools using F_{ST} in a 5000bp windowed analysis. Overall, the genetic basis of size adaptation to high altitude appears to be polygenic, with no striking regions that would indicate alleles of large effect contributing (Figure 3.3). For analysis, windows with an F_{ST} greater than 3 standard deviations from the genomic mean F_{ST} for that cross were considered biologically relevant outliers. For the two crosses sharing a lowland parent, Zi192xEf96 and Zi192xEf81, we see some similarities between the two crosses with 112 outlier windows (total = Zi192xEf96: 421, Zi192xEf81: 552) shared between them. In contrast, the cross with no shared ancestry, Zi418xEf43 (total = 306) shared only 8 outlier windows with Zi192xEf96 and 4 with Zi192xEf81. No windows were considered outliers in all three crosses. Shared windows could indicate either a shared causative allele contributing to shape variation in both crosses or could reflect chance with linked regions of the genome contributing. Because the mutational target size for *Drosophila* wing shape is so large, it is possible that linked genes may both contribute to wing size variation.

In contrast to size, mapping the change in shape between high and lowland populations revealed specific regions of the genome that likely contribute to the shape variation variation (Figure 3.4). Although a large region of differentiation is shared on chromosome 3R in both the Zi192xEf96 and Zi192xEf81 crosses, this region is not differentiated in the Zi418xEf43 cross (Figure 3.4, Figure A2.4). There is a large region of differentiation on

chromosome 2R in the Zi418xEf43 cross that appears to be unique to this cross. No outlier windows, using the mean plus three standard deviations cutoff, are shared between Zi418xEf43 and other crosses (total = Zi192xEf96: 366, Zi192xEf81: 722, Zi418xEf43: 700). There are 253 windows shared between Zi192xEf96 and Zi192xEf81, with all but one of those windows on chromosome 3R. The large genomic regions contributing to shape differentiation make it difficult to identify specific alleles that may be contributing in these regions.

There is also evidence for sex specific alleles contributing to shape differentiation (Figure A2.5). Sexual shape and size dimorphism have been documented for the *Drosophila* wing in these populations (Pesevski and Dworkin 2020). In the case of the QTL on 3R in the Zi192xEf96 and Zi192xEf81 crosses, this region may contribute more in females as the allelic differentiation in this region is greater. In males, regions of the X chromosome are differentiated in males but not in females in the Zi192xEf81 cross. This same pattern on the X chromosome, with the addition of another region on chromosome 2R appearing to contribute more in one sex than the other. These observations can be explained by sampling variance, but it is more likely that there is varying expression of allelic effects between sexes. The abundance of sites on the X in males indicates there may be recessive segregating alleles contributing while on other chromosomes, and on the X, indicating a sex by genotype effect.

3.4.2 Chromosome 3R has a candidate genomic region contributing to shape divergence between populations

The QTL on chromosome 3R that is differentiated in two of the shape crosses is an interesting candidate for future study. To investigate this, genes with alleles predicted to influence gene function in this region were selected for follow up analysis (Supplementary File 2). Knockdown of one gene, *loco*, had a substantial effect on wing shape when compared to controls (Figure A2.6). Because of the large mutational target size of wing shape, it is more useful to investigate the shared direction of the effect of gene knockdown and the altitudinal effect vector. For all 6 examined genes, the correlation between vectors was modest to small (Figure 3.5). The *wge* RNAi vector correlation makes this an interesting candidate gene as it is the only case where the 95% CI does not approach 0 (0.57; CI: 0.34 – 0.65). *loco* (0.46; CI: 0.20 – 0.62) and *takl2* (-0.39; CI: -0.57 - -0.16) knockdowns also demonstrate a moderate level of shared effect direction with the altitudinal effect vector. The shape changes of these three genes is like that of the altitudinal effect vector, making them good candidates for future work (Figures 3.5, A2.7).

In addition to candidate gene knockdowns, we also took a deletion mapping based approach to find an association between smaller genomic regions and shape change. Reaction norm plots showed little effect between populations for most tested deletions (Figure 3.6). For both panels tested, there was no substantial effect of the interaction between population and deletion line (Tables A2.2 A2.3). In the DrosDel panel, there may be different reaction norms between the two populations for the 20515 line (Figure 3.6). This line is predicted to have no deletions in genes that overlap with the previously identified candidates (See supplementary file 2 for full list). In the Exelexis panel, deletion line 7671 is a possible candidate for influencing shape (Figure 3.6). This region contains both *wake* and *wge*. Additionally, deletion 7740 in the Exelexis panel may be a candidate and contains the genes *loco*, *btn* and *ef6a* from the candidate list.

3.4.3 Size and shape divergence have unique genetic bases.

Because size and shape are tightly linked though allometry, we wanted to ask if there was a change to allometric effect vectors in addition to the differences in shape between crosses in this study. As we controlled the environment in these experiments, the majority of phenotypic variation we observe should be explained by genetic variation. Wing size is intermediate in the F20 cross genotypes compared to the parents (Figure A2.8). Using three crosses with a shared Zambian parent but unique Ethiopian parents, we calculated the allometric effect vectors to compare the relationship between size and shape in crosses compared to parental genotypes. There is a significant effect of allometry between genotypes; however, this only explains a small proportion of overall shape variance (R^2 = 0.0013, F = 4.36, p = 0.001, Table A2.4). Despite different allometric effects within Ethiopian parental lines and between Ethiopian and Zambian parents, we observe a shared direction of allometry in all three F20 crosses (Figure 3.7A). However, the overall correlation of allometric effect vectors between the cross and parental populations remains about the same (Figure A2.9). It is important to note the larger magnitude of the allometric effect vector in the parental populations (ZI: 0.22 ,CI: 0.15 – 0.27; EF: 0.11, CI: 0.11 – 0.20) compared to the cross populations (0.06, CI: 0.06 – 0.07)(Figure A2.9). Most of this variation is related to a shift in the position of the L2 and L4 longitudinal veins and a posterior shift in the anterior cross vein between the smallest and largest files (Figure 3.7C). There is a high degree of individual variation within both the crosses and the parental lines (Figure 3.7B, Table 3.1).

We compared the variation in wing shape, after accounting for wing size between genotypes. Overall, the parental lines had a higher variation between lines for all the

estimated statistics (Figure 3.8, Figure A2.10). F20 crosses had lower integration and eccentricity (two measures of sphericity of the covariance matrix) than any of the parental genotypes, indicating that variation within the matrix is spread over many directions, rather than concentrated in a single direction (Figure 3.8A, Figure A2.10). It is important to note that there were far more individuals measured within each F20 cross compared to each parental line, but also a much higher degree of genetic variation in crosses than parental lines, which are near isogenic (Figure 3.7B). The degree of similarity between shape variation within populations is much higher when comparing crosses to each other (cor = 0.96, 95% CI: 0.83 – 1) than comparing inbred lines to other lines from the same population (cor = 0.72, 95% CI: 0.66 – 0.79) (Figure 3.7C). There is also a higher correlation between parental lines used and the F20 cross (cor = 0.89, 95% CI: 0.82 - 0.96) than the crosses and inbred lines that did not contribute (cor = 0.81, 95% CI: 0.76 – 0.86) (Figure 3.8C). Despite the observed shape differences between inbred lines and F20 crosses, the variation along the axis of variation defined by the shape difference between low- and high-altitude populations (altitudinal effect vector), responds as expected, with the F20 cross as an intermediate between high and low altitude populations (Figure 3.8D).

The selection vector used to score wings in the F20 mapping crosses was defined as the difference vector between the three Ethiopian and Zambian lines used for the mapping populations. Because these lines were chosen at random regarding size and shape diversity, this vector does not necessarily provide a perfect representation of the shape change between highland and lowland populations. To address this, we calculated the same shape change vector using additional data from 11 Ethiopian and 10 Zambian lines. The shared direction between difference (altitudinal effect) vectors to the direction of genetic variation in the population, using the approximate **G** matrix, was measured by projecting the mean shape of each line onto the difference vector to calculate a shape score and then calculating the relationship between these vectors and the axis of variation, summarized in PCs. There is a stronger relationship between the direction of greatest variation (PC1) and the altitudinal effect vector using the subset of lines selected for this study (r = 0.61) than the total population (r = 0.22)(Figure A2.11). There is also a relationship between both effect vectors and PC2 (subset: r = 0.54; all data: r = 0.52).

3.5 Discussion

The main goal of this study was to identify the genetic architecture that influences wing shape and size during adaptation to a high-altitude environment, using a F20 advanced intercross to map QTL. We demonstrate a polygenic architecture of adaption for both traits, based on mapping of three crosses (Figure 3.3, 3.4). Analysis of the distribution of shape and size phenotypes in F20 crosses compared to parents demonstrate an intermediate and consistent phenotypic distribution between crosses (Figures 3.8, A2.8). Despite the intrinsic link between shape and size of traits though shape-size allometry, we demonstrated that the alleles contributing to shape divergence and size divergence were unique (Figure 3.3, 3.4). Additionally, despite different allometric shape-size relationships in parental inbred lines, crosses shared an allometric effect vector, indicating that changes to shape or size may not necessarily correlate with changes to the relationship between the two.

Overall, this work provides support for a model in which small shifts in allele frequency for many genes rather than subsequent fixations in alleles for a small number of genes contribute to adaptation for the traits of interest. Wild populations of *D. melanogaster* have large effective population sizes with high genetic diversity (Duchen et al. 2013; Sprengelmeyer et al. 2020). Therefore, new mutations that are concurrent with selection are not required to create the genetic substrate on which selection can act. In the Drosophila genetic resource panel (DGRP), SNPs with replicable effects on wing size were identified in over 30 genes (Vonesch et al. 2016). For shape, over 500 SNPs contributing to variation were identified in the DGRP (Pitchers et al. 2019). In both cases, this is likely an underestimate of the total number of genetic variants contributing to trait variation, as polymorphisms with very small effect sizes are thought to have a substantial effect on variation of complex traits and are difficult to identify with GWAS methods (Rockman 2012; Boyle et al. 2017). Although this study used a modest number of parental inbred genotypes for QTL mapping, the results indicate that there are no fixed effect alleles contributing to the adaptive divergence because there are no QTL shared between all three crosses, representing a total of 3 Ethiopian and 2 Zambian genetic backgrounds, for either size or shape. Alleles may be segregating at a high, but not yet fixed, frequency and we may have sampled from lines with alternate alleles. However, this same polygenic pattern of rapid adaptation following an optimum shift has been previously reported using both simulations (Jain and Stephan 2017) and mapping of life history traits in guppies (Whiting et al. 2022).

This work suggests that small effect alleles, as would be predicted if genetic variants were already segregating in a population, rather than large effect alleles contribute to adaptation. First, the number of QTL contributing to shape variation on the X chromosome identified in hemizygous males indicates that at least some proportion of segregating variants are likely recessive (Figure A2.6). Secondly, the intermediate (relative to parental lines) and similar phenotypes in F20 crosses could be explained by many alleles, each with relatively small phenotypic effects contributing. Previous work to map the alleles contributing to size variation found a maximum estimated effect size of 25% (Sprengelmeyer et al. 2022), however effect sizes in these types of mapping studies are often overestimated (King and Long 2017; Xu 2003). Small phenotypic effects of alleles and large effective population size are two predictors of rapid adaptation with many alleles contributing (MacPherson and Nuismer 2017).

The intermediate phenotypes should also be interpreted with caution as an alternate explanation for these results is differing environmental contributions to wing morphology between cross and parental individuals. Both wing shape and wing size are plastic traits with a large contribution of environmental effects to phenotype (Carreira et al. 2013; Debat et al. 2009). Although it is tempting to understand the results based solely on changes in genetic variation, it is likely that changes in environmental variation have a substantial effect. This is made most clear by comparing the magnitude of the allometric effect vectors between high altitude, low altitude, and cross individuals (Figure A2.9). The larger magnitude of this vector in either parental population indicates a greater size variation in individuals. Because these are nearly isogenic lines with low genetic variance, it is likely that this variance is due to environmental variation.

In follow up experiments, we did investigate one QTL on chromosome 3R and attempted to identify the gene or genes contributing to shape variation between high and low altitude populations in this genomic region. Using both RNAi of candidate genes and deletion mapping in this genomic region (Figure 3.5, 3.6), we were unable to identify a single 'stand out' candidate but possibly identified multiple moderate candidates. One possible explanation for this is that there is not a single allele or single gene in this region contributing to divergence and rather several alleles in LD within the cross. Clusters of many alleles of small effect grouped together in LD and contributing to divergence are predicted both by theoretical (Yeaman 2013) and empirical studies (Orteu and Jiggins 2020). RNAi effect vectors had low to moderate correlations with the altitudinal effect vector (Figure 3.5). It is possible that these effect vectors are poorly estimated and

titrating the knock down effect may help to obtain better estimates. It is also possible that knock down does not correlate with the allelic effect in this region, although previous studies have demonstrated correlation between segregating polymorphisms and genetic knock down effects for wing shape (Pitchers et al. 2019). A quantitative deletion mapping experiment identified two regions that may be related to shape change in the same direction as the altitudinal effect vector (Figure 3.7). One of these regions overlaps with *wge*; the same gene that demonstrated the highest correlation in the RNAi experiment (Figure 3.5). *wge* has been shown to be important for expression of *vestigial*, a key wing patterning gene, in the developing wing tissue (Katsuyama et al. 2005). Although there is a candidate gene in this region, it is not likely "the" gene contributing to divergence between populations as one single large effect allele likely does not exist to explain variation in wing shape.

Changes to wing shape and wing size are linked though shape-size allometry. Although there is evidence that the non-allometric component of shape varies along an altitudinal cline (Pitchers et al. 2013), and we accounted for allometric shape variation in our mapping study, changes in size and shape may be linked either though allometry or through a shared genetic basis. For example, the Hippo developmental network is best known for its role in regulation of organ size, including the size of *Drosophila* wings. Hippo signaling variants are also indicated in influencing wing shape variation (Pitchers et al. 2019)(chapter 2). However, an allele frequency change across many hippo signaling loci following artificial selection for wing shape change did not result in a substantial wing size change (chapter 2). In this study, we also see evidence for independent genetic bases of wing size and wing shape change (Figures 3.3, 3.4). We observe a consistent allometric size-shape relationship in F20 crosses (Figure 3.7), indicating that despite shape changes, this relationship remains consistent. Again, these results should be interrupted with caution as the same caveats of increased environmental variance applied to the comparison of shape variance matrices should be applied here. That is, the environmental effects contributing to shape and size variation may simply be more similar in the crosses than in the parental lines, creating a common phenotypic variance. However, because we still observe the unique genetic basis of both size and shape variation, this is strong evidence that these traits have unique optima and the changes observed are due to selection on the trait and are not explained simply though selection on the other trait.

This study adds to the growing body of evidence that adaptive divergence does not require alleles of large effect or sweeps of alleles and can instead be explained by small

allele frequency shifts across many loci. Further mapping of specific loci contributing to divergence in these populations will be an interesting element in understanding the origin of these alleles, that is if they are segregating in lowland populations or if they are in fact *de novo* mutations arising concurrently with adaptation that have not fixed in high altitude populations. The importance of alleles of large effect contributing to divergence is well established but future questions will need to address what patterns exist that contribute to which alleles are "captured" by divergence.

3.6 Figures and Tables

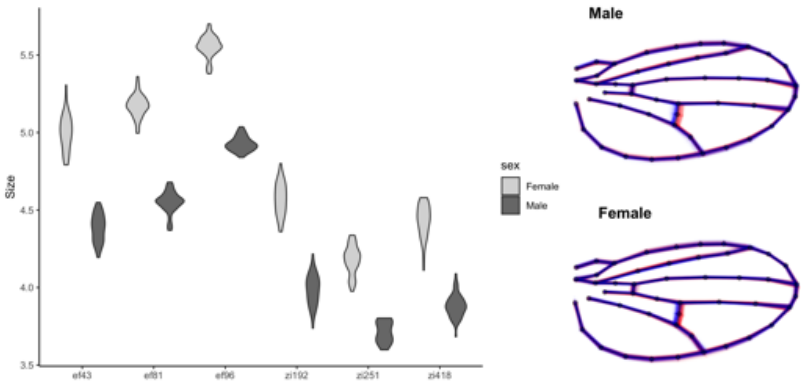

Figure 3.1: Differences in wing size and shape within and between high and low altitude lines used in mapping study. (Left) Distribution of wing sizes, measured with centroid size, within sex for parental lines used for intercrosses in the study. Ethiopian lines are on average larger than Zambian lines. (Right) Distribution of wing shapes within sex between high (red) and low (blue) Altitude populations. 150 wings plotted within each sex and population.

Table 3.1: Pairwise correlations between estimated slope of allometric effects. 95% CI for estimates are indicated in brackets. Vector correlation and 95% CI estimated using residual permutations as implemented by Geomorph package in R.

	EF43	EF81	EF96	ZI192	Zi192Ef43	Zi192Ef81	Zi192Ef96
EF43	1	0.23 (-0.27, 0.75)	0.25 (-0.11, 0.80)	0.90 (0.12, 0.84)	0.71 (0.34, 0.91)	0.90 (0.35, 0.91)	0.79 (0.35, 0.91)
EF81		1	0.54 (-0.22, 0.78)	0.13 (-0.22, 0.78)	0.40 (-0.14, 0.84)	0.39 (-0.14, 0.84)	0.37 (-0.16, 0.84)
EF96			1	0.13 (-0.06, 0.81)	0.67 (0.08, 0.89)	0.58 (0.08, 0.88)	0.58 (0.09, 0.89)
ZI192				1	0.62 (0.42, 0.93)	0.82 (0.41, 0.93)	0.77 (0.44, 0.93)
Zi192Ef43					1	0.88 (0.96, 0.99)	0.82 (0.96, 0.99)
Zi192Ef81						1	0.91 (0.96, 0.99)
Zi192Ef96							1

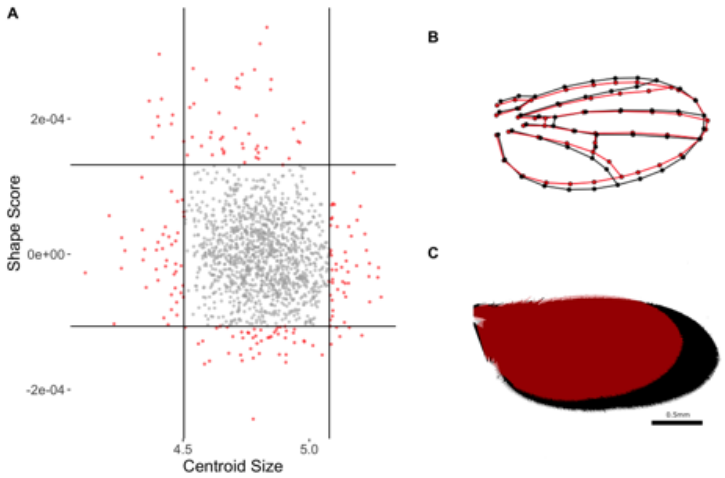

Figure 3.2: Selection of bulk pools used for sequencing from one F20 cross. (A) Distribution of individual phenotypes along the size and shape score axis. The 50 most extreme individuals along each axis were selected for sequencing and are indicated in red. Only males are plotted because of the size dimorphism between males and females. (B) Mean shape difference between individuals in the extreme pools along the shape score axis. Shape change is magnified 2x for visualization. (C) Mean size difference between pools selected for sequencing.

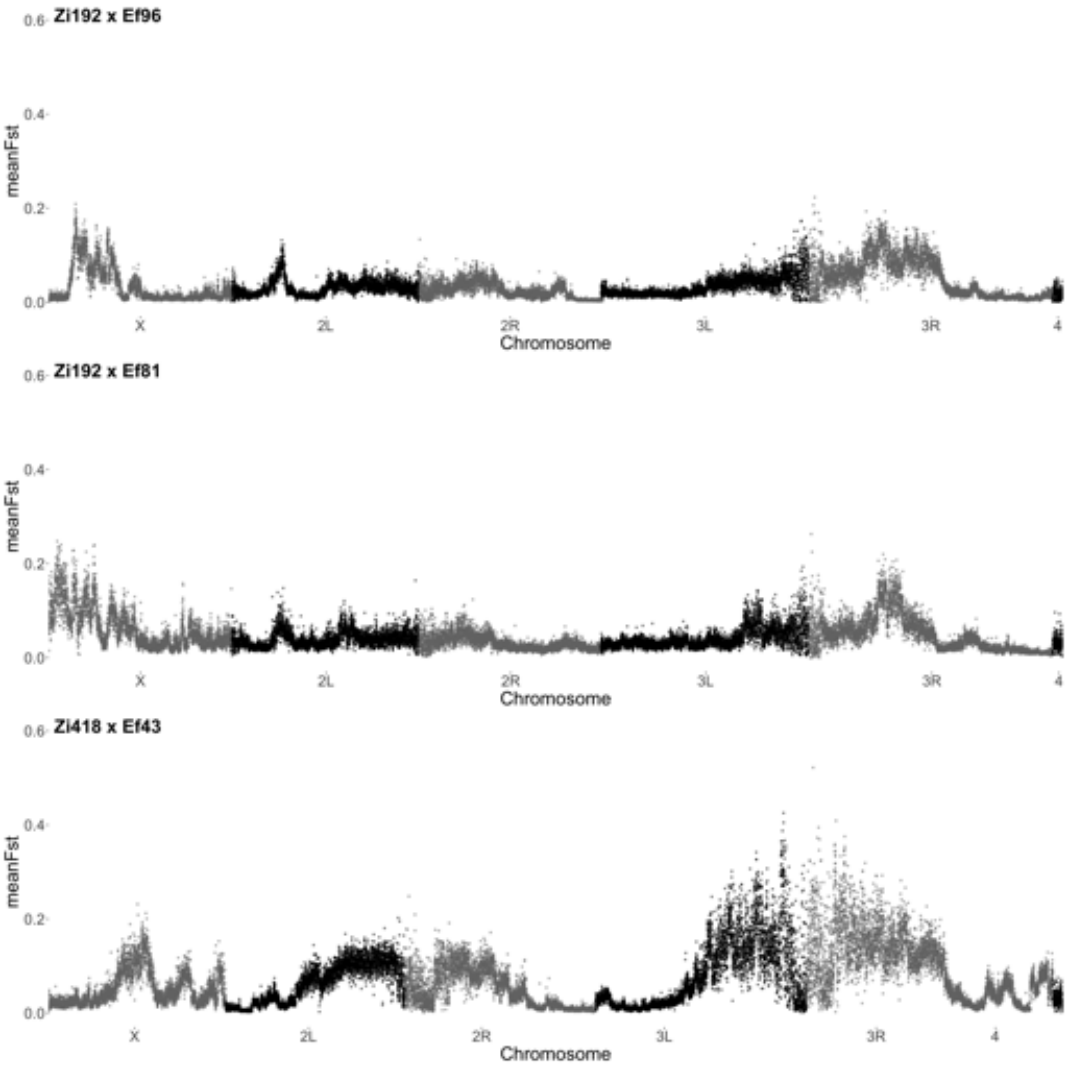

FIGURE 3.3: Genetic differentiation between size bulk pools indicates a polygenic basis of size divergence. F_{ST} between male pools measured in a 5000 bp windowed analysis using PoPoolation2 (Kofler et al. 2019b). Parental genotypes of crosses are indicated above each panel.

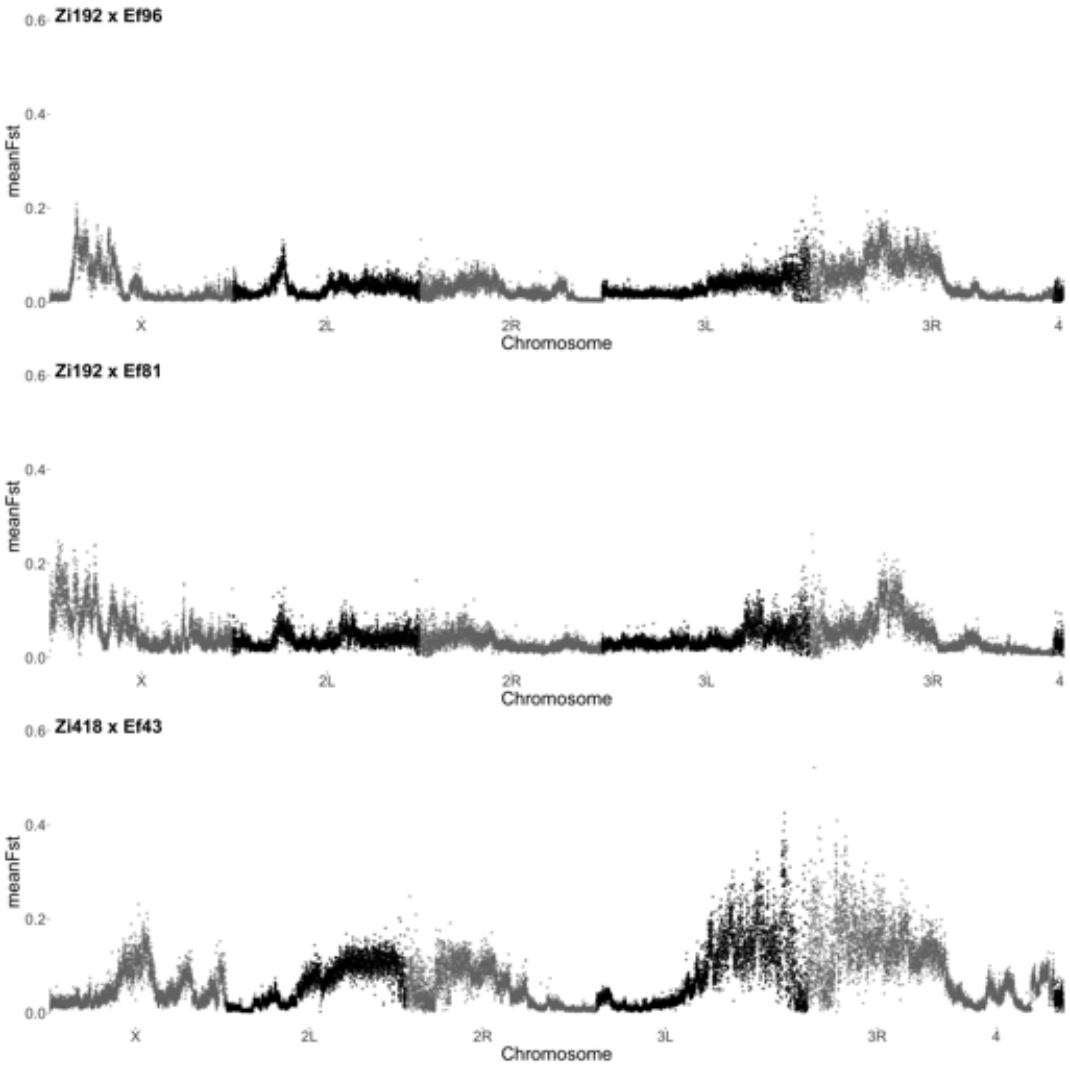

FIGURE 3.4: Genetic differentiation between shape bulk pools indicates a polygenic basis of size divergence. F_{ST} between male pools measured in a 5000 bp windowed analysis using PoPoolation2 (Kofler et al. 2019b). Parental genotypes of crosses are indicated above each panel.

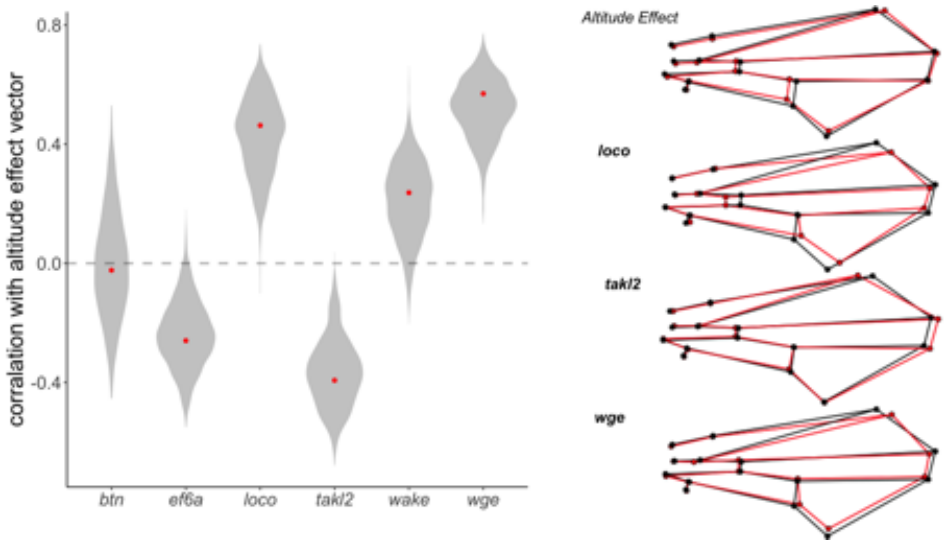

Figure 3.5: RNAi knockdown effects of genes in the chromosome 3R candidate region. Bootstrapped distribution of vector correlation between altitudinal effect vector and RNAi knock down vectors with observed value noted with point. Correlation of 0 indicates no shared direction of effects, noted with dashed lines. Wing shape changes plotted for altitudinal effect and selected RNAi effect vectors. For altitudinal effect vector, black represents the low altitude and red the high altitude shape. For RNAi effect vectors, black represents the control and red the RNAi knockdown. Shape change effects have been magnified for visualization purposes: altitudinal effect 20x; *loco* effect: 1.5x, *takl2* effect: 3x, *wge* effect: 3x.

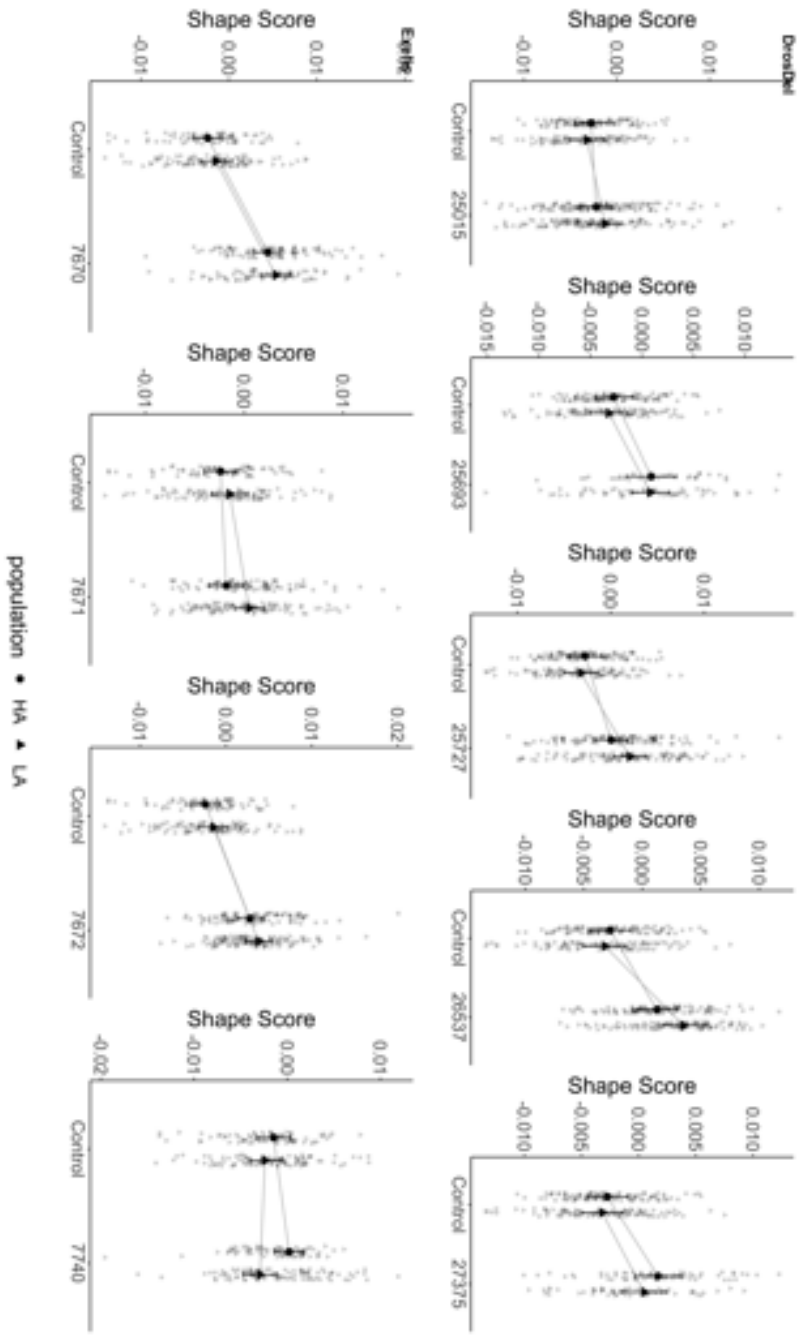

Figure 3.6: Reaction norms for quantitative mapping crosses. Estimated shape scores, calculated from projection onto altitudinal effect vector, between control and deletion cross. 4 high altitude and 4 low altitude lines were used to estimate population means for high altitude (triangles) and low altitude (circles) populations. Raw data for each population is plotted behind (grey). Error bars represent 95% confidence intervals.

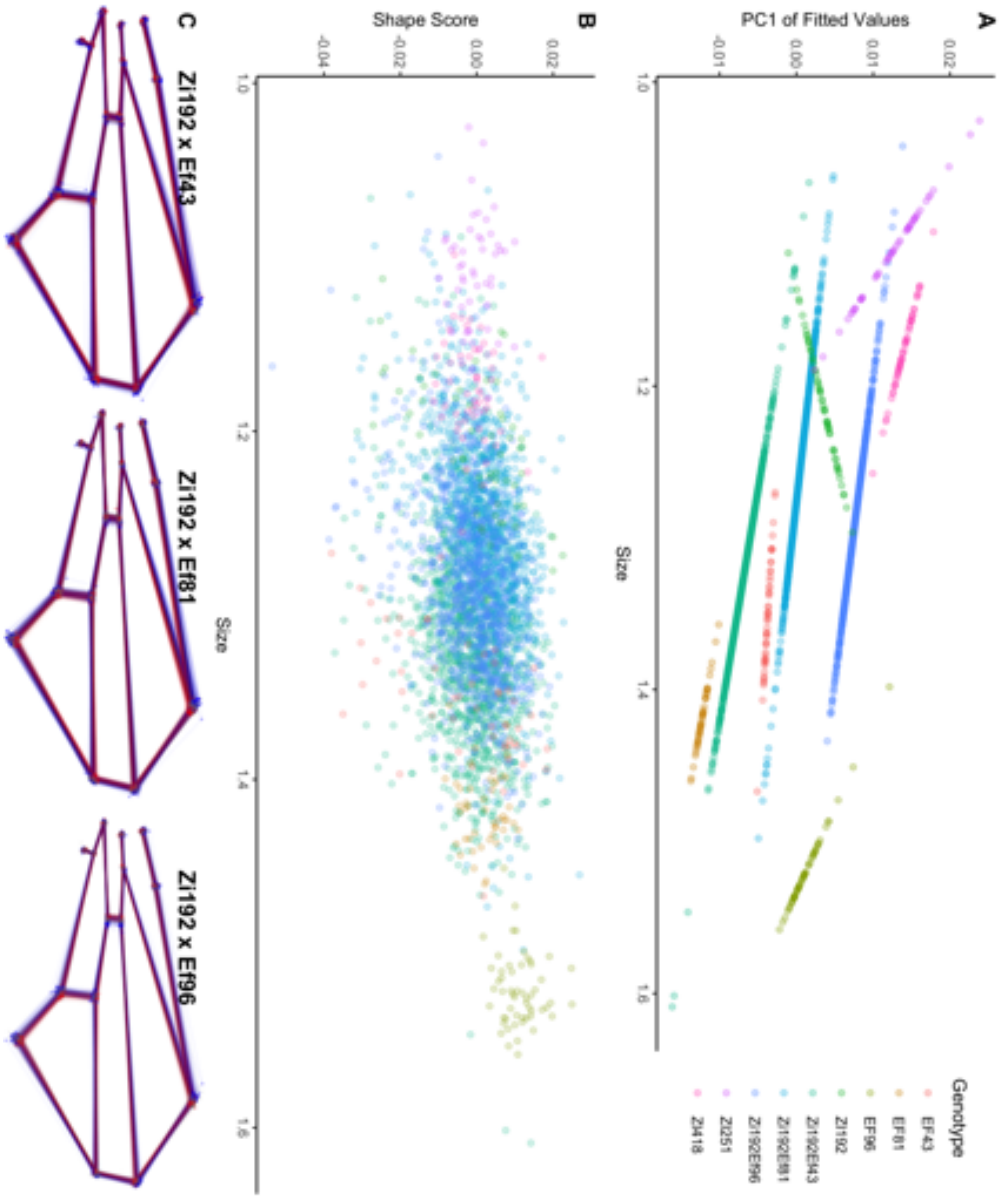

Figure 3.7: Similar allometric component of shape in F20 intercross despite unique relationship in parental lines. (A) Model predicted allometry is represented by slope of lines. PC1 of model fitted shape residuals plotted against wing size. (B) Shape scores of individuals calculated by projection on to the allometric effect vector for each genotype to represent within line variation of allometric relationship. (C) Wire frames demonstrate the shared allometric relationship in F20 crosses. The total diversity of wing shape is plotted in grey with the largest (blue) and smallest (red) wings highlighted.

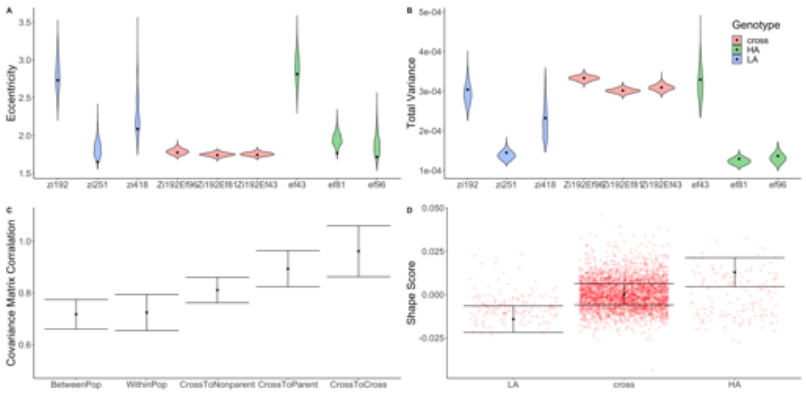

FIGURE 3.8: Shape variation within and between crosses and parental lines. (A) Integration of the VCV matrix for allometry corrected wing shape, measured using the standard deviation of all eigenvalues normalized by the mean eigenvalue. Bootstrapped 95% CI are indicated by violin distribution with the observed value indicated by point. (B) Total variance of VCV matrix, measured by the sum of eigen values. Bootstrapped 95% CI are indicated by distribution with the observed value indicated by point. (C) Estimated covariance matrix correlation with 95% CI between genotypes, given the predicted degree of relatedness in comparison. Matrix correlation was estimated based on the similarity of subspace between two matrices based on principal components, with correlations between PCs weighted by the magnitude of variation in that direction (eigenvalues). These correlations were also corrected for the degree of repeatability of each genotype's VCV matrix based on bootstrapped correlations. BetweenPop comparisons (n = 9) include a comparison of a high altitude line to low altitude, WithinPop comparisons (n = 6) include the comparisons between either high altitude or low altitude lines, CrossToNonparent includes comparisons (n= 12) between F20 crosses and either high or low altitude lines that are not the parents of the F20 cross, CrossToParent includes comparisons (n = 6) between F20 crosses and either high or low altitude lines that are are one of the parents and CrossToCross are comparisons (n = 3) of the crosses to other crosses. (D) Estimated shape score, based on the projection of wing shape onto the altitudinal effect vector. with 95% CI. Red points indicate actual values.

Chapter 4

Quantitative changes in cell size contribute to adaptative divergence of wing shape and size between two populations of *Drosophila melanogaster*

4.1 Abstract

Small, quantitative changes in development lead to morphological variation between populations. Expansion and contraction of signaling domains, cell polarity variation and localized expansions in cell number are just some developmental processes that impact morphology. When the number of alleles contributing to divergence is large, with indifvidually small alleleic effects, changes to developmental systems can be assayed to understand the important mechanisms underlying the morphologic change. *Drosophila* populations living at high altitude have many adaptions, including a larger wings and different wing shape compared to lowland counterparts. Although phenotypic changes have been extensively documented, underlying mechanisms contributing are not known. For both traits, adaption to high altitude has a polygenic architecture. We demonstrate that larger wings in highland populations are explained both by larger cells and more cells in the wing. With two possible 'traits' for selection to act on, this helps to explain the polygenic basis observed in the mapping study. Additionally, we demonstrate that variation in cell size within the wing co-varies with shape, indicating that this is an important mechanism contributing to adaptive shape change. Together, this work

demonstrates the important contribution of wing cell size to high altitude adaptation and hints at a developmental mechanism important for this morphological variation in a case where single loci are uninformative.

4.2 Introduction

Small, quantitative changes in development are common in nature and often have important consequences for adult fitness. For example, beak size variation in Galapagos finches can be explained in part by quantitative changes to the expression domain of *bmp4* in the developing beak, with the size of the *bmp4* expression domain in the developing beak correlated with adult beak size (Abzhanov et al. 2004). This is an example of the relationship between genotype and phenotype being mediated in the developmental space. The developmental space encompasses the creation and realization of developmental signals, encoded in the genome, to create a structure, the phenotype (Orgogozo et al. 2015; Félix and Barkoulas 2015). There is a non-linear relationship between genotype and phenotype, with substantial perturbations needed to result in phenotypic changes (Orgogozo et al. 2015). To this end, many studies map the alleles contributing to phenotypic change and then use forward genetics to understand changes to development underlying phenotypic change.

For many studies mapping the 'alleles of evolution', this approach has been a successful. For example *mc1r* and the regulation of melanin production in mice (Hubbard et al. 2010), *pitx1* as a developmental regulator of pelvic spines development in sticklebacks (Coyle et al. 2007) are two classic examples where alleles contributing to divergance have been mapped. However, these single alleles of large effect explaining the majority of phenotypic difference between populations may represent special cases. Increasingly, the role of polygenic adaptation, many sites throughout the genome with small individual effects contributing to differentiation, has become apparent (Barghi et al. 2020; Höllinger et al. 2019; Pritchard and Di Rienzo 2010). In these cases, identifying particular alleles contributing to phenotypic divergence is nearly impossible without enormous sample sizes (Rockman 2012). Rather than focusing on mapping all the alleles contributing to divergence in these cases, understanding the changes to the developmental program underlying the observed phenotype may help to provide a better understanding of the processes of evolution (Travisano and Shaw 2013).

Developmental systems, or the morphogenic signals used to create adult structures,

can be robust to genetic (mutational) perturbations. Mutations that reduce the expression of *Fgf8* in mouse embryos by over 50% have little effect on the craniofacial morphology of neonates (Green et al. 2017). With this high level of genetic robustness, it may seem surprising that any allelic effect generates enough genetic variation for selection to act upon. In *Drosophila melanogaster*, alleles of moderate effect along a severity spectrum have increased variance both within and between genetic backgrounds (Chandler et al. 2017). However, the alleles with the smallest effect on expression have little effect on phenotype (Chandler et al. 2017). Both these examples use mutations in single focal genes to study robustness in the developmental system; however, adaptation is often polygenic with many alleles of small effect contributing. Genetic variation for complex traits is thought to be concentrated though a small number of 'core' regulatory pathways (Boyle et al. 2017) and in *Drosophila* it has been demonstrated that selection can act on alleles with aligned effects within a developmental pathway (chapter 2). By assaying changes at the developmental level, we may be able to make predictions about important developmental pathways contributing to divergence between populations, even when individual allelic effect sizes are very small.

Shape and size of the *D. melanogaster* wing are widely used for both evolutionary and developmental studies. Not only are the developmental processes underlying these traits well understood, but there is also extensive genetic and environmental variation influencing quantitative morphological variation within and between populations found in nature (Matamoro-Vidal et al. 2015). In some cases this variation is associated with adaptive variation along latitudinal (Land et al. 1999) or altitudinal (Lack et al. 2016b; Pitchers et al. 2013) clines. Populations of *D. melanogaster* in Sub-Saharan Africa have adapted to a high-altitude environment with high altitude flies developing darker pigmentation (Bastide et al. 2014), greater thermal tolerance (Pool et al. 2016), larger body size (Lack et al. 2016b), in addition to larger wings and distinct changes to wing shape (Pitchers et al. 2013; Pesevski and Dworkin 2020) from low altitude ancestral populations. Identifying the genetic basis of wing shape and size adaptation to high altitude has revealed a polygenic, but unique, basis of adaptation for these traits (Sprengelmeyer et al. 2022)(chapter 3). With variants in many genes contributing, it can be hard to identify specific developmental pathways that may be contributing and give context to the identified alleles. Variation in the proteome of developing wing discs is much lower than expected from genetic variation, suggesting that buffering mechanisms exist in the developmental program (Hubbard et al. 2010). The variation that escapes these buffering mechanisms and is expressed in developmental changes may provide clues to specific developmental pathways that are important for adaptation.

Strains derived from high-altitude population have a greater number of wing vein abnormalities, due in large part to increased mutational sensitivity, rather than mutation load (Groth et al. 2018; Lack et al. 2016a; Pesevski and Dworkin 2020). As a loss of robustness in development is hypothesized to be associated with rapid adaptation (Visser et al. 2003), it has been hypothesized that the rapid increase in wing size in high-altitude populations relative to their low-altitude ancestors resulted in a loss of robustness, and can explain the increased number of abnormalities. The large size of high-altitude wings is explained both by the contribution of more cells in the wing and larger cells in the wing. Interestingly the high altitude population has on average much larger cells than are generally observed in other large bodied *D. melanogaster* strains (Lack et al. 2016a; Pesevski and Dworkin 2020). It has been suggested that larger wing cells are contributing to the loss of robustness; however, a simple examination suggested that variation in cell size within the wing does not correlate with increased wing abnormalities (Pesevski and Dworkin 2020), but these studies used inbred strains derived from each population. These analyses were not specifically suited for disentangling genetic sources of variation influencing wing size, shape and the relative contribution of cell size and number on overall wing morphology. Using the advanced intercross created for the previous mapping study (chapter 3), we can specifically ask questions about the relationship between cell size and abnormalities in the wing. If increased abnormalities could be explained by larger cells in highland populations has yet to be tested because previous work used inbred lines where changes in wing size and wing shape are linked. Using an F20 intercross between inbred high and low altitude populations, we can ask if these two processes can be separated, and if so, if large cells are associated with a loss of robustness.

The developing *Drosophila* wing tissue, or wing disc, is composed of a monolayer of columnar cells. By the end of the third larval instar, regions of the wing disc have defined fates, with the nostrum going on to fuse with the body wall, the hinge forming the region where the wing meets the body and the wing pouch fated to become the wing blade (Bryant 1975). By this time in development, much of the pattern of the adult wing has been established. Expression of Wingless and Notch mark the D/V boundary of the wing, the region that will ultimately become the wing margin of the adult structure(Celis and Bray 1997; Micchelli et al. 1997). Egfr, Dpp and Notch signalling is establishes the relative locations of longitudinal veins and intervein regions (reviewed in: (Tripathi and Irvine 2022)). In late third instar, three folds also develop in the epithelium of the wing disc: one between the nostrum and hinge region, one within the hinge region and one between the hinge region and wing pouch. Quantitative changes in wing morphology

in adults can be related to quantitative changes in the developing wing; that is, similar shape changes are seen in both structures (Matamoro-Vidal et al. 2018). This observation allows us to investigate the relationship between quantitative changes in development of the wing, using those changes to understand what genes expression may be altered to create variation in the adult wing.

Over the course of development, cells in the developing wing undergo many rounds of division, growing from about 30 cells in the embryo to 30000 cells (Martín et al. 2009) in the larvae to 50000 cells (Garcia-Bellido and Merriam 1971) in the adult wing. Wing size is tightly regulated in *Drosophila*, with wings typically becoming larger though increased cell number rather than larger cells in laboratory experiments (Bryant and Levinson 1985; Partridge et al. 1999) and along latitudinal clines (Zwaan et al. 2000). This makes the observation that an increase in wing size in high-altitude populations is in part explained by an increase in cell size very interesting. By inhibiting cell division in the disc, the loss of cell number can be compensated with larger cells so that regular wing morphology is not inhibited (Neufeld et al. 1998; Weigmann et al. 1997). However, increased cell size is associated with decreased fitness in artificially selected populations (Trotta et al. 2007). Many of the genes involved in patterning the wing disc, including *wnt*, *dpp* and *vg*, also have a role in regulating wing disc size (reviewed in: (Tripathi and Irvine 2022)). One such example is that of Hippo signaling, a key pathway in regulating the size of the wing (Pan et al. 2018). Polymorphisms in this pathway are also important for wing shape variation in wild populations, independent of regulation of wing size (Pitchers et al. 2019)(chapter 2)

We assayed quantitative differences between strains derived from high- and low-altitude populations as well as an advanced intercross to help understand the relative contributions of cell size and number on wing shape and size variation. With this, we can provide better context to QTL mapping studies and understand what alleles may be most important for the adaptive divergence between populations. Changes in cell size and cell number can be separated though many generations of recombination in the F20 intercross, indicating that there is at least a partially distinct genetic basis for them, and they can independently contribute to overall organ form variation, providing a partial explanation for the polygenicity of wing size divergence observed in mapping studies. Additionally, cell size variation across the wing is associated with shape variation in the adult wing so that localized changes to cell cycle regulation may then represent a candidate mechanism for changes to wing shape between populations. Despite the clear changes in adult tissues, we did not observe the same changes in the larval wing

disc. This may reflect technical limitations of the data collection or could indicate that changes in cell size and number are not determined at the single timepoint assayed and that observations need to me made over developmental time. Together, these results indicate key developmental mechanisms that may be targets of selection and can help to provide context to QTL mapping studies.

4.3 Methods

4.3.1 Generation of Synthetic Outbred Populations

To counter any effects of inbreeding on our traits of interest, two synthetic outbred (SO) populations were created, one from low altitude lines (LA) and one from high altitude lines (HA). HA inbred lines are derived from a population captured in Fiche, Ethiopia (3000m) while LA lines are derived from a population captured in Siavonga, Zambia (500m) (Lack et al. 2016b). Zambian lines used were: Zi445, Zi192, Zi337, Zi331, Zi159, Zi360, Zi357, Zi124. Ethiopian lines used were: Ef117, Ef98, Ef81, Ef112, Ef119, Ef43, Ef134, Ef16. Lines from within each population were crossed together using a pairwise design for the first generation with reciprocal crosses used to ensure that the contribution of X chromosomes was equal for each line. Progeny from these crosses were crossed using a round robin design, again to create equal genetic contributions from each line. In the final two generations of crosses, populations were again crossed together as contributing lines had X chromosomes with mixed ancestry present at this point. All crosses were performed in vials, using high protein food (3L water, 22.4g blackstrap molasses, 22.4g fancy molasses, 142.8g RedStar yeast, 39.2g cornmeal, 15g Carrageenan, 4.9mL Propionic Acid, 10mL 1% tegosept in 95% ethanol). High protein food was chosen as it maximizes body size, and provides a clearer indication of variation between populations. After the F4 generation, when all lines were combined, the SO populations were maintained at low density in 175 ml bottles. To ensure low density, 20 males were crossed with 20 females that were allowed to lay eggs for 24-36 hours and then transferred onto new food for 2-3 passages. Outcrossing populations were maintained for 2 more non-overlapping generations in bottles until the start of the experiment.

To collect both larval discs and adult wings for experiments, adults from the SO populations were allowed to lay eggs on apple juice agar plates seeded with a small amount of yeast paste prepared with orange juice. Eggs were collected into vials of the same high protein food on which crosses were maintained. Egg density was kept low in vials (50 eggs) to limit environmental effects. Vials from the same cage were combined

for analysis with different cages treated as biological replicates. Wing imaginal discs were dissected from late 3rd instar larvae that had been staged based on reaching the wandering stage; when larvae stop feeding and wander up the sides of the vial prior to pupation. For more details on the dissection and fixation of larvae, refer to the immunostaining section below. Adults were collected 24-48 hours after eclosion, to allow for sclerotization of the wings, and stored in 70% ethanol until wings were dissected for imaging using the same methods as described in chapter 3. Only male individuals were used in for both the larval and adult wing analysis to control for sex-specific effects. A total of 28 HA and 28 LA discs were used for analysis and 54 HA and 48 LA adult wings.

4.3.2 Parental and F20 Outcrossed Individuals

All wings from the African inbred lines and F20 outcrossed individuals were collected and imaged as part of a previous study (3, Figure A3.1). Three HA and three LA lines were included in the analysis. HA lines, with sample sizes indicated in brackets, were EF43 (males: 25; females: 27), EF81 (males: 22; females 19), EF96 (males: 18; females: 10). LA lines used were: ZI192 (males: 33; females: 26), ZI251 (males: 28; females: 27), and ZI418 (males: 29; females:27). For the Zi418 x Ef 43 cross, 942 females and 1026 males were included in the analysis and for the Zi192 x Ef96 cross 669 females and 673 males were included in the analysis. For more specific details of the crossing scheme used and husbandry conditions as well as an analysis of the wing shape and size changes between these groups, refer to chapter 3. A single inbred high altitude and single low altitude line were crossed for 20 non overlapping generations to create the F20 populations. All individuals were stored in 70% ethanol until dissected and mounted for imaging, described in chapter 3. Defects were scored in images based on the presence of: extra veins, loss of cross veins or loss of longitudinal veins (Figure A3.2). Wings with vein loss that resulted in landmark loss for shape analysis were dropped from the data set, with a total of 856 female and 912 male wings without abnormalities and 86 female and 114 male wings with abnormalities included in this analysis.

4.3.3 Immunofluorescence

Late third instar larvae were bisected and the anterior component was inverted to expose imaginal tissues to reagents. However, wing discs were not dissected away from other tissues prior to fixation and staining. Only male larvae were dissected to control for sex-specific effects. All staining steps were done on a nutator in "baskets" (created by fastening fine mesh to the top of a screw topped vial with a hole drilled in the cap), apart from the fixation step which was done in a 1.5mL microfuge tube. Inverted larval

"heads" (parts of the larvae containing wing and other imaginal disc tissues) were fixed in 4% paraformaldehyde in phosphate buffered saline (PBS) for 20 minutes at room temperature. Following this, tissues were washed three times with PBT (2% Tween-20 in PBS) for 20 minutes per wash. To reduce non-specific binding of antibodies, tissues were blocked overnight in blocking solution (2900 μL PBT, 60μL Goat Serum, 40μL Bovine Serum Albumin (BSA)) at 4°C. Primary antibodies were used at the following concentrations: α-wingless (Developmental Studies Hybridoma Bank) 1:1000, α-patched (Developmental Studies Hybridoma Bank) 1:50. Tissues were incubated at 4°C with primary antibodies overnight. Tissues were then washed four times for 15 minutes with PBT before a secondary blocking step for 3 hours at room temperature. Tissues were incubated overnight with secondary antibodies. Secondaries were used at the following concentrations: α-mouse (GFP 475 flourofor) 1:2000. Then tissues were washed one time in PBT for 15 minutes then incubated for 1 hour in a 1:5000 DAPI in PBS solution to stain nuclei, followed by two more 15-minute PBT washes before tissues were stored in antifade mounting solution until dissected. Fine dissections and mounting of wing imaginal discs were done in antifade mounting solution. Discs were imaged with an Olympus DP305 camera, mounted on a Olympus BX51 microscope with a 20X objective lens (total 200X magnification) with samples illuminated and examined with appropriate fluorescent filters (DAPI and GFP filters).

4.3.4 Wing shape, size and cell size measurements from adult wings

Collection of wing size and shape from adult wings was previously described in chapter 3. For the inbred Ethiopian and Zambian lines and F20 crosses, the same shape and size data was used for both analysis and was collected with the 48 landmark/semi landmark WINGMACHINE pipeline. The SO data was collected as a part of this study using the 15-landmark method. For each SO replicate, 20 wings per replicate within each population (~60 individuals per population) were measured using the 15 landmark collection method. Cell density in the wing was estimated by counting trichomes on the wing surface of each wing as each trichome originates from a single cell (Dobzhansky 1929; Garcia-Bellido and Merriam 1971). Trichomes were measured in 16 0.0065mm^2 (150x150 px) areas, distributed over the wing (Figure 4.1D) using the FijiWings macro (v2.2) (Dobens and Dobens 2013).

4.3.5 Wing shape, size and cell size measurements from larval wings

All images were converted to 8-bit colour for downstream analysis. To count cell number, the total number of maxima, each representing a single nucleus, were measured in a 16

$0.0065mm^2$ (150x150 px) area of the wing, near the centre of the wing pouch. Three measurements at slightly different locations were taken and averaged to account for some variation in cell density across the disc. Landmarks were chosen for wing discs based on the immunofluorescence staining pattern of Wg and Ptc in the disc as well as the location of the wing pouch-hinge fold (Figure 5A). Landmarking was done using the program TPSdig (v2.3.2).

4.3.6 Association between wing shape and size and cell size in adults

To ensure our results for high and low altitude wing size and cell size matched previous work (Pesevski and Dworkin 2020; Lack et al. 2016b), we estimated wing size and cell density by fitting a linear mixed model with terms for population, sex and their interaction and random slopes for sex across isogenic lines. Estimated marginal means for wing size or cell density, averaged over the entire wing, for each sex within population were estimated using the emmeans package (v 1.7.2). Because cell density can vary over the wing, we also wanted to analyze the variation in density between measured regions. First, the variation structure between groups was explored using a PCA of the trichome counts across 16 wing regions. Variation within regions was estimated using a mixed model with main effects of population, sex and wing region plus a random slope for each line within sex and random intercept for individual wings.

We took advantage of the 3 distinct F20 intercrosses generated as a part of chapter 3 to assay the relationship between wing size, shape and cell size following 20 generations of recombination between the parental strains (each derived from either the Zambian or Ethiopian population). First, to investigate the relationship between wing size and cell density (proxy for cell number) in the wing we fit a linear model with the effects of wing size, sex and the interaction on the average cell density of the wing. Additionally, we fit a mixed model to test how much cell density varies over the wing, with terms for wing size, sex and wing region as well as a random effect for individual wings to account for repeated measures. A PCA was also used to examine the (co)variation of cell densities across the wing and associations with overall wing size variation. The first 4 PCs from this model were then used as predictors in a model, along with sex and the interaction between PCs and sex to test the relationship with wing size. To ask if there is a relationship between cell density and wing shape, we fit a model testing the effects of wing size, sex and cell density averaged over the entire wing on shape using the Geomorph package (v 4.0.7) (Adams and Otárola-Castillo 2013; Collyer and Adams 2018). To assess multivariate covariation between patterns of local variation in cell density with wing shape, a 2-block partial least squares (PLS) analysis was done using the methods

proposed in (Rohlf and Corti 2000) and implemented in geomorph. This method describes the axes of greatest covariation between the data sets then projects data onto these vectors for plotting, with the PLS1 vector in the direction of greatest covariation. Correlation between data projections onto the first vector (greatest covariance) are reported and significance determined by permutation testing, where individuals in one block are randomly shuffled and the PLS-1 correlation calculated for 999 iterations.

4.3.7 Association between cell density and wing abnormalities

We took advantage of the recombined genomes and separation of large cell size and increased cell density in large wings as a test of the hypothesis that larger cells in high altitude populations result in a loss of robustness. The Zi418 x Ef43 cross had an increased incidence of wing abnormalities and was used in this study. Due to loss of landmarks and technical limitations of shape collection, the lines missing cross veins were dropped from this analysis; this does create a limitation of our tests as some of the most extreme wing abnormalities were not included in analysis. To assess the effects of wing size and cell density on abnormalities in the wing, we fit a generalized linear model with a binomial distribution with sex, average cell density and wing size, as well as the interactions between the three as predictors. Because wing size and cell density are on vastly different scales, z-scores for the predictors were calculated prior to model fitting. The slope of the response (increase in probability per standard deviation of predictor) was estimated using emtrends function within the emmeans package (V1.7.2) and plotted. Because the crossveinless wings were both the most extreme wing abnormalities observed and were dropped from the analyses as shape data could not be collected, we wanted to test if including them changed the results of the wing size analysis. For a small subset of Zi418 x Ef43 wings and Zi 251 x Ef 43 wings, we measured wing area using imageJ and repeated the analysis. To ask if there was a shape change associated with having defects in the wing, we fit a model with centroid size, sex and if the wing had an abnormality, as well as all interaction terms using procD.lm in the geomorph package. Cell density was not included in this model as it had a negligible effect on wing shape in the previous analysis.

4.3.8 Changes in wing shape and cell size in developing and adult wings in the SO

To test for differences in size in the SO population wing disc size, a linear mixed model with the effect of wing size with a random effect of replicate collection was fit. Estimated marginal means were estimated from this model. The relationship between cell density

and wing disc size, a linear mixed model with effects for cell density, population and their interaction plus a random effect for replicate collection was fit. The fitted line for each population was estimated. Shape variation effects were estimated using a model fit with procD.lm function in the geomorph package with the effects of cell density, population, their interaction as well as replicate collection. Significance testing in this package uses a residual resampling permutation procedure.

To demonstrate that wing size varied between the adults in the high and low altitude SO populations, a mixed linear model was fit testing the effect of population with a random effect of replicate collection and marginal means estimated. Trends of the relationship between cell density and wing size were tested using a mixed linear model with the effects of cell density, population and their effect plus a random effect of replicate vial.

4.4 Results

4.4.1 Wing Shape and Size Vary With Cell Density in Adult Wings

As seen in previous studies, we observe a lower cell density (χ^2 = 16.9, df = 1, p = 4.0e-05) and larger wing size (χ^2 = 34.7, df = 1, p = 3.8e-09) in high altitude populations when compared to low altitude (Figure 4.1)(Lack et al. 2016b; Pesevski and Dworkin 2020). There is substantial variation between regions within wings, as well as differences between wing regions between sexes and populations (Figure A3.3). Variation in cell density between wing regions is correlated with wing size variation (Figure A3.4). This is seen most clearly with PC1, which explains 49% of total variance for wing cell density and is correlated with wing size (r = 0.70, 95% CI: 0.63 – 0.75).

Using an F20 intercross derived from a cross between a high and low altitude strain, we wanted to ask if the relationship between larger cells and larger wings was genetically separable. Wing size variation is strongly correlated with cell density (Figure 4.2B, Table 4.1). However, the predictors of wing size, sex and their interaction only explain about half of the variability in cell size variability (R^2_{adj} = 0.51). Interestingly, we did not find a significant effect of wing size by sex on cell density in the wing (Table 4.1). In addition, when the distribution of cell densities in the largest and smallest wings and a subset of intermediate wings are plotted, there is a clear bimodal distribution of cell densities in the largest wings (Figure 4.2A). The right side of this distribution largely overlaps with a sample taken from intermediate sized wings. Because higher density indicates more

cells, rather than larger cells, this indicates that a subset of large wings have more cells and a subset of wings have larger cells in the F20 population.

Variation in cell density between wing regions varies within wings regions (Figure 4.3C). Similarly, in the F20 the direction of greatest variation in cell density within the wing (PC1 = 54% of variance) was correlated with wing size variation (r = 0.69, 95% CI: 0.66 – 0.71, Figure 4.2). Using the PCs for cell density variation within the wing, there is a relationship between not only PC1 but also the other PCs (Table 4.2). However, the estimated slope of the relationship between PC2 and PC4 appears to be sex dependent (Figure 4.2D). The first 4 PCs were selected as model predictors as there was no clear separation based on sex after PC4 (Figure A3.5).

As we observed differences in cell density across the wing, we wanted to test if there were changes in wing shape associated with cell density variation. Although there was a significant effect of average cell density over the entire wing on wing shape, the variation accounted for by this relationship was very small ($R^2 = 0.002$) and wing size and sex had a much greater effect on shape (Table 4.3). Despite the lack of substantial relationship between cell density and wing shape, there is substantial shared variation structure between wing shape and variation of cell density across the wing (r = 0.58, p < 0.01, Figure 4.3).

Because shape wing shape and size have at least partially independent genetic architectures (chapter 3), I wanted to replicate the initial findings in a second, genetically distinct intercross. This second cross shares neither the high or low altitude parent with the cross used in the above analysis. As in the first cross, cell density was associated with wing size (F = 450.8, df = 1, p = 2.2e-16) (Figure A3.6) and the direction of greatest variation in cell density was correlated with wing size (r = 0.77, 95% CI: 0.76 – 0.79 , Figure A3.6). When examining cell density in the largest and smallest wings in this cross, we see a different pattern than the first cross. There is no bimodal distribution of the cell densities in the largest wings, with the distribution largely overlapping with a sample of intermediate sized wings as well as a longer left tail (larger cells) in the smallest wings (Figure A3.6A). Variation in cell density between regions is associated with wing size and is sexually dimorphic in this genotype (Table A3.1, Figure A3.6D). Although there is a significant effect of cell density on wing shape, the effect size is very small ($R^2 = 0.002$, Table 4.1). However, there is also significant covariation between cell density variation within the wing and wing shape in this cross (Figure A3.7), even if the effects of average cell density are subtle (Table A3.2). The direction of greatest covariation between wing shape and cell density is largely shared between the two crosses

and demonstrated by a high correlation between PLS-1 vectors calculated in the two cases ($PLS-1_{shape}$ r = 0.94; $PLS-1_{density}$ r = 0.83)

4.4.2 Loss of robustness in HA populations cannot be explained by increased cell size

Because previous work had hypothesized that the loss of robustness could be explained by larger cells in high altitude population (Groth et al. 2018; Pesevski and Dworkin 2020; Lack et al. 2016a), the F20 intercross gave us the unique opportunity to ask the probability of wing abnormalities increases with larger cells. The Zi418 x Ef43 cross showed increased levels of wing abnormalities compared to parental lines, while there were a negligible number of abnormalities observed in the Zi192 x Ef96 cross (Figure A3.2). Neither variation in wing size nor trichome count were particularly associated with increased probability of wing abnormalities (Figure 4.4, Table A3.2). However, there was a large degree of uncertainty in these estimates that may be explained by other factors that we could not account for (Figure 4.4). Additionally, there was a significant but very small shape change associated with the presence of defects in the wing (Table 4.5). However, there is more variance in shapes of wings with defects compared to those without, within sex (difference in disparity = females: 3.93e-5, p = 0.045; males: 4.07e-5, p = 0.022, Table A3.3).

Because wings missing cross veins were dropped from this study as shape data could not be collected from these wings, we are excluding the wings with the most extreme phenotypes in terms of wing abnormalities from the analysis. For a subset of the wings for the Zi418 x Ef43 and Zi251 x Ef43 crosses, we measured wing size directly in all wings. For the Zi251 x Ef43 cross, males were slightly more likely to have wing abnormalities with larger wings, but this result was not seen in the Zi418 x Ef43, which was the genotype used in the previous analysis (Figure A3.8).

4.4.3 No change in size of larval wing discs, despite larger adult wings

We created synthetic outcrossed populations from inbred high and low altitude lines to decrease the effects of inbreeding when comparing high and low altitude populations. After 6 generations of recombination between lines used for this study, the high altitude SO remained substantially larger ($\beta_{altitude}$ = 0.402, 95% CI: 0.34 – 0.48) than the low altitude population (χ^2 = 225.43, df = 1, p < 2.2e-16, Figure 4.5E). As observed for the inbred lines, there was an effect of cell density on wing size, with lower density (larger cells) associated with larger wings (χ^2 = 8.66, df = 1, p = 0.0033, Figure 4.5F). Within

the SO populations, there was no association between average cell density in the wing and shape change (p = 0.85, Table A3.4). However, like in the F20 populations, there was significant co-variation between wing shape and variation in cell density within the wings in the adult SO wings (r = 0.48, p = 0.003, figure A3.9).

In contrast, there was only a modest and non-statistically significant change in wing disc size in the larval tissue, measured by centroid size (estimated diffrence = 25.4 centroids, 95% CI = -59.7 - 111, p = 0.44 Figure 4.5C). For wing discs, we observe the opposite relationship in high altitude populations in the larval wing tissue when compared to adults in the relationship between size and cell density (Figure 4.5D). In this case, larger wing discs had lower cell density or more cells compared to smaller discs but this same relationship was not observed for the low altitude population, which trends in the expected direction. Although the overall relationship between cell density and wing size remains positive ($\beta_{CellDensity}$ = 7.38, 95% CI: 3.49 - 11.3), none of the tested predictors have a substantial effect on in larval wing disc shape (Figure 4.5B, Figure A3.10, Table 4.6)

4.5 Discussion

Divergence of complex traits is often explained by allele frequency shifts at many loci, as is the case for *D.melanogaster* wing shape and size. With many alleles contributing to divergence, it can be hard to identify individual alleles that may be important for phenotypic change. Quantitative genetic models predict that although variation for quantitative traits can be explained by many sites across the genome, particular core pathways will contribute more to the variation than others, usually at the level of gene or protein activity (Boyle et al. 2017). Thus, assaying quantitative changes to developmental processes may help to identify those important core pathways contributing to adaptive divergence. The goal of this work was to assay and describe quantitative changes in wing development between high and low altitude populations of *Drosophila* that have diverged for both wing shape and wing size. We demonstrate that variation in wing size due to cell size and cell number are, at least partially, genetically independent (Figure 4.2, A3.6). Although there are no associations between average cell size (averaged over the whole wing) and wing shape change, variation of cell size within the wing co-varied with wing shape in the intercross (Figure 4.3, A3.7). Additionally, we demonstrate no substantial difference in size or shape in larval wing discs (Figure 4.5) across populations. However, there were some technical limitations of this experiment, and the results should be interpreted with caution.

Despite evidence from artificial selection on increased cell size in the wing showing decreased fitness for populations with larger cell size (Trotta et al. 2007), high altitude populations of *Drosophila* have evolved a larger wing size in part via this mechanism (Lack et al. 2016b; Pesevski and Dworkin 2020). This work demonstrates that the developmental program for cell size and number can be genetically separated, and thus be (partially) independents targets for selection. Increasing the number of developmental programs that can be selected on can facilitate rapid evolution as there becomes more than one set of alleles that can be selected on to achieve the same outcome (Barghi et al. 2019). As high altitude populations diverged from low altitude ancestors only 3000 years ago, phenotypic divergence has been rapid (Sprengelmeyer et al. 2020). It is possible that the increased evolvability as a result of the increased mutational target size may overcome the fitness drawbacks of utilizing larger wing cells to make the wing bigger during the adaptive process. The large mutational target size is also in line with the polygenic basis of adaptation observed for wing size adaptation (Sprengelmeyer et al. 2022)(chapter 3).

Wing shape and cell density within the wing co-vary in adults. To some degree, this finding is unsurprising due to the influence of wing size on both shape and cell size variation. Trait shape and size are linked through size-shape allometry, which describes the non-linear (non-isometric) changes in shape associated with size changes (Klingenberg 2016). Generally, this allometric shape-size variation is the greatest direction of shape variation within a population. Here, we also demonstrated that the direction of greatest variation in cell density across the wing was also correlated with size (Figure 4.2, A3.6). It is not surprising that this direction of variation was shared between populations. However, because co-variation between these two traits extended to other directions of variation as well, this may provide clues to some of the developmental changes creating shape changes in high altitude populations. As growth in a particular region of the developing wing, that is in any intervein regions, can be locally determined, changes to cell proliferation within particular regions may drive shape changes in the adult wing (Resino et al. 2002). Although other morphogenic processes, such as oriented cell divisions are also probably related to shape changes (Baena-López et al. 2005).

Previous work has hypothesized that larger wing cells are the underlying cause of increased wing abnormalities in the high altitude population (Lack et al. 2016a; Pesevski and Dworkin 2020). Although there is a loss of robustness associated with the rapid adaptation to high altitude (Lack et al. 2016a; Groth et al. 2018), it may not be associated with cell size change. In the F20 intercross, both wing size and cell size were

poor predictors of wing abnormalities (Figure 4.4). Additionally, in two F20 intercross lines and the inbred high altitude parental line (EF43), wing abnormality frequency is at about 25% (Figure A3.2), or what would be expected for a segregating Mendelian polymorphism in the population. A seggregating allele in the population can create the observed loss of robustness rather than as a by-product of having larger wings or larger cells alone. Future mapping studies should be done to identify this polymorphism to better understand the loss of robust wing development. It is also possible that there is an effect of wing size and cell size on wing abnormalities but because we dropped the most severe cases of abnormalities (those with vein loss as shape landmarks were no longer present) we created a biased sample and could not detect these effects.

We did not observe any quantitative developmental changes to wing discs between low and high synthetic outbred populations despite clear differences in adult wings (Figure 4.5). One difference we did observe was that in the high-altitude population, larger wing discs appeared to have smaller cells, while this relationship was not seen in the low altitude population. If we assume that the largest wing discs come the largest wings, this finding may suggest that morphogenic changes later in development, specifically during pupal development, are required to create larger cells in the larger wings. As an important step in pupal development is the "flattening" of previously columnar cells by morphogenic forces (Diaz de la Loza and Thompson 2017; Tripathi and Irvine 2022), this is a plausible explanation. However, this is a strong assumption. Additionally, the way that density was measured in the wing discs could not account for variation across the disc, which this work has demonstrated is important in the adult wing. Because we collected discs after the creation of morphogenic folds, it is impossible to count all the cells in the disc using our methods as there is 3D structure. Counting cells earlier in development across the whole disc or using a method that can capture the 3D structure, such as confocal microscopy, to get a better picture of the total number of cells in the wing disc may produce better estimates. The lack of shape change between samples was not particularly surprising as the markers used in this study were important for the formation of critical morphological structures such as the wing margin and wing hinge. Rather, comparing the morphology of protoveins in the wing disc may be a better test for shape changes in the adult wing. Because of these caveats, the lack of changes in the larval discs should be interpreted with caution.

Although we did not observe the expected changes in wing discs, further work is needed to test some of the technical shortcomings that could explain these results. The changes observed in adult wings suggest variable developmental processes underlying

the morphologic changes seen between populations. Understanding how changes to cell density within the developing disc can be translated into differences in adult wings can help to understand the developmental underpinnings of adaptive divergence between high and low altitude populations. Additionally, the separation of cell size and cell number to large wings in intercrosses is interesting and helps to explain the polygenicity of wing size adaptation previously observed. However, an outstanding question is if there is a fitness disadvantage of these larger cells in high altitude populations as has been observed in other systems. Together, this work suggests that changes to cell size between high and low altitude populations helps to explain the polygenicity of wing size adaptation and regional variation in cell size within the wings may help to explain wing shape divergence.

4.6 Figures and Tables

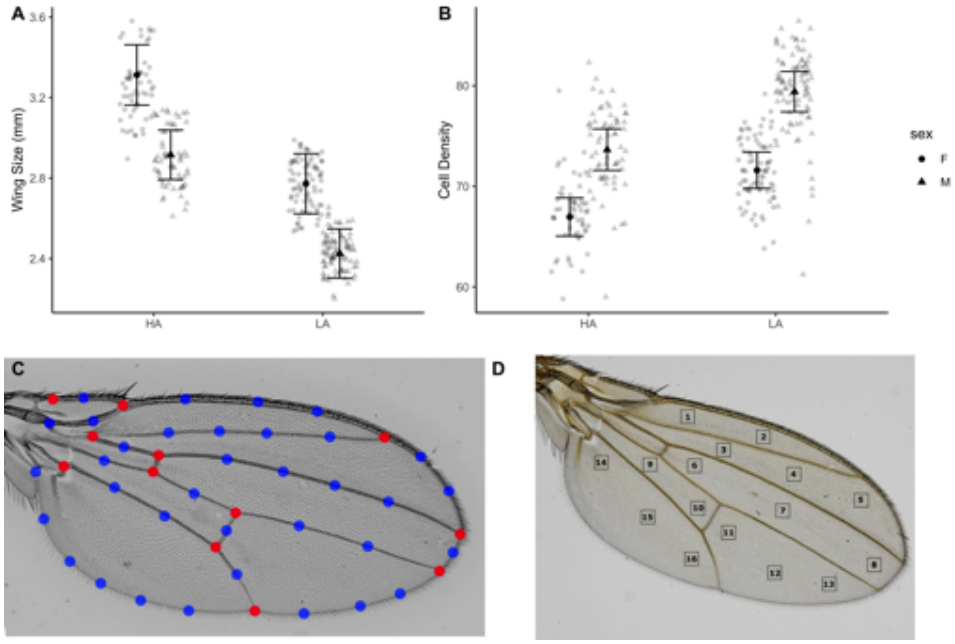

FIGURE 4.1: Wing size and cell Density varies between high and low altitude populations. (A) Estimated mean wing size in mm, estimated based on data from 3 high altitude (HA) and 3 low altitude (LA) inbred lines. Error bars indicate 95% confidence intervals. (B) Estimated mean cell density, averaged over the entire wing. Estimates are based on 3 HA and 3 LA wings. Error bars indicate 95% confidence intervals. (C) Landmark (red) and semi-landmark (blue) location for shape data collection. (D) Location of 16 $0.0065mm^2$ (150 x 150 px) regions used to measure cell density across the wing.

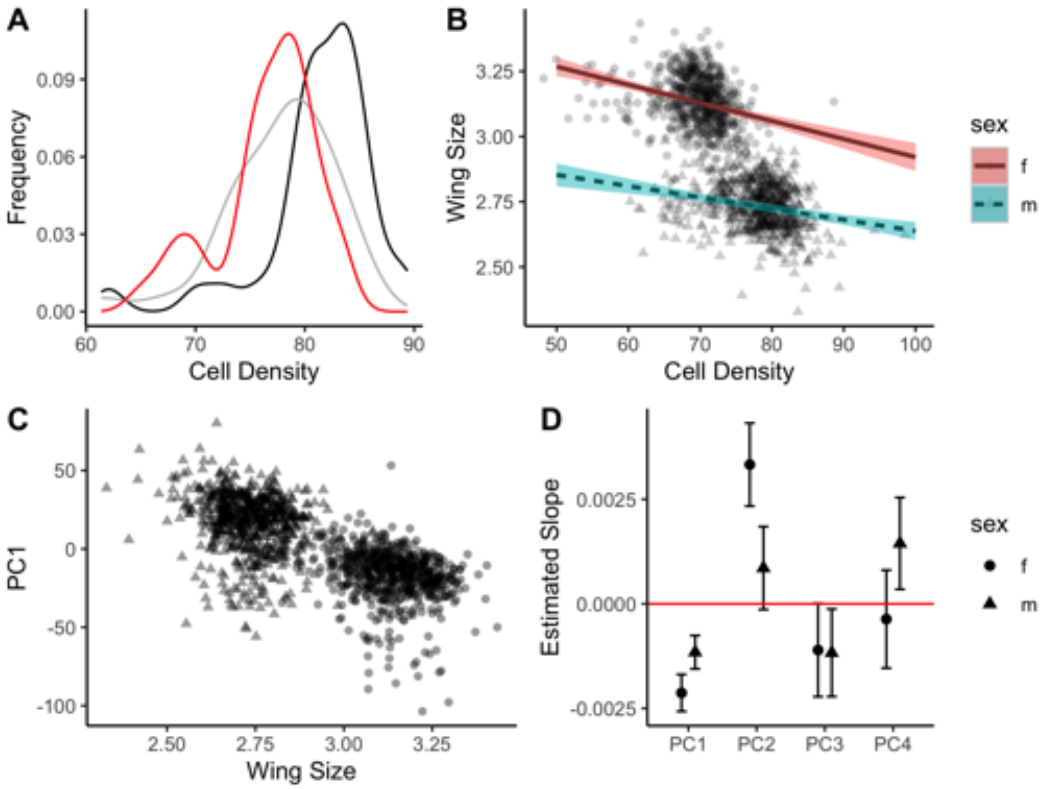

Figure 4.2: Relationship between wing size and cell density in Zi192 x Ef96 F20 intercross. (A) Density plot of cell density in the largest (red), smallest (black) and equal sized sample from the intermediate sized wings (grey) in F20 intercross. Lower density is related to a larger cell size. (B) effect of cell density on wing size, within sex. Estimates of the regression are indicated by lines, with shaded 95% CI. (C) PC1 of variation in cell density between wing regions is correlated with wing size. (D) Estimated slope of regression of PCs from cell density onto wing size. Error bars indicate 95% CI. Red line indicates a slope of 0, or no relationship.

Table 4.1: ANOVA for effect of wing size on cell density in ZI192 x EF96 F20 cross.

	Sum Sq	DF	F-value	Pr(>F)
Wing Size	1588.2	1	85.0	2.2e-16
Sex	1118.3	1	59.9	2.01e-14
Wing Size:Sex	0.9	1	0.046	0.83
Residuals	25023.5	1339		

Table 4.2: ANOVA for the effect of cell density variation between wing regions on wing size in ZI192 x EF96 F20 cross.

	Chisq	Df	Pr(>Chisq)
Sex	1802.6	1	2.2e-16
PC1	111.7	1	2.2e-16
PC2	34.2	1	5.03e-09
PC3	8.58	1	3.4e-3
PC4	2.15	1	0.14
PC1:Sex	10.3	1	1.34e-3
PC2:Sex	12.0	1	5.44e-4
PC3:Sex	0.0070	1	0.93
PC4:Sex	4.89	1	2.71e-2

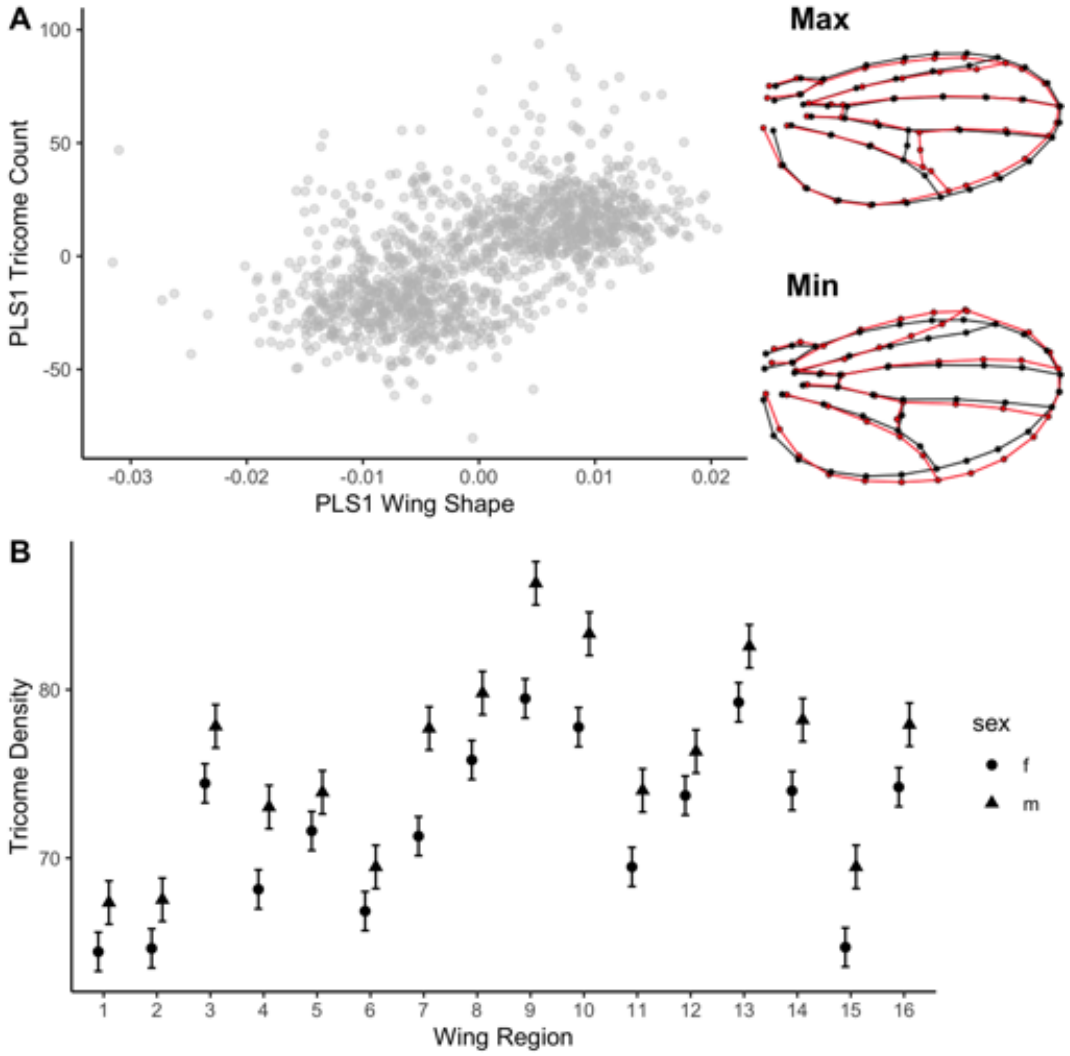

Figure 4.3: Substantial co-variation between wing shape and wing cell size in the Zi192 x Ef96 F20 intercross. (A) 2 block partial least squares correlation between the first dimension of variation for wing shape and cell density variation within the wing, indicated similar covariation structure. Wire frames on the left demonstrate the shape change (red) from mean shape (black) at the maximum and minimum wing shape PLS-1 values (B) Cell density varies between wing regions.

Table 4.3: ANOVA for the effect of size, cell density and sex on wing shape in ZI192 x EF96 F20 cross. Model fit using residual resampling permutation test using RRPP/Geomorph.

	Df	SS	MS	R^2	F	Z	P(>F)
WingSize	1	0.069	0.069	0.13	198.34	12.11	0.001
Sex	1	0.010	0.010	0.018	28.70	7.58	0.001
CellDensity	1	0.0013	0.0013	0.002	3.76	3.60	0.001
WingSize:Sex	1	4.9e-4	4.9e-4	7.1e-4	1.41	1.10	0.013
WingSize:CellDensity	1	7.1e-4	7.1e-4	0.0014	2.05	1.91	0.028
Sex:CellDensity	1	5.1e-4	5.1e-4	9.5e-4	1.48	1.13	0.13
WingSize:Sex:CellDensity	1	7.7e-4	7.7e-4	0.001	2.23	2.14	0.014
Residuals	1314	0.46	3.4e-4	0.85			
Total	1321	0.54					

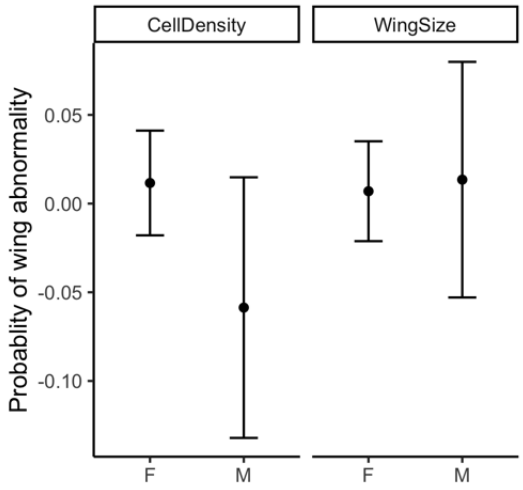

Figure 4.4: Unclear relationship between increase in wing abnormalities and cell density or wing size. Probability of increased wing abnormalities with standard deviation increase in trait values (larger wings, increased cell density), by sex. Z-scores are used for both wing size and cell density. Error bars represent 95% confidence intervals.

Table 4.4: ANOVA of wing size and cell size effects on presence of wing abnormalities in Zi418 x Ef43 F20 intercross

	Chisq	Df	Pr(>Chisq)
WingSize	0.36	1	0.55
CellDensity	3.51	1	0.061
Sex	5.29	1	0.021
WingSize:CellDensity	3.26	1	0.071
WingSize:Sex	0.044	1	0.83
CellDensity:Sex	5.17	1	0.023
WingSize:CellDensity:Sex	0.26	1	0.61

Table 4.5: ANOVA for the effect of size, wing abnormalities and sex on wing shape in ZI418 x EF48 F20 cross. Model fit using residual resampling permutation test using RRPP/Geomorph.

	Df	SS	MS	R^2	F	Z	P(>F)
WingSize	1	0.15	0.15	0.22	564.68	9.32	0.001
Sex	1	8.9e-3	8.9e-3	0.013	34.03	9.01	0.001
WingAbnormality	1	4.1e-3	6.0e-3	0.002	15.66	6.21	0.001
WingSize:Sex	1	1.6e-3	1.6e-3	2.3e-3	6.10	4.20	0.001
WingSize:WingAbnormality	1	4.2e-4	4.2e-4	6.2 e-4	1.59	1.32	0.103
Sex:WingAbnormality	1	2.6e-4	2.6e-4	3.8e-4	0.99	0.21	0.417
WingSize:Sex:WingAbnormality	1	4.5e-4	4.5e-4	6.6e-4	1.71	1.50	0.066
Residuals	1960	0.52	2.6e-4	0.76			
Total	1967	0.68					

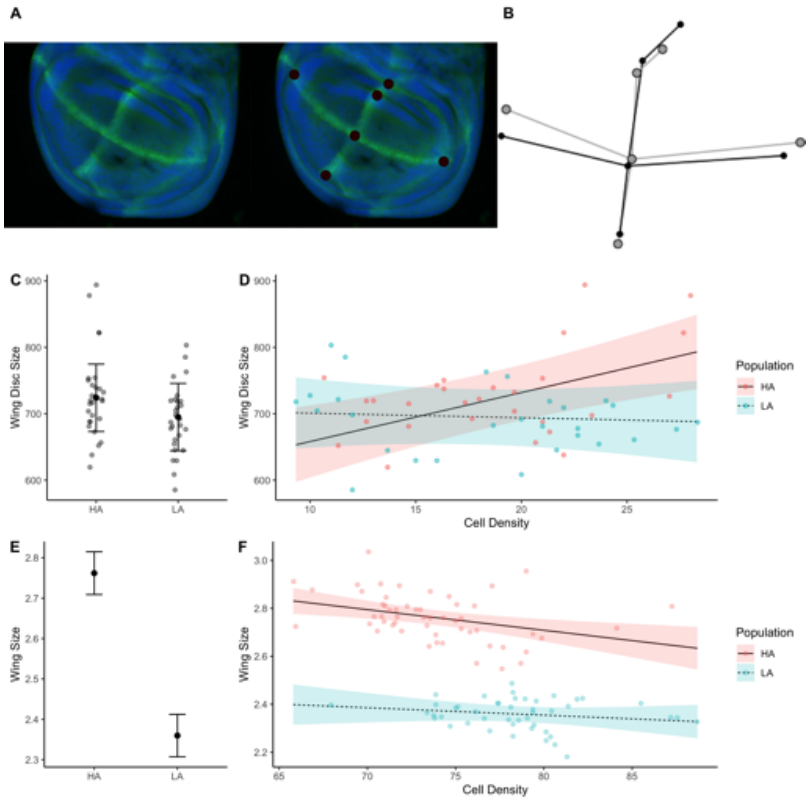

Figure 4.5: Wing size and cell size in larval and adult wings in synthetic outbred populations. (A) Larval wing disc with DAPI (blue) and patched/wingless (green) staining indicated. Landmark locations are indicated on the right. (B) Mean shape change for larval discs for low altitude (red) and high altitude (black) discs. Effects magnified 5x. (C) Estimated wing disc size, based on centroid size of wing data for high altitude (HA) and low altitude (LA) populations indicated by black point, with error bars representing 95% confidence intervals. Observed data is plotted in grey. (D) Relationship between cell density and wing disc size (centroid size) in larval discs. Fitted line with 95% confidence bands for each population with observed data points plotted behind. (E) Estimated wing size (centroid size) of low and high altitude SO population adult wings, error bars representing 95% confidence intervals. (F) Relationship between cell density and wing size for adult SO population wings. Fitted line with 95% confidence bands for each population with observed data points plotted behind. All analyses for SO population included only males.

Table 4.6: ANOVA for the effect of centroid size of disc, population and on wing disc shape of larval wing discs in synthetic outbred populations. Model fit using residual resampling permutation test using RRPP/Geomorph and type II sum of squares.

	Df	SS	MS	R^2	F	Z	P(>F)
Population	1	0.017	0.017	0.025	1.43	0.80	0.23
Size	1	0.010	0.010	0.014	0.83	0.015	0.49
Replicate	4	0.055	0.014	0.080	0.82	-0.54	0.71
Population:Size	1	0.0074	0.0074	0.011	0.44	-0.68	0.75
Residuals	49	0.58	0.012	0.84			
Total	56	0.69					

Chapter 5

Conclusions

Drosophila melanogaster wing shape and size are two particularly well studied traits, with some of the earliest mapped mutants in this species affecting the wing and making *Drosophila* wing shape and size excellent models for understanding the genetic architecture of complex traits. In this work, I used wild *Drosophila* populations to map alleles contributing to phenotypic variation both within (chapter 2) and between populations (chapter 3). I also used comparative developmental biology to investigate quantitative changes between populations that may help to explain the alleles contributing to divergence (chapter 4). Together this work has contributed to our understanding of the genetic architecture of adaptation for complex traits.

From artificial selection experiments based on *ds* shape change in chapter 2, I demonstrate that there is an alignment of genotypic effects within a developmental signaling pathway and that selection can act on many loci simultaneously. However, the same genetic effects could not be replicated in wild populations, despite a strong alignment of phenotypic variation and *ds* shape change. These results demonstrate not only the complexity of understanding genetic architecture of traits in wild populations due to low allele frequencies and environmental factors but when alleles are segregating at a high enough frequency on which selection can act, selection can simultaneously act on many alleles with aligned effects. This results is further demonstrated with the experiment based on *emc* shape change, where we observe a response at hippo (the developmental pathway to which *ds* belongs) signaling loci but only a modest response at *emc*, likely explained by the available genetic diversity within the starting population. Together, these experiments demonstrated important factors influencing what alleles can be 'used' by selection.

Using altitudinally divergent populations, I mapped QTL contributing to divergence for wing shape and size. This mapping study revealed a polygenic basis of adaptation,

with evidence for many alleles of small effect contributing. In this study, I used two unique lowland and three unique highland lines as parents for the advanced intercross. For both size and shape, no QTL were shared between all three crosses, suggesting that the adaptive alleles are not fixed in the high-altitude population. This work adds to the growing evidence that rapid evolutionary divergence can be explained by small shifts in the allele frequency at many sites, rather than requiring subsequent fixations of adaptive alleles though selective sweeps (Barghi et al. 2020).

My final chapter examines the quantitative developmental changes between high and low altitude populations, specifically focusing on changes to cell size and cell number in the wing. As seen in previous work (Pesevski and Dworkin 2020; Lack et al. 2016b), both cell size and cell number contribute to the larger wings in high-altitude populations. Using F20 intercrosses, I demonstrated that these two programs can be separated though recombination, and suggest that an increased mutational target can contribute to the rapid phenotypic change observed between high and low altitude populations. I did not observe this same change in developing wing tissue, but it is not clear if this is due to technical limitations or reflective of the biology of the system. Further work should focus on quantifying developmental changes between high and low altitude populations as this may provide clues to the pathways contributing to adaptive divergence in this system.

Although many studies have successfully identified 'alleles of evolution' contributing to adaptive divergence between populations, these large effect alleles explaining the majority of variance may represent special cases and are not fully representative of the genetic architecture of adaptation. As generation of genomic data has become cheaper and easier, increasing our power to detect variants of smaller effect size and map variants in more populations, it has become apparent that adaptive divergence of complex traits often has a polygenic basis (Dittmar et al. 2016; Barghi et al. 2020). As more alleles contribute to phenotypic variance, individual effects of alleles are expected to become very small (Fisher 1930) and with models predicting that every site in the genome can contribute to phenotypic variance (Boyle et al. 2017), individual allelic effects may be very small. Because of this, mapping the individual alleles contributing to divergence in many cases will not be informative as each allele contributes so little to overall variation (Rockman 2012). Rather, focusing on mechanistic differences between populations and patterns within alleles that do contribute to divergence may provide more fruitful insights into the targets of selection between populations (Bomblies and Peichel 2022; Travisano and Shaw 2013). These ideas are demonstrated in this thesis, as our mapping study (chapter 3) revealed a polygenic basis of adaptive divergence for both wing size and

wing shape. Using comparative developmental biology, I demonstrate the important role of cell size variation to shape and size divergence (chapter 4). Additionally, using artificial selection, we demonstrated the alignment and correlated selection of variants within a single signaling pathway (chapter 3). By using these 'inverted' approaches, artificial selection based on an important genetic effect and comparative developmental biology, we were able to gain more insight into mechanisms of selection that can lead to developmental divergence than if we used mapping alone to identify the alleles of adaptation.

Appendix A

Chapter 2 Supplement

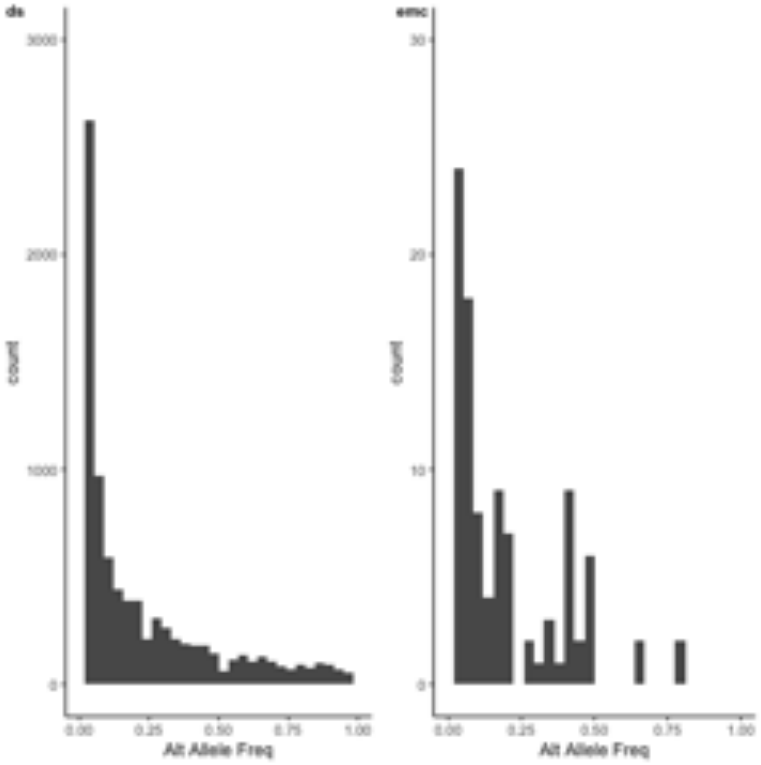

FIGURE A1.1: Allele Frequency spectra demonstrate more variation at *ds* compared with *emc* in the synthetic outbred population used for artificial selection. Figures show estimated alternate allele frequencies at *ds* and *emc*. Alternate allele frequencies are estimated using parental strain genotype data and assuming an equal contribution from each parent to the founding population. Note the different y axis scale between *ds* and *emc*.

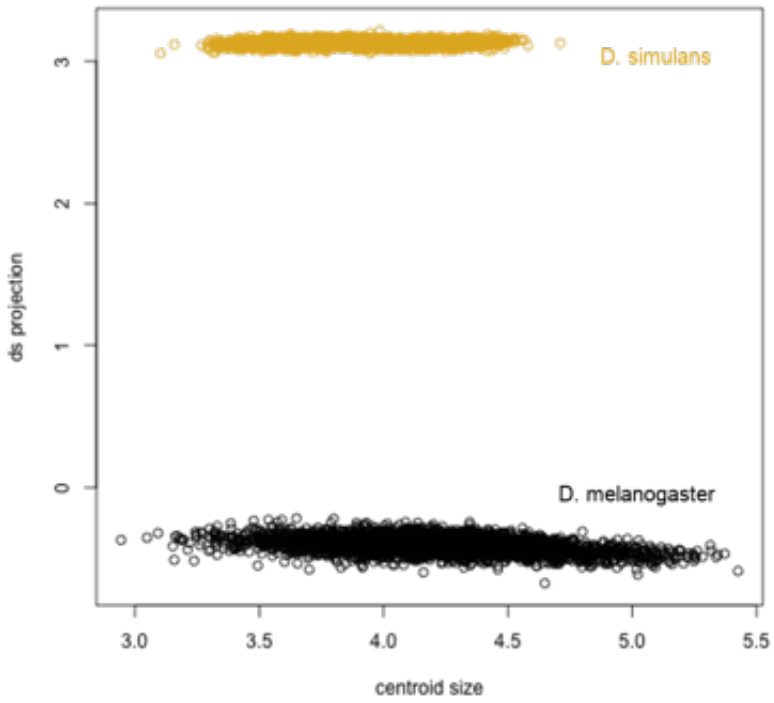

Figure A1.2: Projection of FVW14 wings onto *ds* shape change vector shows clear distinction between *D. melanogaster* and *D. simulans*. Clear separation between the FVW14 samples (black) and *D. simulans* data (gold) indicates that *D. melanogaster* females were accurately identified.

Table A1.1: Number of individuals used for BSA from each wild-caught cohort

Collection	Females Phenotyped	Males Phenotyped	Females – "up" pool	Females – "down" pool	Males – "up" pool	Males – "down" pool
FVW13	0	2184	0	0	75	75
FVW14	403	797	59	0	16	75
PHO	0	1232	0	0	75	75
CMO	0	1001	0	0	75	75

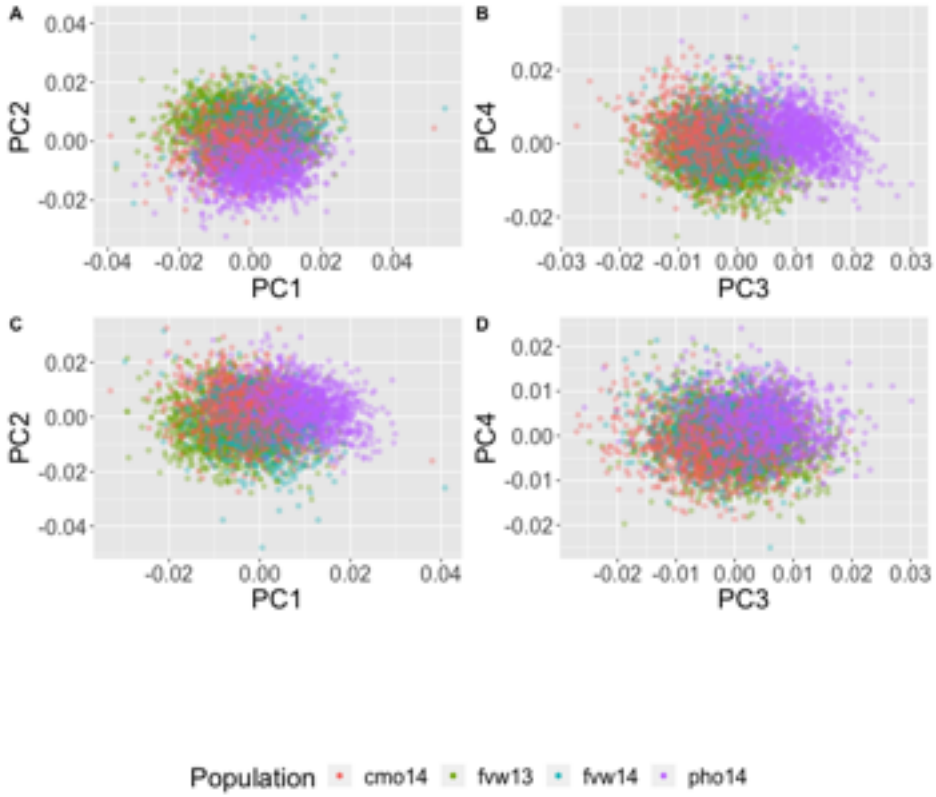

Figure A1.3: Principal component analysis of shape variation within and among populations for wild collected *Drosophila*. First four axes from the PCA for shape variation are shown. (A) and (B) PCA includes all shape variation. (C) and (D) use the 'allometry corrected' landmarks, (residuals from a model regressing landmarks onto centroid size of wings).

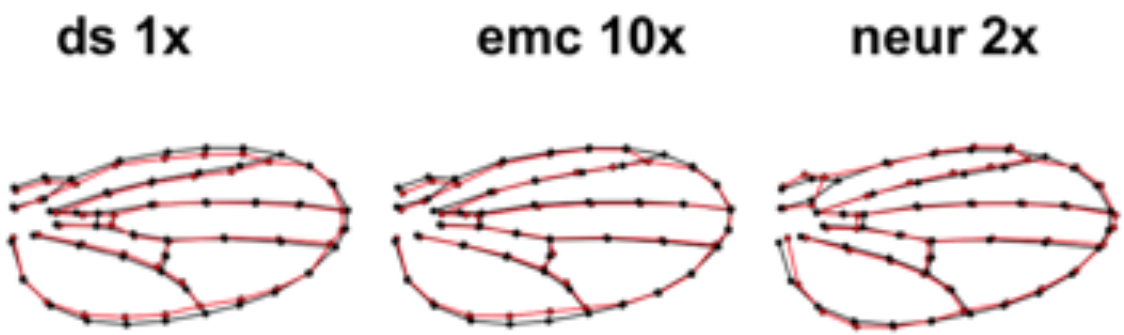

FIGURE A1.4: Shape change effects due to RNAi knockdown of *ds*, *emc* and *neur*. Scaling of effects provided to aid in visualization of shape changes. Different magnifications are provided to account for the disparate magnitudes for estimated shape change vectors: $ds = 5.5$, $emc = 0.44$, $neur = 2.8$. The vectors from these analyses were used for projections in this study.

TABLE A1.2: Directions of major axes of variation differ somewhat between the among line (DGRP) covariance matrix and the wild caught cohorts, likely due to a combination of differences in allele frequencies and the major contribution of environmental variation (and potentially GxE) in the wild caught individuals. Correlations for the first three eigenvectors computed from among the DGRP, wild-cohorts (all populations) and CMO shape variation. |Estimates| $< 10^{-}15$ are treated as 0.

.	dgrp.PC1	dgrp.PC2	dgrp.PC3	wild.PC1	wild.PC2	wild.PC3	cmo.PC1	cmo.PC2	cmo.PC3
dgrp.PC1 0.066	1	0	0		-0.17	-0.46	0.26	-0.35	-0.54
dgrp.PC2		1	0	-0.18	-0.21	0.61	-0.10	-0.60	-0.27
dgrp.PC3			1	0.56	-0.12	0.40	-0.32	0.27	-0.71
wild.PC1				1	0	0	-0.39	0.68	-0.29
wild.PC2					1	0	0.90	0.31	-0.061
wild.PC3						1	0.056	-0.55	-0.74
cmo.PC1							1	0	0
cmo.PC2								1	0
cmo.PC3									1

TABLE A1.3: Top 50 enriched GO terms of linked differentiated sites following artificial selection based on *ds* shape change

See GitHub Data Repo

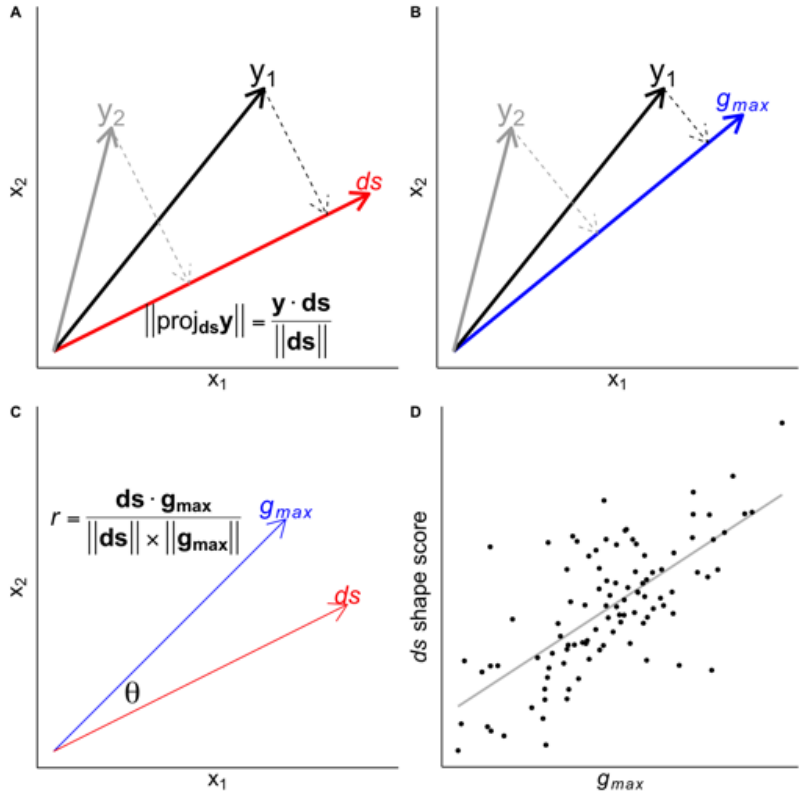

FIGURE A1.5: Illustration of projections onto shape vectors to generate shape scores used in this study. The *ds* shape change vector is used for demonstration. (A) Calculating shape score using projection. y1 and y2 represent vectors of landmarks for two representative individuals. Dotted arrows represent projection of y1 and y2 onto the shape change vector defined by *ds* RNAi to generate the *ds* shape score. (B) Similarly, y1 and y2 are projected onto the g_{max}(PC1) vector, representing the direction of maximum genetic variation in the genetic variance-covariance matrix, **G**. (C) Comparing $g_{max}$and shape change vectors, using the correlation (r) of vectors directly, or via the angle q, between vectors. (D) Hypothetical relationship between *ds* shape scores and g_{max}, indicating a relationship between directions of *ds* induced shape change and the direction of genetic variation in shape variation.

TABLE A1.4: Top 50 enriched GO terms of linked differentiated sites following artificial selection based on *emc* shape change

See GitHub Data Repo

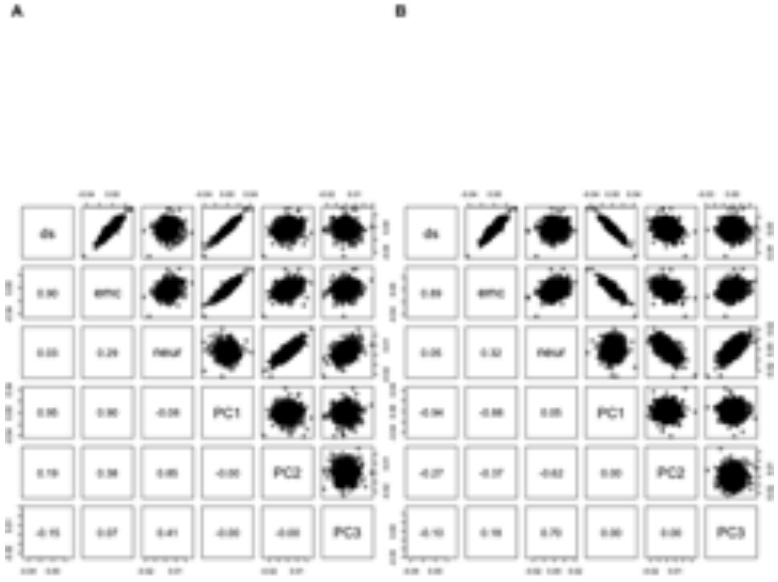

Figure A1.6: Including wild-caught females in the analyses does not change interpretation for FVW14 data. Correlation between projection of shape data from FVW14 population onto ds, emc and neur shape change vectors and the first three PCs are calculated from shape data from all wings in the FVW14 population. (A) male only data, (B) females and male data. Inclusion of female data does not change the conclusions drawn from the relationships between directions shape change vectors and PCs. Note that the "flipped" directions of the PCs between (A) and (B) represents the arbitrary sign of the set of eigenvectors for the PCA (i.e. the set of eigenvectors can equivalently be multiplied by -1).

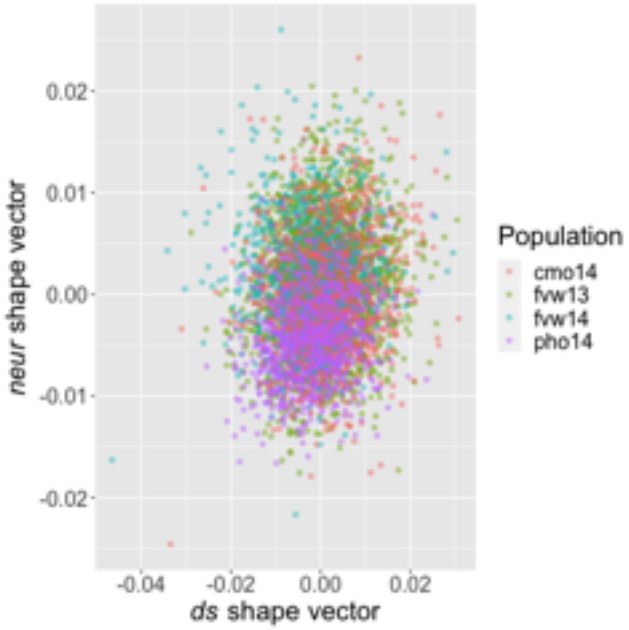

Figure A1.7: Shape variation in field collected samples by projecting individual shape data onto *ds* and *neur* shape change vectors. Projections were performed used size "adjusted" landmark data onto *ds* and *neur* shape change vectors. The correlation between the *ds* and *neur* shape scores is r = 0.12. In linear models with shape scores (*ds* and *neur* respectively) regressed onto population and wing size, the partial R2 for population effects is 0.040 (*ds*) and 0.18 (*neur*).

Table A1.5: Pairwise Procrustes (Euclidian approximation) distances between mean shapes across wild cohorts. Pairwise comparisons between population means estimated from a model with fixed effects for centroid size and population. Z-score and p-value are calculated using permutation of residuals as implemented in the RRPP package using a null model with only the effect of centroid size. Comparisons to the PHO samples, which show the largest pairwise differences are in bold.

Population Comparison	Distance	95% permutation threshold	Z-score	p
CMO-FVW13	0.0070	0.0011	9.70	0.001
CMO-FVW14	0.0084	0.0014	11.0	0.001
CMO-PHO	**0.021**	**0.0013**	**15.2**	**0.001**
FVW13-FVW14	0.0065	0.0012	7.25	0.001
FVW13-PHO	**0.022**	**0.0012**	**13.0**	**0.001**
FVW14-PHO	**0.022**	**0.0014**	**13.5**	**0.001**

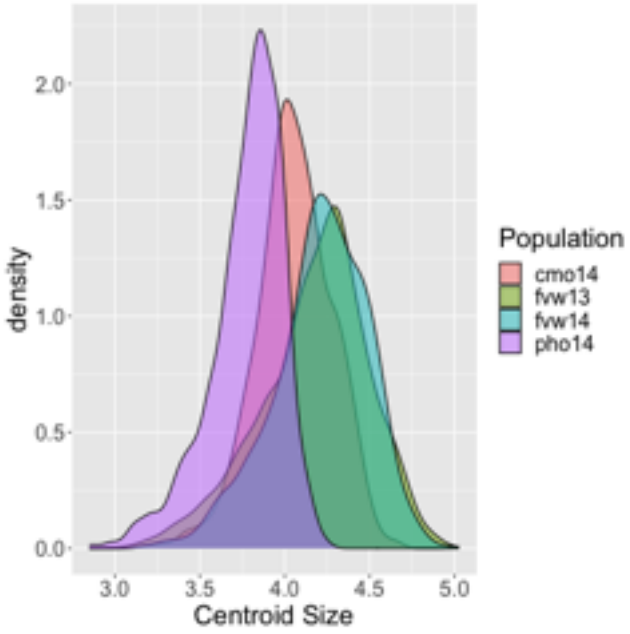

Figure A1.8: Distribution of wing sizes (males only) in wild caught cohorts. When size is linearly regressed onto population, model $R^2 = 0.27$.

Table A1.6: Significantly differentiated sites when PHO population is left out of CMH test.

See GitHub Data Repo

Table A1.7: GO analysis of significantly differentiated sites found in CMH test when PHO population is left out of analysis

See GitHub Data Repo

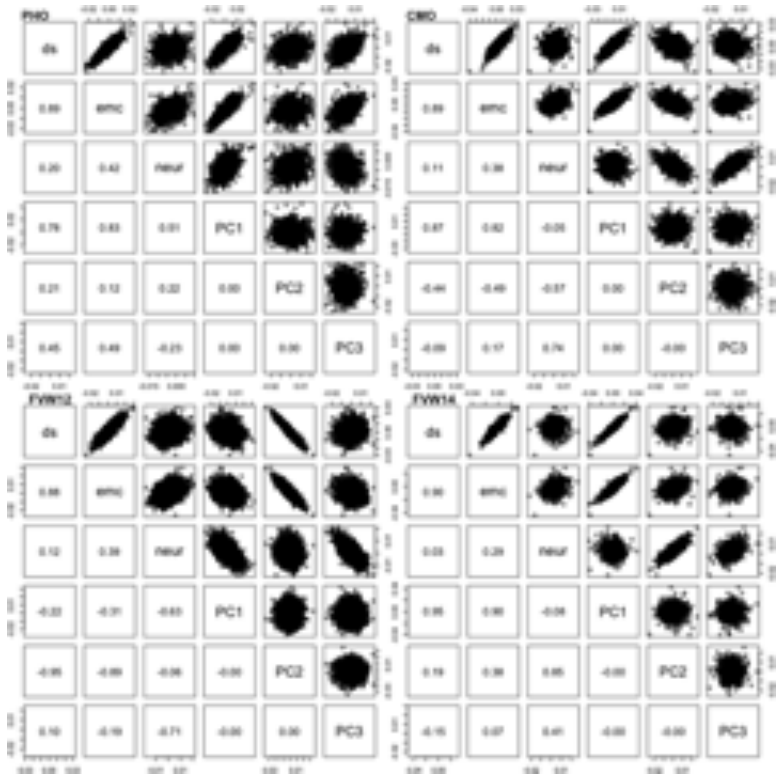

Figure A1.9: Projections of data onto RNAi shape change vectors are correlated with major axes of shape variation in wild-caught *Drosophila* from each population. Correlation between projection of shape data from wild cohorts onto *ds*, *emc* and *neur* shape change vectors and the first three PCs are calculated from shape data from all wings in each cohort independently. Note that the "flipped" directions of the PCs for FVW12 represents the arbitrary sign of the set of eigenvectors for the PCA (i.e. the set of eigenvectors can equivalently be multiplied by -1). Note that the eigenvectors representing PC1 and PC2 in FVW12 have "swapped" because of similarities in variance accounted for.

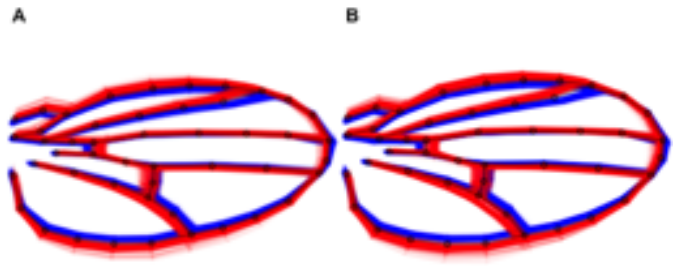

Figure A1.10: Variation in wing shape among individuals from artificial selection along the *ds* shape change vector. All wings from generation 7 of up (red) and down (blue) selection lineages plotted, with females in (A) and males in (B). Black wireframe is mean shape from the experiment.

Table A1.8: Significantly differentiated variants for *ds* shape change from the wild-caught cohorts (BSA).

Location	CMH p-value (FDR corrected)	Gene	FlyBase ID	Distance from ORF (bp)
X:14833408	5.42 x 10^{-5}	CG14411	FBgn0030582	0
X:14833412	3.29 x 10^{-5}	CG14411	FBgn0030582	0
X:15381676	7.54 x 10^{-5}	CG9164	FBgn0030634	0
X:16037404	2.21 x 10^{-4}	*Muc14A*	FBgn0052580	0
X:22956575	4.58 x 10^{-2}	*lncRNA:CR45502*	FBgn0267058	1501
X:4118816	9.49 x 10^{-3}	*tyf*	FBgn0026083	0
X:4130993	9.84 x 10^{-3}	*GlcAT-I*	FBgn0066114	218
2L:14793860	1.15 x 10^{-2}	CG18420	FBgn0028866	656
2L:1480390	3.03 x 10^{-2}	CG31928	FBgn0051928	11905
2L:20626829	7.29 x 10^{-4}	*lncRNA:CR44909*	FBgn0266214	623
2L:4481772	1.54 x 10^{-2}	*dpy*	FBgn0053196	0
2L:4481788	3.70 x 10^{-2}	*dpy*	FBgn0053196	0
2L:4843588	4.62 x 10^{-2}	*mxt*	FBgn0031637	0
2R:11876761	2.73 x 10^{-2}	CG13185	FBgn0033661	0
2R:16405045	3.70 x 10^{-6}	*Sema2b*	FBgn0264273	0
2R:9943212	5.15 x 10^{-3}	*Mef2*	FBgn0011656	0
3L:19082031	4.49 x 10^{-3}	*Mkp3*	FBgn0036844	0
3L:19082032	2.73 x 10^{-3}	*Mkp3*	FBgn0036844	0
3L:23237904	3.05 x 10^{-2}	*nAChRalpha4*	FBgn0266347	0

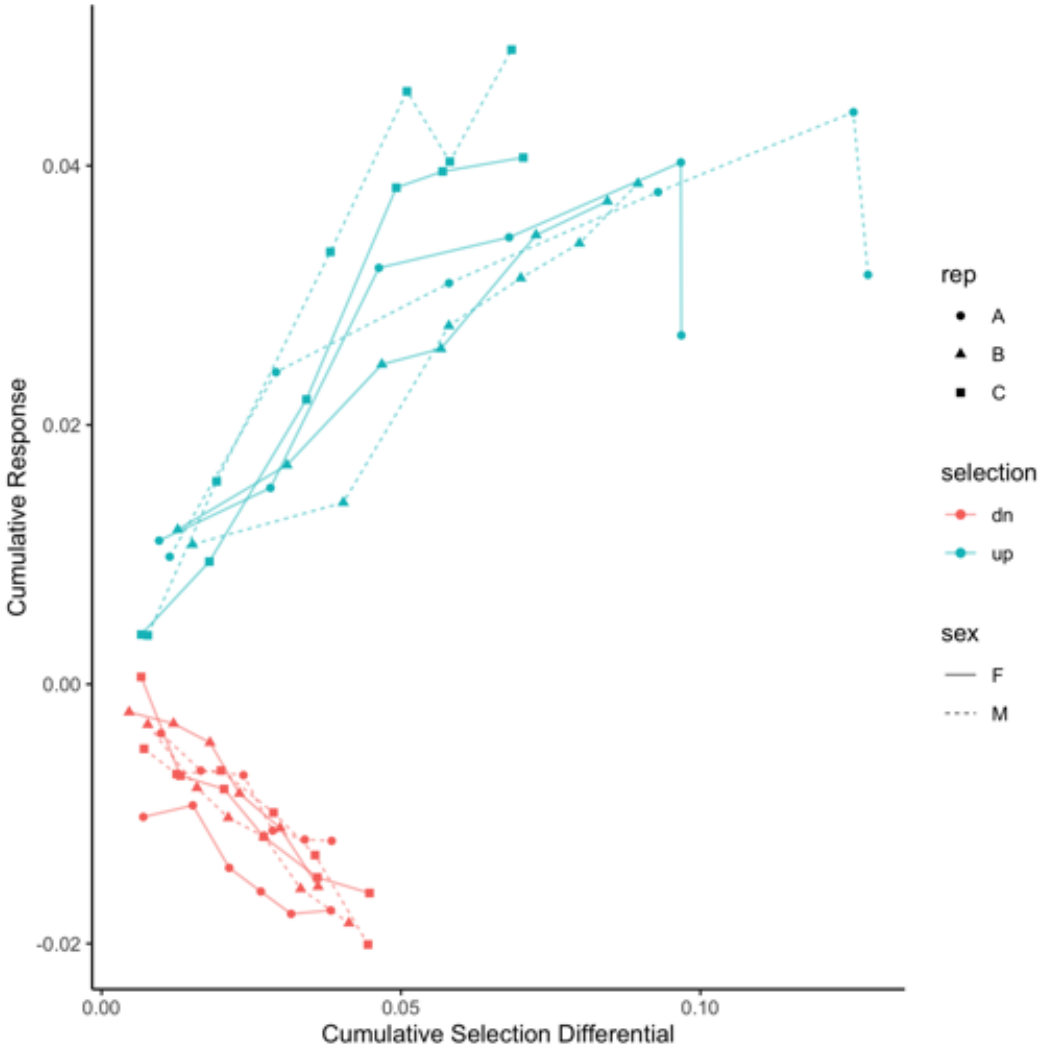

FIGURE A1.11: Response to artificial selection along the *ds* shape change vector. Regression of cumulative selection differential onto cumulative response was used to estimate realized heritability in both treatments ("up" "down") independently.

TABLE A1.9: Significantly differentiated variants for *neur* shape change from the wild-caught cohorts (BSA).

Location	CMH p-value (FDR corrected)	Gene	FlyBase ID	Distance from ORF (bp)
2L:15775767	0.026	CG43760	FBgn0264260	675
2L:15967220	0.017	*Beat-Ib*	FBgn0028645	4785
2L:15967222	0.017	*Beat-Ib*	FBgn0028645	4787
2L:8651597	0.015	*Sema1a*	FBgn0011259	0
3R: 21898160	0.024	CG6678	FBgn0038917	0

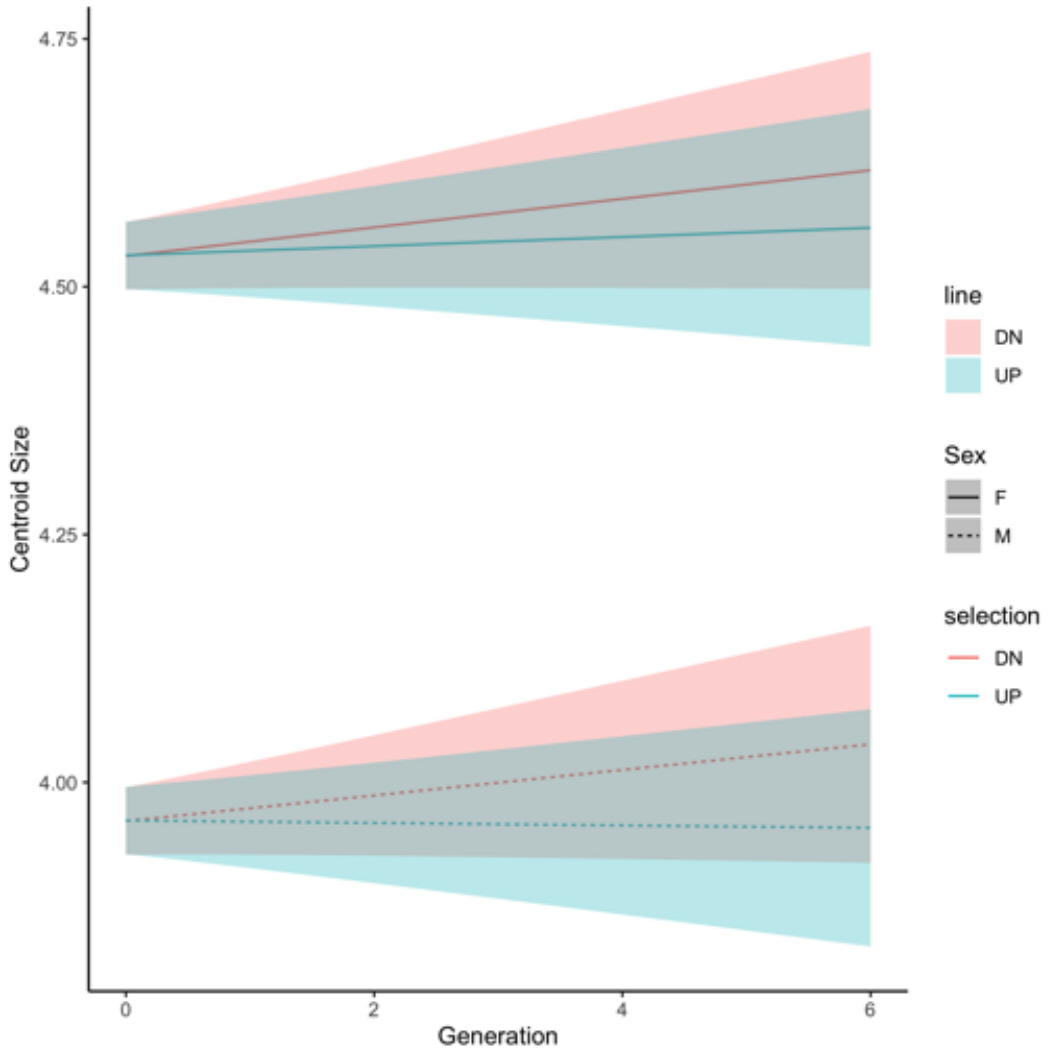

Figure A1.12: Modest (and not significant) changes in wing size following artificial selection based on *ds* shape change. Mean size estimated for up and down *ds* selection lineages estimated from a linear mixed model with replicate lineage fitted as a random effect. Shaded regions represent 95% confidence bands for the correlated response to selection.

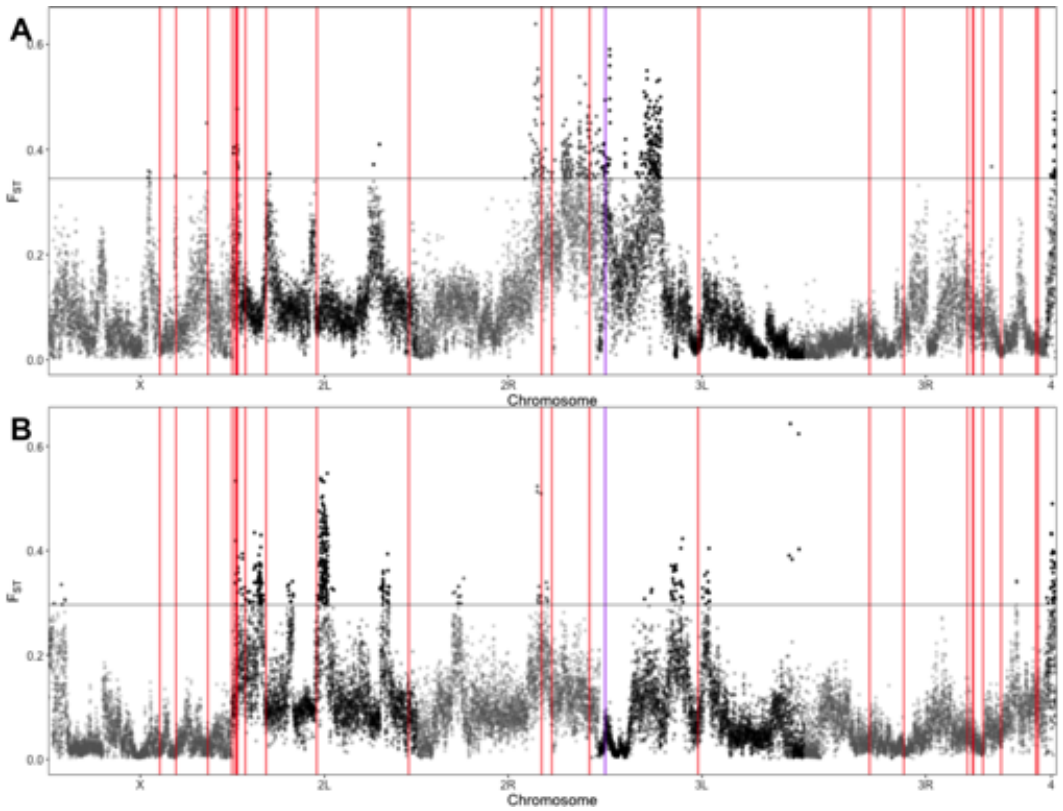

FIGURE A1.13: Genetic differentiation between artificial selection pools (Figure 2.3), with core hippo signaling loci (red) and *emc* (purple) marked. Genomic differentiation between up and down selection lineages (F_{ST}) measured in 5000bp windows for the artificial selection along *ds* (A) and *emc* shape change vectors (B). Horizonal grey lines represents 3sd from mean F_{ST}.

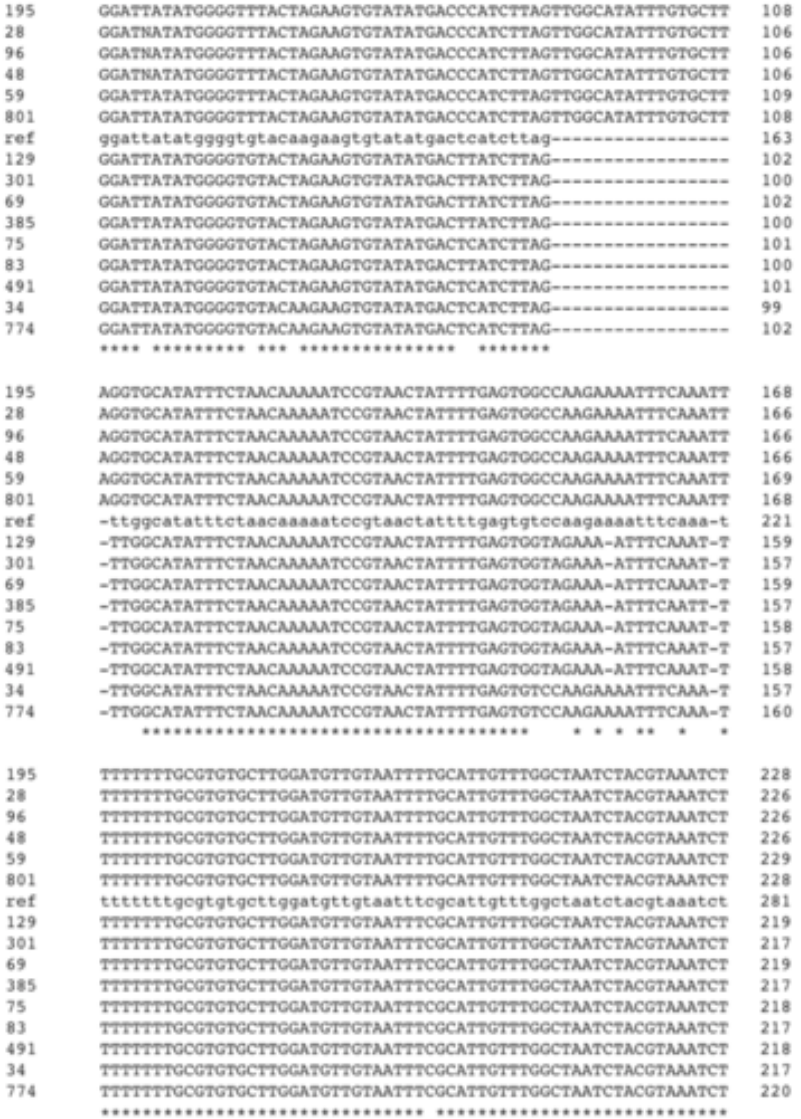

Figure A1.14: Alignment of sanger sequencing of the region containing the *ds* polymorphism from several DGRP lines (line numbers indicated at line starts) to reference sequence (from *Drosophila melanogaster* genome). DGRP lines are indicated with DGRP 195, 28, 96, 48, 59 and 801 predicted to have the insertion, and, DGRP 129, 301, 69, 385, 75, 83, 491, 34 and 774 without. In addition to the insertion in these lines, several other associated SNPs are found linked to the insertion.

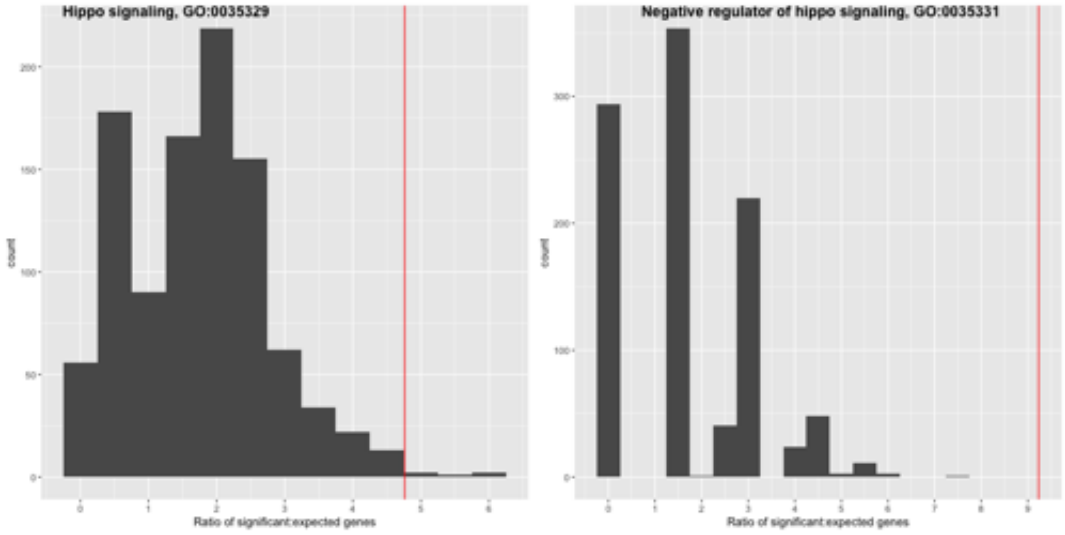

Figure A1.15: Permutation test for over representation of hippo signaling terms in outlier regions. The red line represents the observed ratio of significant to expected genes in outlier windows (F_{ST} greater than 3 standard deviations from the mean). The permutation test selected random windows from the genome, equal in number to those identified as outliers. For each random draw of loci, the ratio of significant to expected genes in the term of interest was calculated for 1000 permutations.

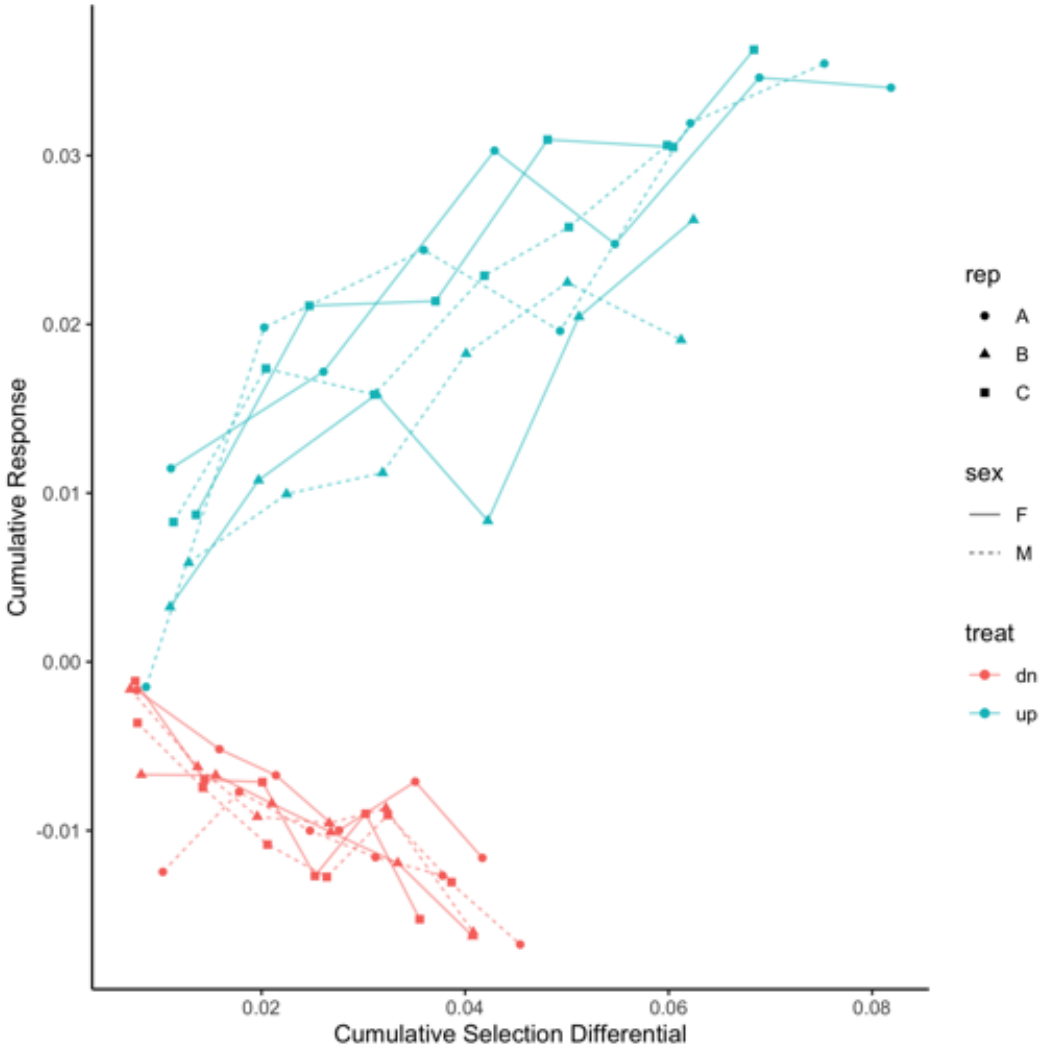

Figure A1.16: Response to selection based on projections onto *emc* shape change vector. Regression of cumulative selection differential onto cumulative response was used to estimate realized heritability in both "up" and "down" selection regimes independently.

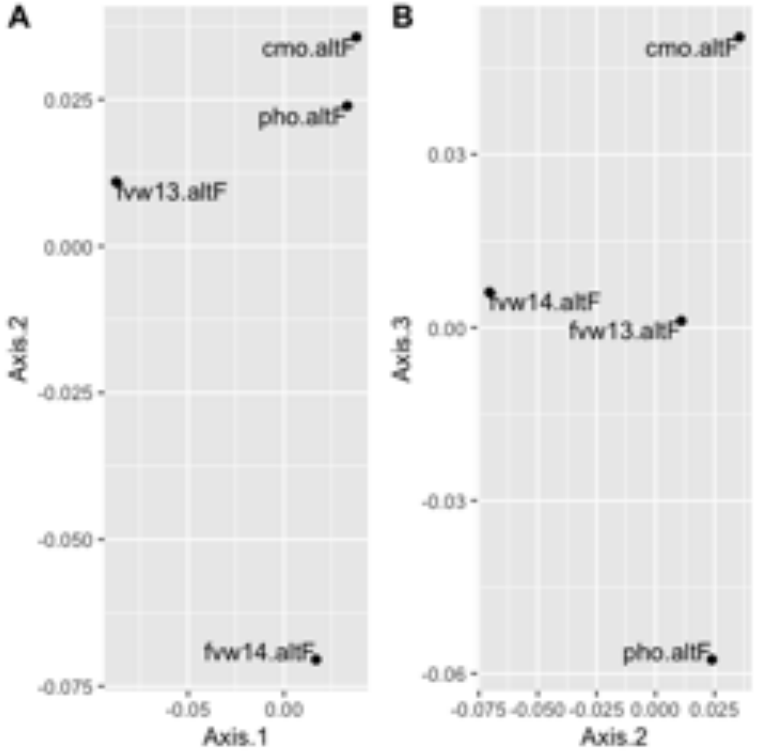

Figure A1.17: Minimal genetic structure among wild populations used in this study. Principal coordinate plot calculated from Bray's distances estimated from allele frequency data (altF), between the four wild cohorts used in this analysis. Axis 1-3 explains 45%, 30% and 25% of the variance in genetic distances respectively.

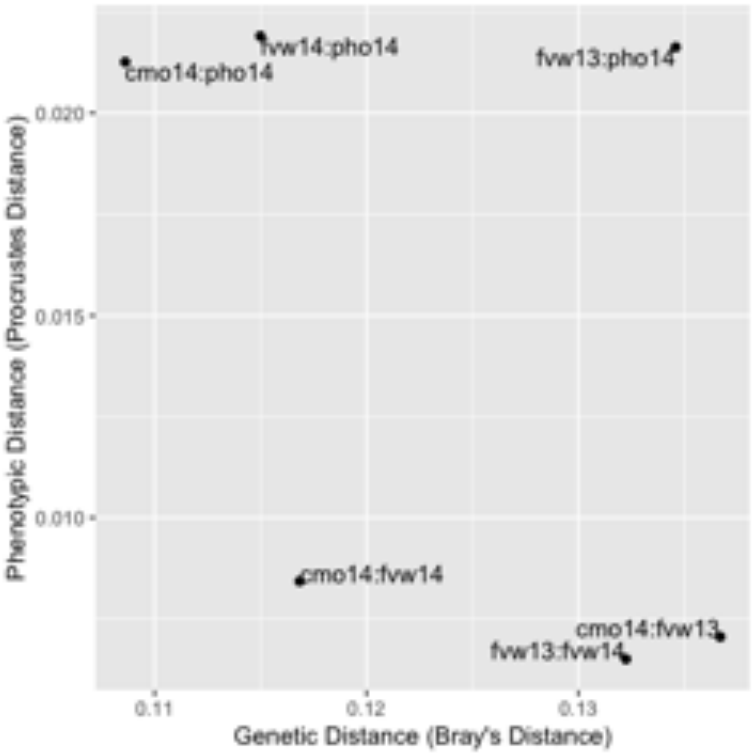

Figure A1.18: Genetic distance is not correlated with phenotypic distance among wild cohorts used in this study. Phenotypic distances are the Euclidian distances from model estimated shape vectors for each population from a multivariate regression of shape onto for population and wing centroid size.

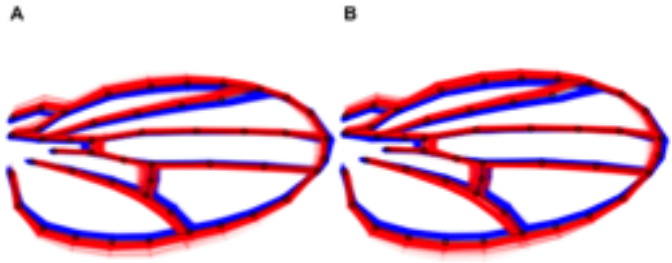

Figure A1.19: Shape variation within *ds* selected pools for bulk segregant analysis by population. Wings within selected pools (one red and one blue, representing the "up" and "down" pools) are plotted to show the phenotypic extremes for the shape scores used for selecting individuals within and between pools. Black line indicates mean shape between pools.

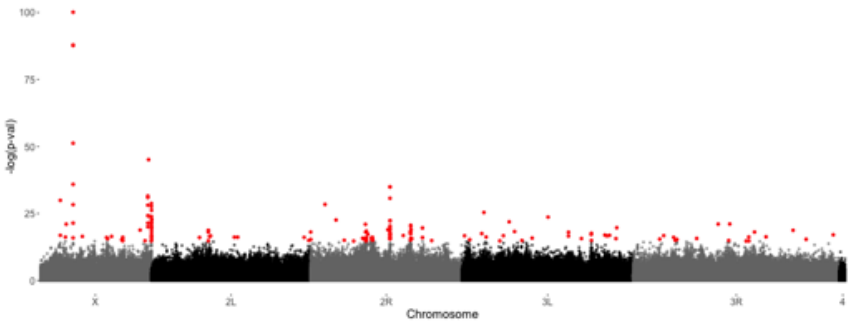

Figure A1.20: Removing PHO from the BSA analysis increases the number of differentiated sites between *ds* shape change pools. Genome-wide scan for differentiated loci between pools selected based on *ds* shape change vector using the CMH test using ACER. Variants in *ds* are still not implicated in this analysis. Points in red indicate sites with significant differentiation based with a FDR of 0.05.

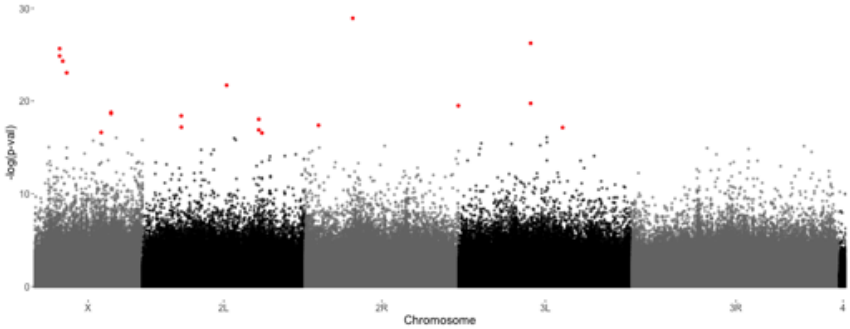

Figure A1.21: Down sampling genome coverage does not impact results for CMH tests substantially. When all pools are sampled to a coverage depth of 75 reads, while preserving allele frequency, we do not find an increase in number of differentiated sites. Although the sites identified as significantly differentiated do change somewhat, in part due to sampling procedure as any sites without a minimum depth of 75 reads in each of the 4 populations was dropped from this analysis. Variants in *ds* are still not implicated in this analysis.

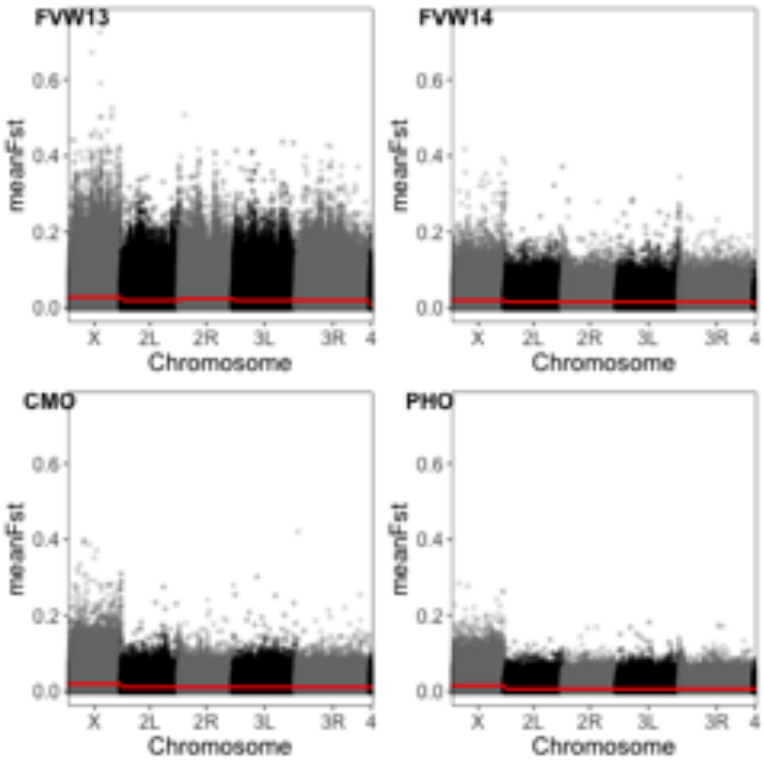

Figure A1.22: F_{ST} between pools of individuals selected along the *ds* shape change axis within each population. Calculated in 100 bp windows using PoPoolation2 program. Elevated F_{ST} on the X chromosome is due to sampling of fewer X chromosomes, relative to autosomes as most pools, with the exception of FVW14, consist of only males. Red line indicates the mean F_{ST} for the chromosome, which as expected is very low.

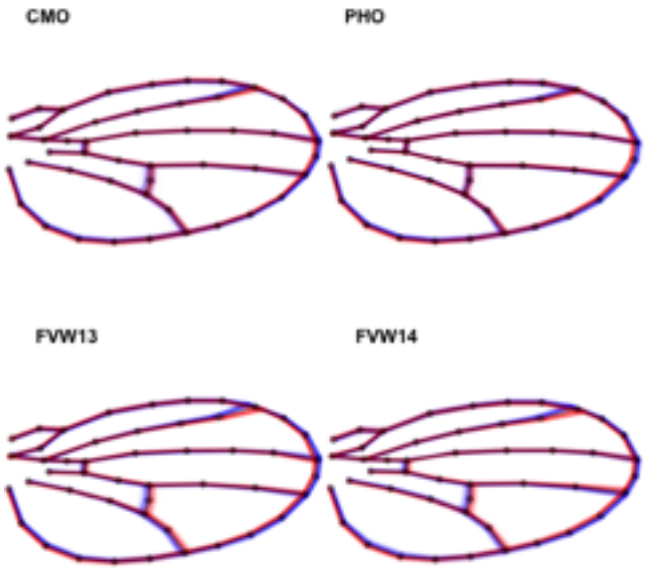

Figure A1.23: Shape variation within *neur* selected pools for bulk segregant analysis by population. Wings within selected pools (one red and one blue, representing "up" and "down" extreme pools respectively) are plotted.

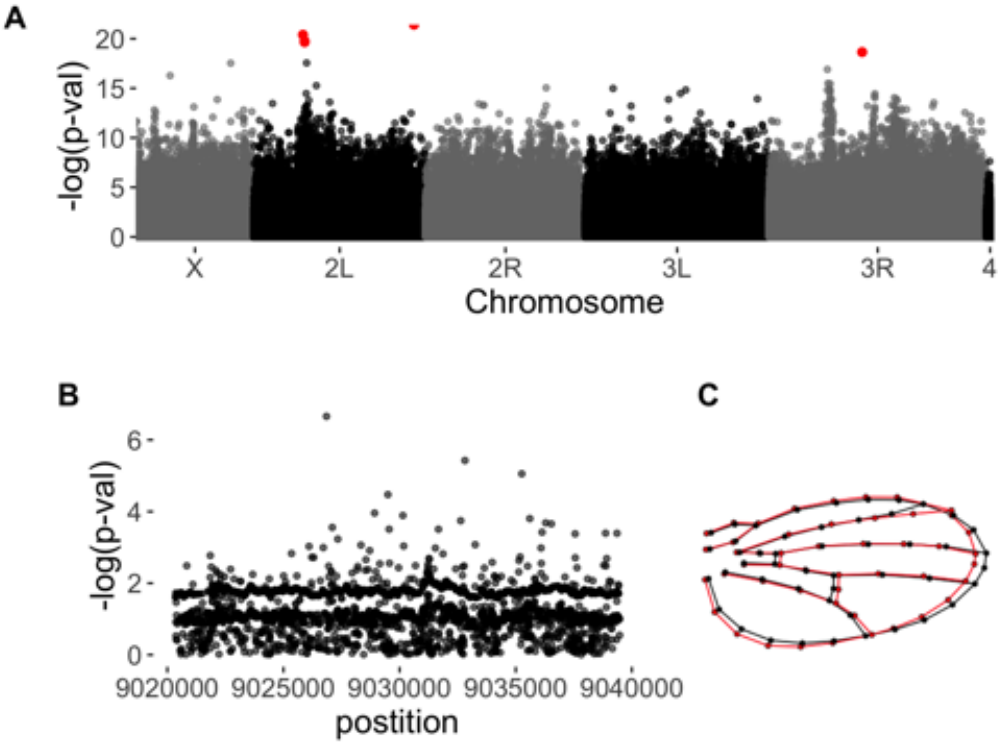

Figure A1.24: Genome-wide scan for differentiated loci between pools selected based on *neur* shape change vector using the CMH test implemented with ACER. (A) Whole genome scan for differentiation. Points in red indicate sites with significant differentiation based with a FDR of 0.05. (B) No significantly differentiated sites within *neur*. (C) shape change between selected pools based on neur shape change vector, effect size is multiplied by 2 for visualization.

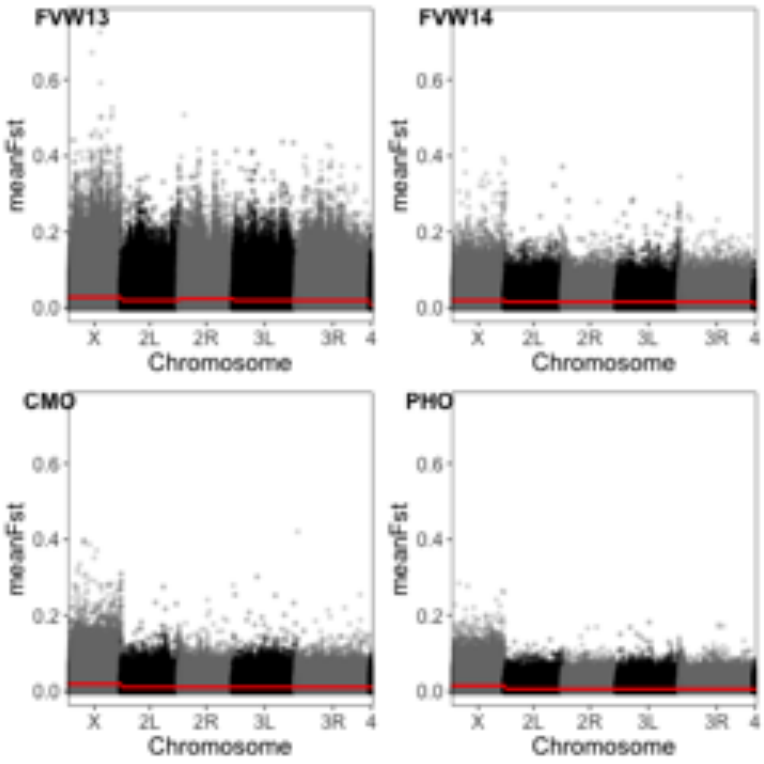

Figure A1.25: F_{ST} between pools of individuals selected along the *neur* shape change axis within each population. Calculated in 100 bp windows using PoPoolation2 program. Elevated F_{ST} on the X chromosome is due to sampling of fewer X chromosomes, relative to autosomes as most pools, with the exception of FVW14, consist of only males. Red line indicates the mean F_{ST} for the chromosome.

Appendix B

Chapter 3 Supplement

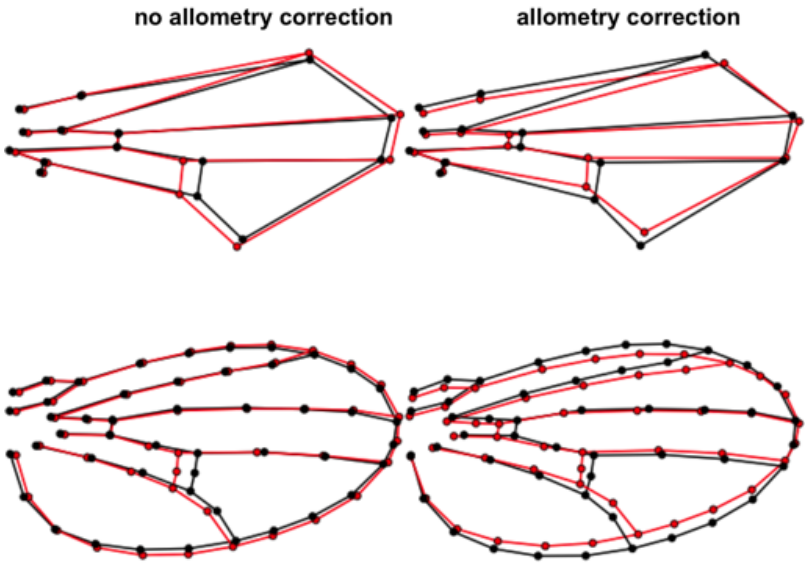

FIGURE A2.1: Shape change between high and low altitude populations is equivalent between methods. 15 point (top) and full spline method (bottom) shape change is about equivalent between high (black) and low (red) altitude populations. Before correcting for allometry, we observe a posterior cross vein shift as well as a small shift in the L2 andL5 longitudinal veins. After the allometric correction, there is a shift in the position of both cross veins as well as a more prominent shift in the longitudinal L2 and L5 veins. All effects are magnified by 2x.

Table A2.1: RNAi lines and appropriate controls for RNAi experiment. All experimental crosses were to the same *nubbin-Gal-4* line (BDSC:25754). In all cases, the TRiP control was (BDSC:36303), the third chromosome insertion line. *w-* were flies carrying the white mutation in the samerkand (SAM) background.

GOI	RNAi line ID	TRiP Panel	Control
loco	BDSC 32456	Y	*loco* RNAi X *w-*
takl2	BDSC 53985	Y	*nb-GAL4* X TRiP Control
ef6a	BDSC 64659	Y	*nb-GAL4* X TRiP Control
wge	BDSC 26813	N	*wge* RNAi X *w-*
wake	BDSC 61232	Y	*nb-GAL4* X TRiP Control
btn	BDSC 42530	Y	*nb-GAL4* X TRiP Control

Table A2.2: ANOVA table for the effect of deletion background from the DrosDel panel and wing size on wing shape.

	Chisq	Df	Pr(>Chisq)
Size	50.02	1	1.53e-12
Deletion Line	115.22	5	2.2e-16
Population	0.88	1	0.35
Size:Deletion line	20.62	5	0.00095
Size:Population	7.81	1	0.0052
Deletion line:Population	9.80	5	0.081

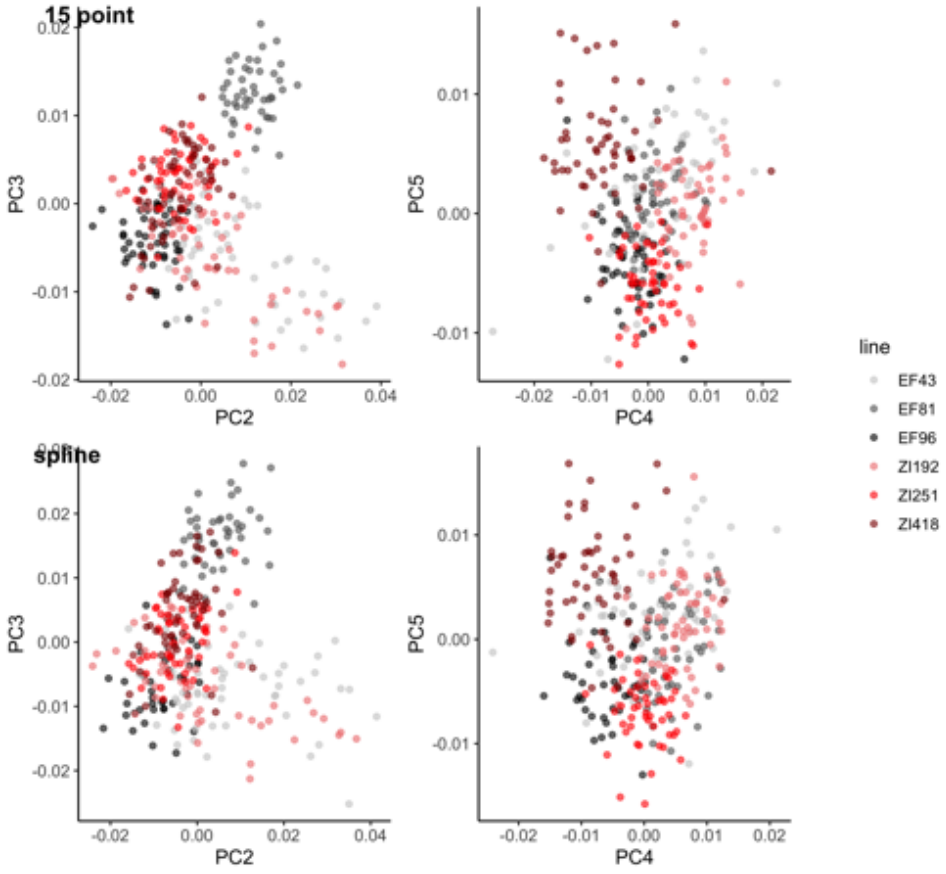

Figure A2.2: Two methods of shape collection do not substantially change the variance structure of parental populations. PCA of shape residuals for variation in high (black/greys) and low (reds) altitude populations based on inbred lines used in this analysis. PC1 is not included in this as it captures the allometric component of shape. Top panel is shape residuals captured using the 15 landmark method and bottom panel is shape residuals from the complete landmark and semi landmark method.

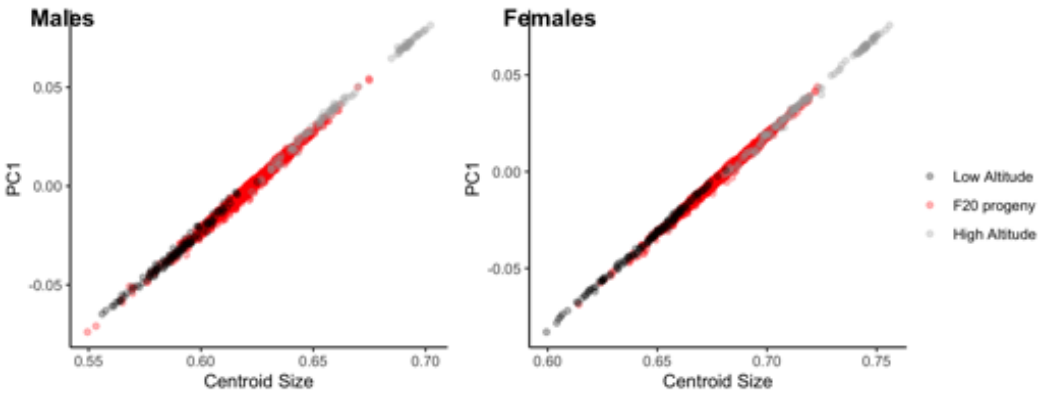

Figure A2.3: Centroid size is correlated with PC1 when log(CS) is included in PCA. Using this method, PC1 represents the allometric component of shape variation in addition to size variation. Representative data plotted for Zi192 x Ef96 cross and six inbred parental lines, but the relationship is consistent between different genotypes.

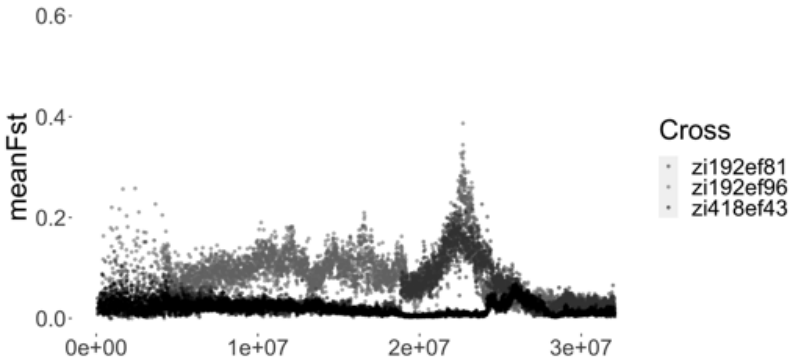

Figure A2.4: Region of genetic differentiation on chromosome 3R for shape mapping crosses. Plotting of mean FST calculated between male bulk pools in three different F20 mapping crosses, measured in 5000bp windows. X axis represents position. Shared genomic location of QTL between Zi192 x Ef81 and Zi192 x Ef96 cross can be see (greys) while small region of differentiation in Zi41 x Ef43 cross (black) is not in the same genomic region.

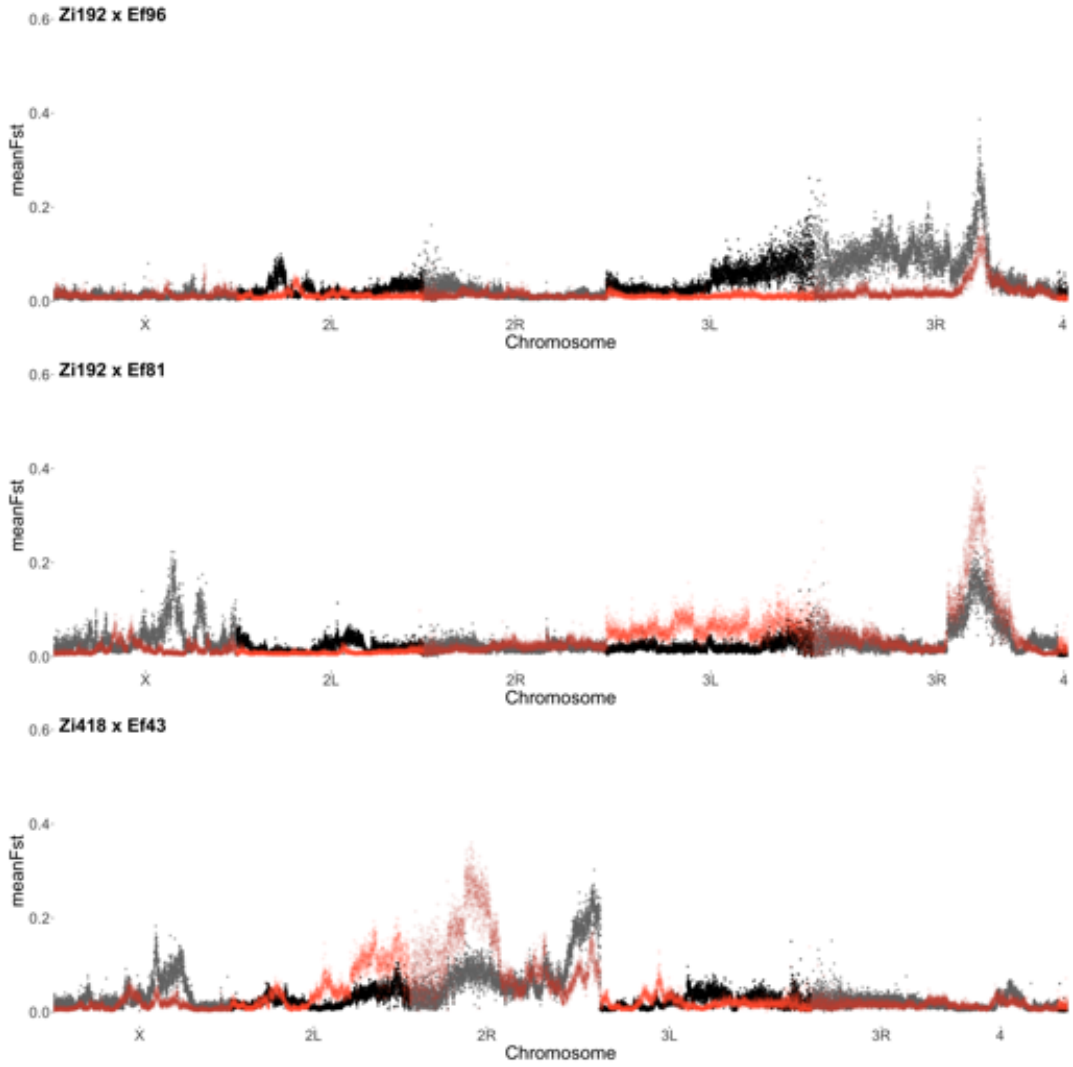

FIGURE A2.5: Sex specific contributions of to shape variation between high and low altitude populations. F_{ST} measured in 5000 bp windows between bulk pools within sex. Comparison between male pools (black/grey) and female pools (reds), show a similar but not completely overlapping genetic basis . This is particularly apparent on the X chromosome, which is hemizygous in males.

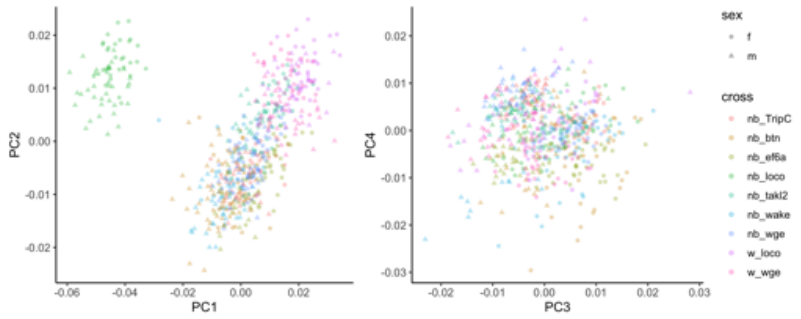

Figure A2.6: PCA of shape variation in RNAi knockdown. For the cross genotype, the *nubbin*-GAL4 line or white- control is indicated before the underscore and the UAS-GOI-RNAi or TRiP control genotype is indicated after the underscore.

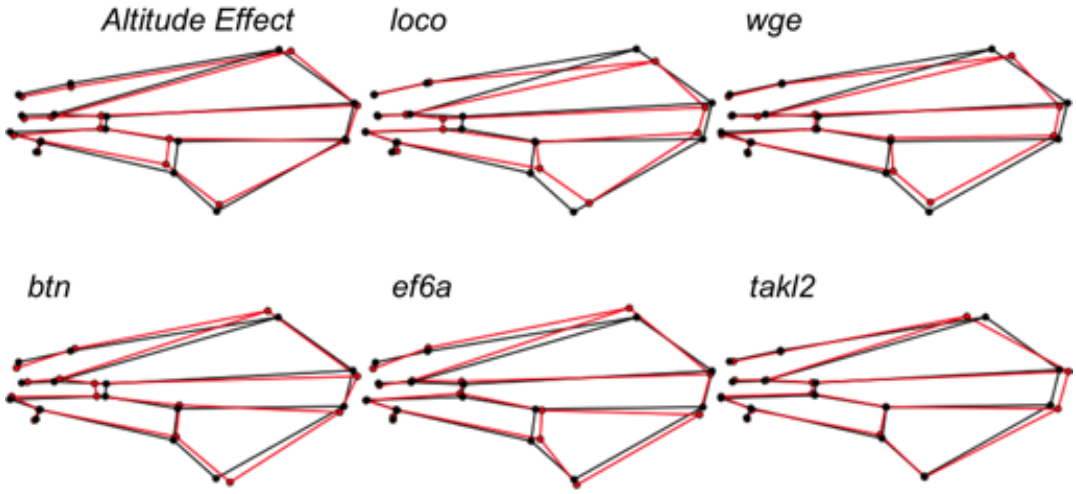

Figure A2.7: Effect on shape from knock down of candidate genes by RNAi in males. Shape change between RNAi knockdown (red) and control (black) is plotted. Altitude effect plots the shape change between high and low altitude population means, estimated from three inbred lines within each population. Effects are magnified for visualization: altitude effect: 10x ; *loco* 1.5x; *wge* 3x; *btn* 5x; *ef6a* 3x; *takl2* 3x. Unequal magnification required due to different magnitudes of estimated effect vectors.

Table A2.3: ANOVA table for the effect of deletion background from the Exelixis panel and wing size on wing shape.

	Chisq	Df	Pr(>Chisq)
Size	54.04	1	1.96e-13
Deletion Line	207.94	4	2.2e-16
Population	4.49	1	0.034
Size:Deletion line	13.12	4	0.011
Size:Population	0.56	1	0.45
Deletion line:Population	3.87	4	0.42

Table A2.4: ANOVA table for the effect of genotype, size and the interaction on shape for the F20 cross genotypes compared to parental inbred lines. Model fit using residual resampling permutation test using RRPP/Geomorph.

	Df	SS	MS	R^2	F	Z	P(>F)
Size	1	0.079	0.079	0.055	258.3	11.91	0.001
Genotype	8	0.22	0.028	0.16	93.4	18.32	0.001
Size:Genotype	8	0.010	0.0013	0.0074	4.37	7.36	0.001
Residuals	3655	1.12	0.000031	0.78			
Total	3672	1.44					

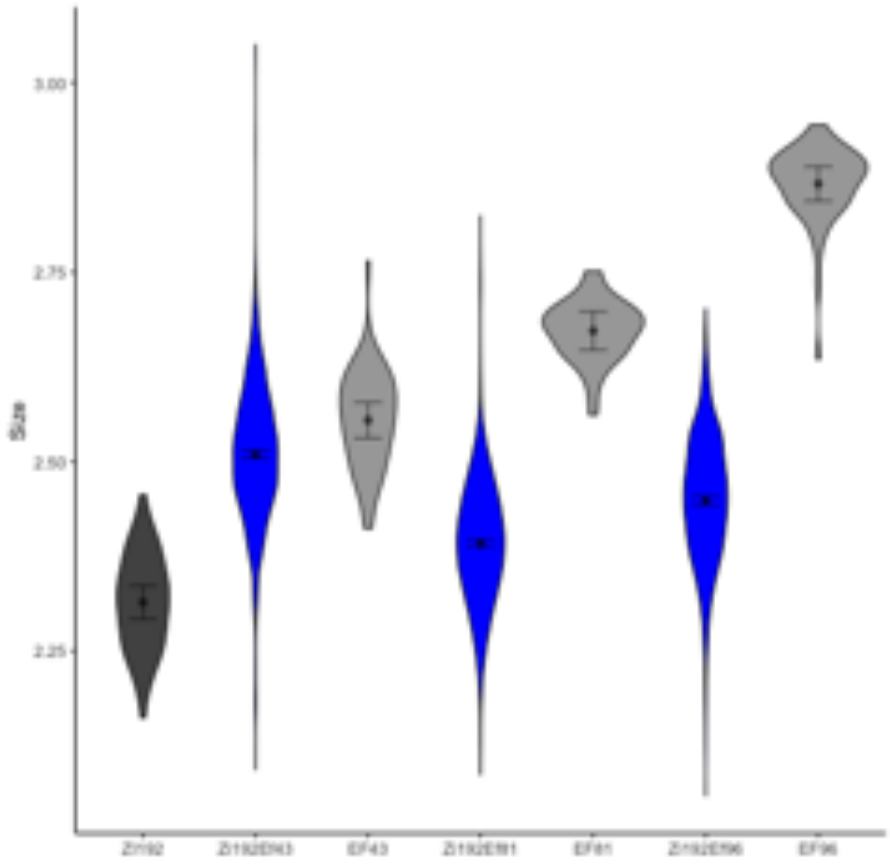

Figure A2.8: Male size variation within and between parental isogenic lines and F20 intercross males. Observed size, measured in centroid size in parental (greys) and F20 cross lines (blue). Low altitude parent is indicated in darker gray than high altitude parents. Estimated mean size with 95% CI indicated within violin plot. It should be noted that sample size is not equal between parental and cross groups, with parental lines represented by 50 individuals and crosses represented by >800 individuals.

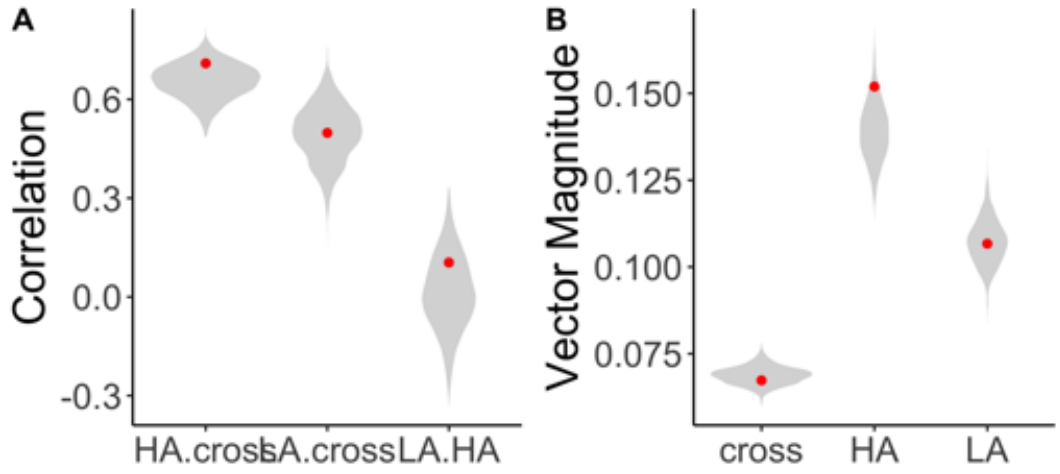

FIGURE A2.9: Comparison of allometry vectors between parental populations and F20 crosses. (A) Pairwise comparisons of allometric vector of shape variation between parental populations (3 HA, 3LA) or F20 cross (3 genotypes). Red points indicate observed value from data with 95% CI from 1000 bootstraps indicated in grey. (B) Magnitude (l2 norm) of allometry effect vector estimated for parental and cross genotypes. Red points indicate observed value from data with 95% CI from 1000 bootstraps indicated in grey. LA: low altitude, HA: high altitude population.

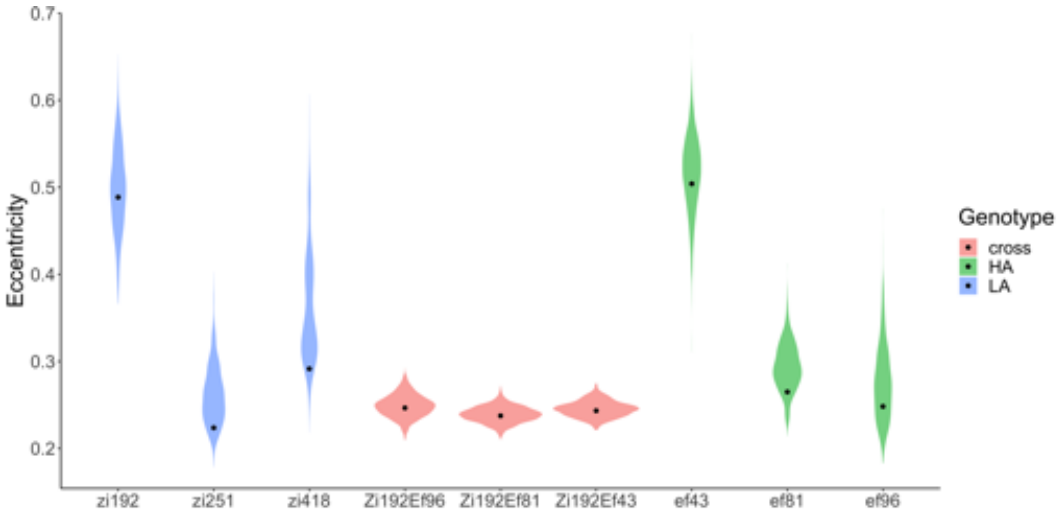

FIGURE A2.10: Eccentricity of VCV matrix by genotype. Eccentricity is measured by the proportion of variance in the direction of greatest variance (PC1). Observed values are indicated with black points with 95% CI calculated by the distribution of 1000 bootstraps in represented by the violin distribution.

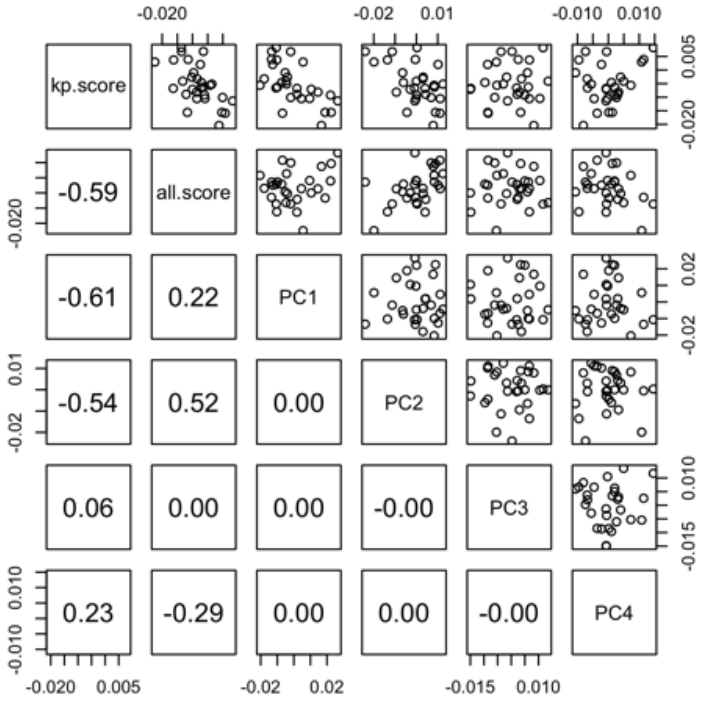

Figure A2.11: Correlation between shape scores and directions of phenotypic variation in African wings in males. Principal components of shape variation estimated from allometry corrected shape residuals of landmark data from inbred African lines from this study as well as Pesevski and Dworkin 2022. Two shape scores calculated by projecting mean line shapes onto the altitude effect vector were calculated to compare the direction of shape variation assisted with adaptation to high altitude with the directions of greatest shape variation within the populations. Kp.score is calculated based only on the lines used in this paper while all.score uses all the available lines.

Appendix C

Chapter 4 Supplement

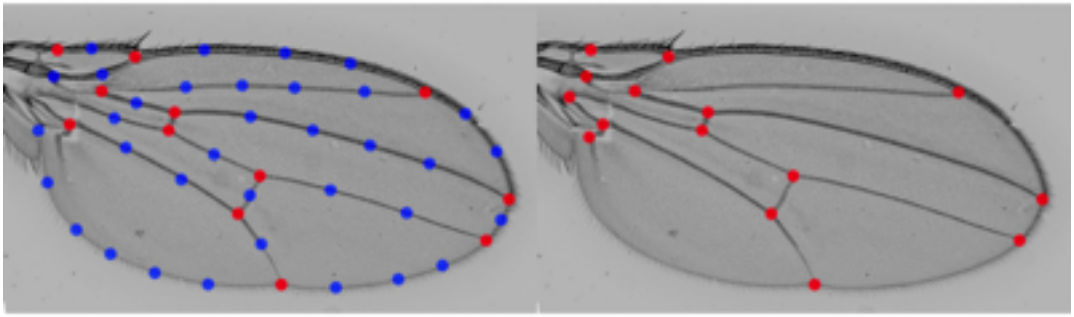

FIGURE A3.1: Spline and 15 point landmark locations. Locations of landmarks for adult wing shape collection using WINGMACHINE method (left) and 15 point shape collection (right) methods. Landmark locations are indicated in red and semi-landmarks in blue. For a complete description of shape data collection methods, see chapter 3.

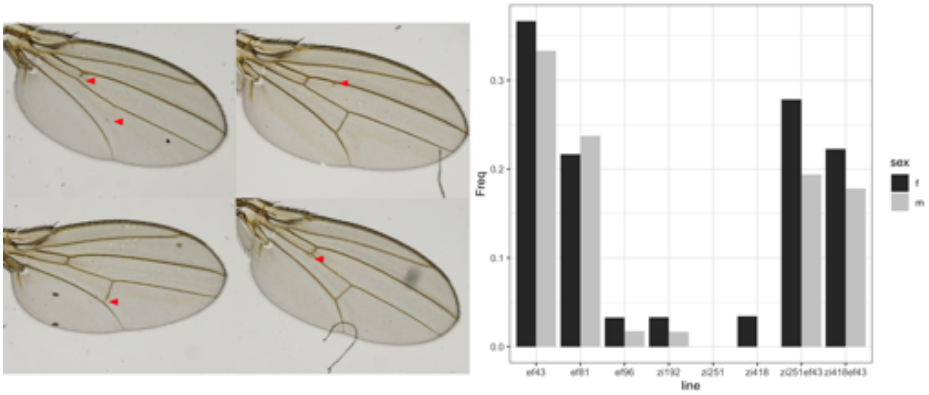

FIGURE A3.2: Scoring wing abnormalities in African inbred lines and F20 intercross. Using wing images collected as part of the chapter 3 study, wings were scored for abnormalities based in vein development. Examples of abnormal development on the right, with specific abnormalities indicated with an arrow. Frequencies of abnormalities indicated on the right for parental lines and F20 crosses (with both parental genotypes indicated on the x axis). In this work, the zi418 x ef43 cross was used for analysis.

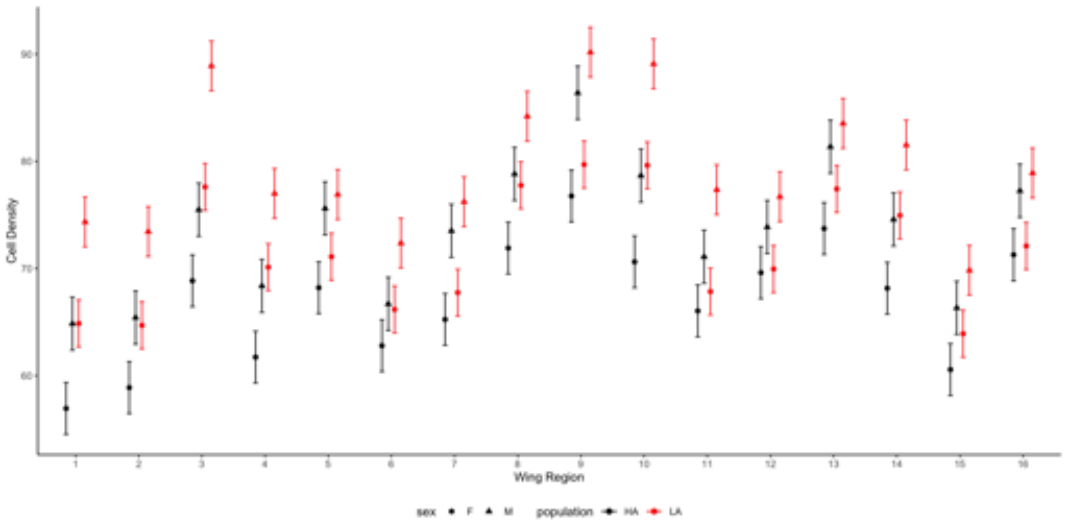

FIGURE A3.3: Cell density varies between wing regions between both populations and sexes. Points indicate mean cell density estimated from three inbred high attitude (HA) and three low altitude (LA) lines across 16 wing regions.

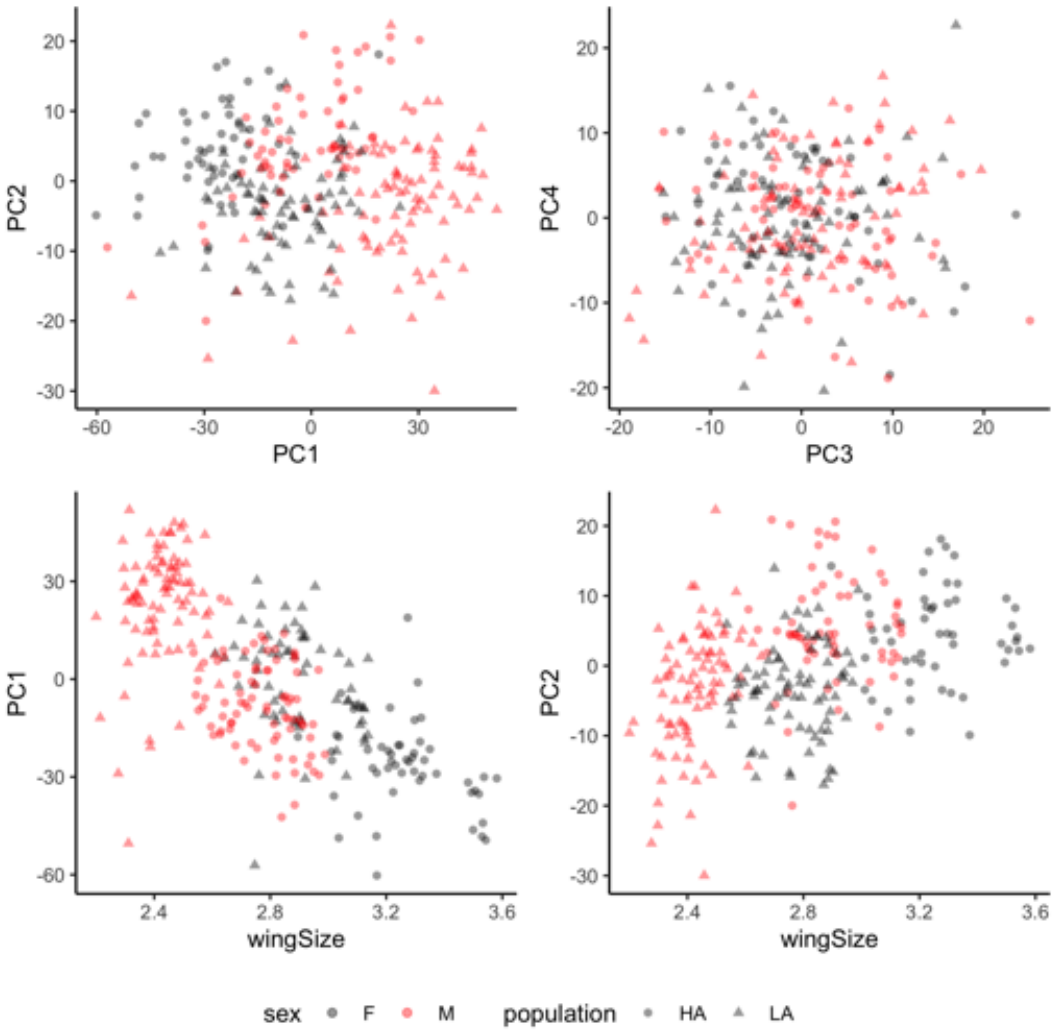

Figure A3.4: PCA of cell density across 16 wing regions for high altitude (HA) and low altitude (LA) populations. Cell density among wing regions is correlated with wing size variation across inbred lines. Proportion of variance explained by PC1 = 0.49; PC2 = 0.067, PC3 = 0.056, PC4 = 0.044. Wing size is measured by centroid size from morphometric analysis.

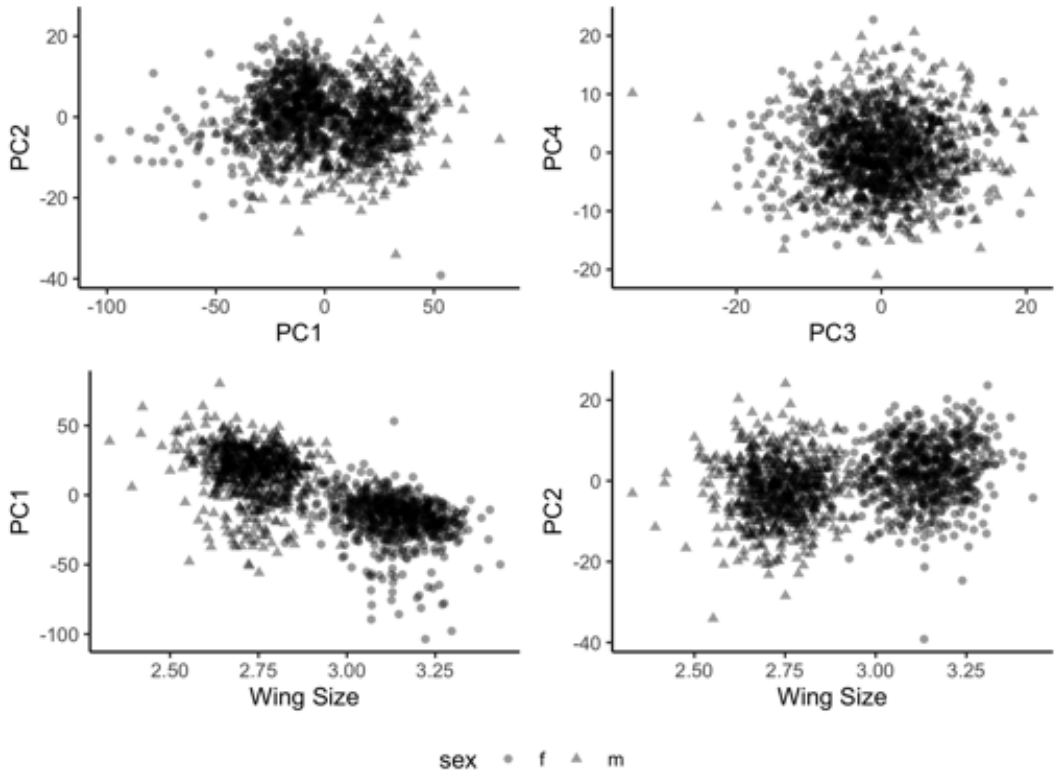

Figure A3.5: Variance of cell densities across 16 measured wing regions in Zi192 x Ef96 F20 intercross wings. Proportion of variance explained by PC1 = 0.55; PC2 = 0.056, PC3 = 0.040, PC4 = 0.036. Wing size is measured in centroid size.

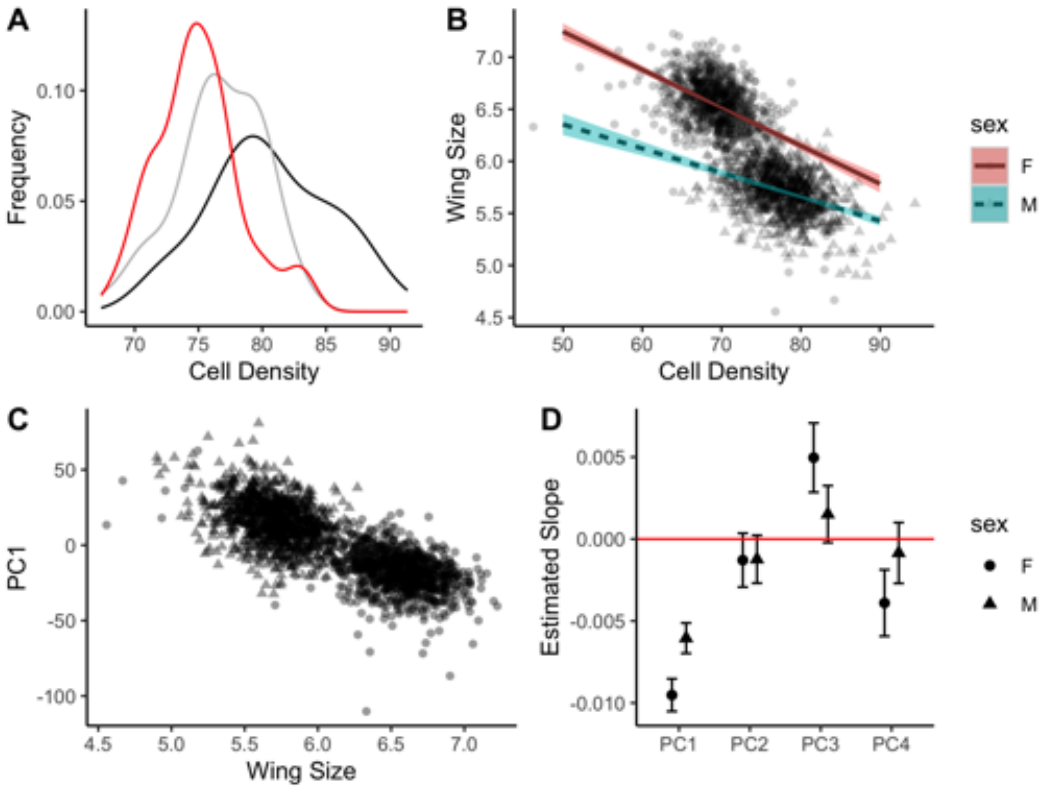

Figure A3.6: Relationship between wing size and cell density in Zi418 x Ef43 F20 intercross. (A) Density plot of cell density in the largest (red), smallest (black) and equal sized sample from the intermediate sized wings (grey) in F20 intercross. Lower density is related to a larger cell size. (B) effect of cell density on wing size, within sex. Estimates of the regression are indicated by lines, with shaded 95% CI. (C) PC1 of variation in cell density between wing regions is correlated with wing size. (D) Estimated slope of regression of PCs from cell density onto wing size. Error bars indicate 95% CI. Red line indicates a slope of 0, or no relationship.

Table A3.1: ANOVA for the effect of cell density variation between wing regions on wing size in ZI418 x EF43 F20 cross.

	Chisq	Df	Pr(>Chisq)
Sex	1246.81	1	2.2e-16
PC1	491.44	1	2.2e-16
PC2	5.12	1	0.023
PC3	18.07	1	2.13e-05
PC4	10.30	1	0.0013
PC1:Sex	10.3	1	5.51e-07
PC2:Sex	0.0026	1	0.96
PC3:Sex	6.11	1	0.013
PC4:Sex	4.74	1	0.030

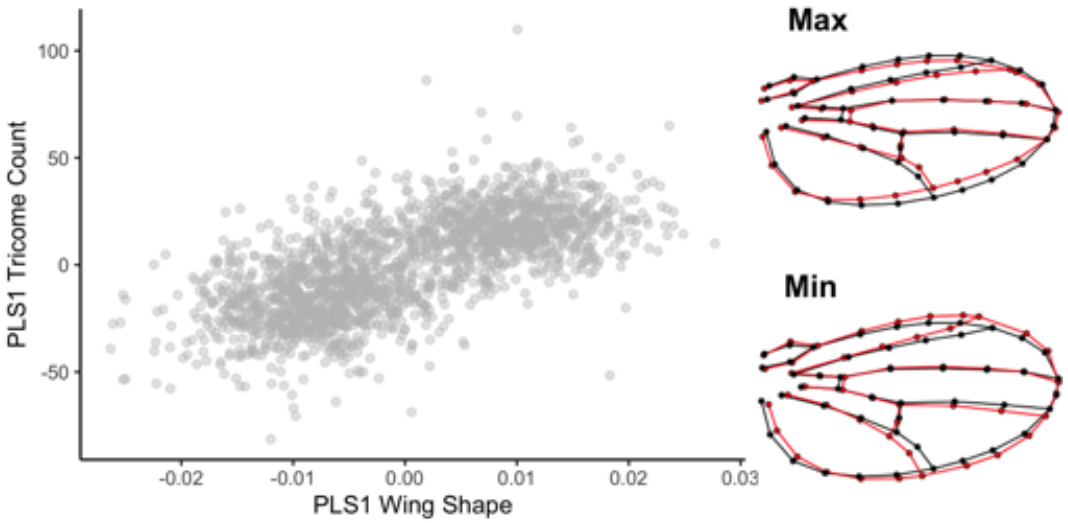

Figure A3.7: Substantial co-variation between wing shape and wing cell size in the Zi192 x Ef96 F20 intercross. 2 block partial least squares correlation between the first dimension of variation for wing shape and cell density variation within the wing, indicated similar covariation structure. Wire frames on the left demonstrate the shape change (red) from mean shape (black) at the maximum and minimum wing shape PLS-1 values

Table A3.2: ANOVA for the effect of size, cell density and sex on wing shape in ZI418 x EF43 F20 cross. Model fit using residual resampling permutation test using RRPP/Geomorph.

	Df	SS	MS	R^2	F	Z	P(>F)
WingSize	1	0.15	0.15	0.22	564.0	8.61	0.001
Sex	1	0.0084	0.0084	0.012	31.81	6.56	0.001
CellDensity	1	0.0016	0.0016	0.0024	6.01	3.99	0.001
WingSize:Sex	1	0.0014	0.0014	0.0021	5.28	3.83	0.001
WingSize:CellDensity	1	0.00062	0.00062	0.00091	2.09	18.32	0.013
Sex:CellDensity	1	0.00079	0.00079	0.0012	2.97	2.61	0.003
WingSize:Sex:CellDensity	1	0.00026	0.00026	0.00038	0.98	0.30	0.377
Residuals	1944	0.52	0.00027	0.76			
Total	1951	0.67764					

Table A3.3: Pairwise distance between variances in shape (disparity) for wings with and without abnormalities. Estimated disparity for each group is: female, normal = 0.00027; male, normal = 0.00025; female, abnormal = 0.00031; male, abnormal = 0.00029

	d	UL(95%)	Z	Pr >d
Female, Normal:Male, Normal	1.42e-05	1.69e-05	1.32	0.083
Female, Normal:Female Abnormal	3.93e-05	3.74e-05	1.68	0.045
Female, Normal:Male Abnormal	2.65e-05	3.48e-05	1.14	0.130
Male, Normal:Female Abnormal	5.35e-05	3.69e-05	2.31	0.007
Male, Normal:Male Abnormal	4.07e-05	3.46e-05	1.89	0.022
Female Abnormal:Male Abnormal	1.29e-05	4.69e-05	-0.21	0.589

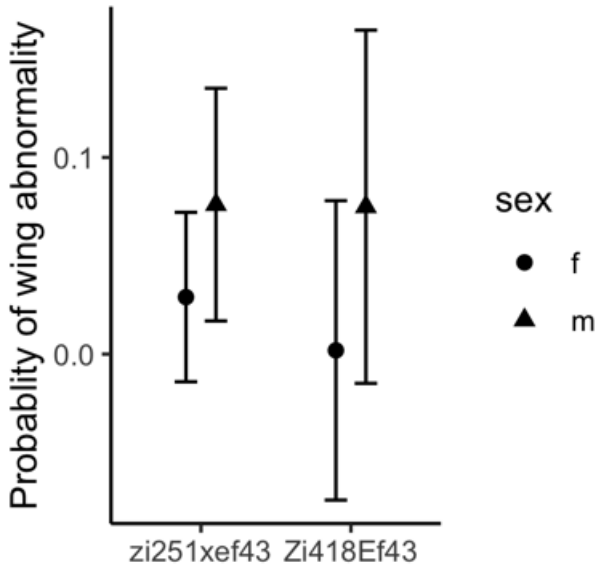

Figure A3.8: relationship between increase in wing abnormalities wing size, including cross veinless wings. Probability of increased wing abnormalities with standard deviation increase in trait values (larger wings, increased cell density), by sex. Z-scores are used for both wing size and cell density. Error bars represent 95% confidence intervals.

Table A3.4: ANOVA for the effect of size, population and cell density on wing shape of adult wings in synthetic outbred populations, using a type II ANOVA.

	Df	SS	MS	R^2	F	Z	P(>F)
WingSize	1	0.0011	0.0011	0.032	4.42	3.04	0.003
Population	1	0.0011	0.0011	0.032	4.44	3.09	0.001
CellDensity	1	0.00014	0.00014	0.004	0.54	-0.98	0.82
Replicate	4	0.0025	0.00063	0.072	0.55	-1.31	0.90
WingSize:Population	1	0.00019	0.00019	0.0053	0.73	-0.33	0.62
WingSize:CellDensity	1	0.00024	0.00024	0.0067	0.91	0.068	0.47
Population:CellDensity	1	0.00038	0.00038	0.011	1.46	1.01	0.16
WingSize:Population:CellDensity	1	0.00033	0.00033	0.0095	0.68	0.30	0.26
Residuals	91	0.023	0.00023	0.66			
Total	102	0.035					

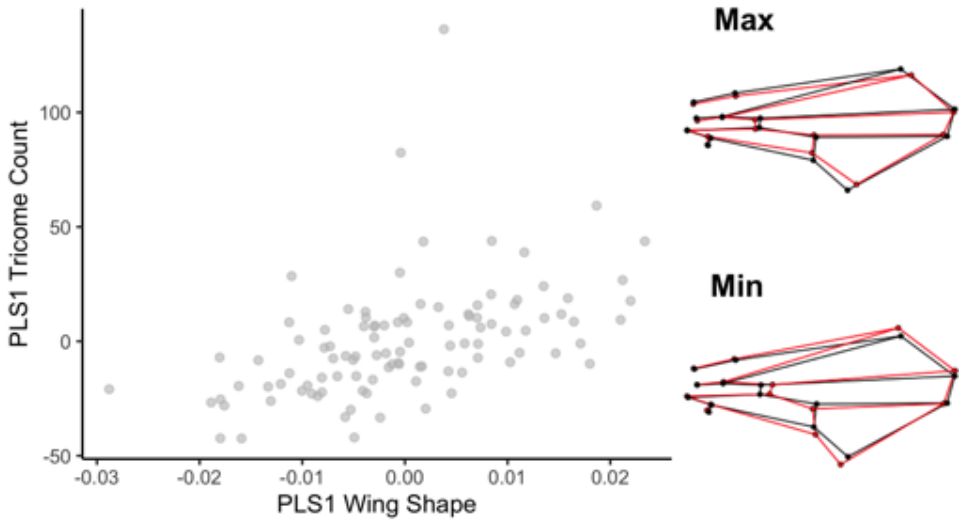

Figure A3.9: Substantial co-variation between wing shape and wing cell size in the SO adult wings. 2 block partial least squares correlation between the first dimension of variation for wing shape and cell density variation within the wing, indicated similar covariation structure. Wire frames on the left demonstrate the shape change (red) from mean shape (black) at the maximum and minimum wing shape PLS-1 values

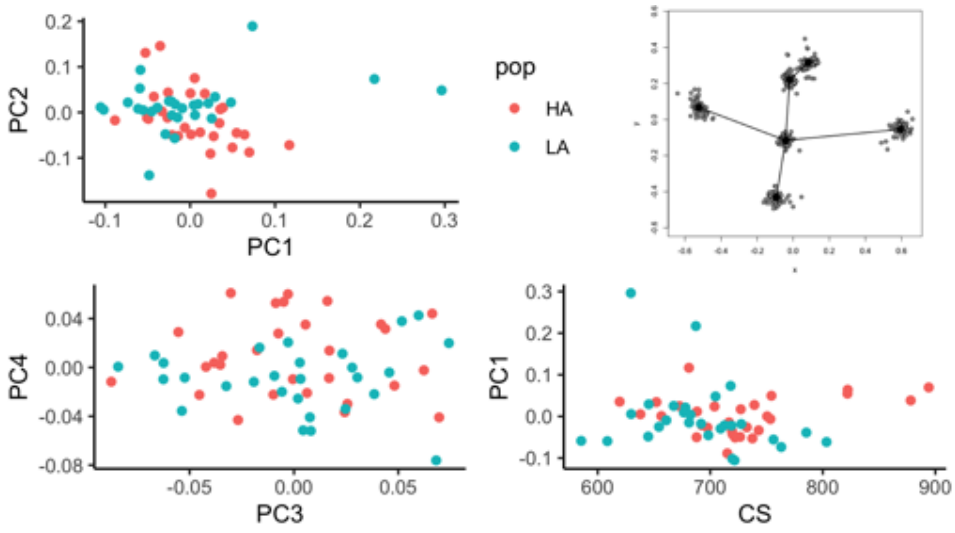

Figure A3.10: Shape variation in larval wing discs from SO populations. PCA of shape residuals for larval wing discs. Top right pannel shows landmark variation in superimposed wing disc shape data, mean shape is indicated by black points.

Bibliography

Abzhanov, A., Protas, M., Grant, B. R., Grant, P. R., and Tabin, C. J. (Sept. 2004). Bmp4 and Morphological Variation of Beaks in Darwin's Finches. *Science* 305(5689), 1462–1465. ISSN: 0036-8075, 1095-9203.

Adams, D. C. and Otárola-Castillo, E. (Apr. 2013). geomorph: an R package for the collection and analysis of geometric morphometric shape data. *Methods in Ecology and Evolution* 4(4). Ed. by E. Paradis, 393–399. ISSN: 2041210X.

Alexa, A., Rahnenfuhrer, J., and Lengauer, T. (July 2006). Improved scoring of functional groups from gene expression data by decorrelating GO graph structure. *Bioinformatics* 22(13), 1600–1607. ISSN: 1367-4803, 1460-2059.

Baena-López, L. A., Baonza, A., and García-Bellido, A. (Sept. 2005). The Orientation of Cell Divisions Determines the Shape of Drosophila Organs. *Current Biology* 15(18), 1640–1644. ISSN: 09609822.

Barghi, N., Hermisson, J., and Schlötterer, C. (June 2020). Polygenic adaptation: a unifying framework to understand positive selection. *Nature Reviews Genetics*. ISSN: 1471-0056, 1471-0064.

Barghi, N., Tobler, R., Nolte, V., Jakšić, A. M., Mallard, F., Otte, K. A., Dolezal, M., Taus, T., Kofler, R., and Schlötterer, C. (Feb. 2019). Genetic redundancy fuels polygenic adaptation in Drosophila. *PLOS Biology* 17(2). Ed. by G. Gibson, e3000128. ISSN: 1545-7885.

Barrett, R. D. H., Rogers, S. M., and Schluter, D. (Oct. 2008). Natural Selection on a Major Armor Gene in Threespine Stickleback. *Science* 322(5899), 255–257. ISSN: 0036-8075, 1095-9203.

Barton, N. H. and Keightley, P. D. (Jan. 2002). Understanding quantitative genetic variation. *Nature Reviews Genetics* 3(1), 11–21. ISSN: 1471-0056, 1471-0064.

Bastide, H., Betancourt, A., Nolte, V., Tobler, R., Stöbe, P., Futschik, A., and Schlötterer, C. (June 2013). A Genome-Wide, Fine-Scale Map of Natural Pigmentation Variation in Drosophila melanogaster. *PLoS Genetics* 9(6). Ed. by P. Wittkopp, e1003534. ISSN: 1553-7404.

Bastide, H., Lange, J. D., Lack, J. B., Yassin, A., and Pool, J. E. (Nov. 2016). A Variable Genetic Architecture of Melanic Evolution in *Drosophila melanogaster*. *Genetics* 204(3), 1307–1319. ISSN: 0016-6731, 1943-2631.

Bastide, H., Yassin, A., Johanning, E. J., and Pool, J. E. (Dec. 2014). Pigmentation in Drosophila melanogaster reaches its maximum in Ethiopia and correlates most strongly with ultra-violet radiation in sub-Saharan Africa. *BMC Evolutionary Biology* 14(1), 179. ISSN: 1471-2148.

Benjamini, Y. and Hochberg, Y. (1995). Controlling the False Discovery Rate: A Practical and Powerful Approach to Multiple Testing. *Journal of the Royal Statistical Society: Series B (Methodological)* 57(1), 289–300. ISSN: 00359246.

Blows, M. W. and McGuigan, K. (May 2015). The distribution of genetic variance across phenotypic space and the response to selection. *Molecular Ecology* 24(9), 2056–2072. ISSN: 09621083.

Bolger, A. M., Lohse, M., and Usadel, B. (Aug. 2014). Trimmomatic: a flexible trimmer for Illumina sequence data. *Bioinformatics* 30(15), 2114–2120. ISSN: 1367-4803.

Bomblies, K. and Peichel, C. L. (July 2022). Genetics of adaptation. *Proceedings of the National Academy of Sciences* 119(30), e2122152119. ISSN: 0027-8424, 1091-6490.

Boyle, E. A., Li, Y. I., and Pritchard, J. K. (June 2017). An Expanded View of Complex Traits: From Polygenic to Omnigenic. *Cell* 169(7), 1177–1186. ISSN: 00928674.

Briševac, D., Peralta, C. M., and Kaiser, T. S. (Feb. 2023). An oligogenic architecture underlying ecological and reproductive divergence in sympatric populations. *eLife* 12, e82825. ISSN: 2050-084X.

Bryant, P. (1975). Pattern formation in the imaginal wing disc of Drosophila melanogaster: fate map, regeneration and duplication. *The Journal of experimental zoology* 193(1). Place: New York Publisher: Wiley Subscription Services, Inc., A Wiley Company, 49–77. ISSN: 0022-104X.

Bryant, P. J. and Levinson, P. (1985). Intrinsic growth control in the imaginal primordia of Drosophila, and the autonomous action of a lethal mutation causing overgrowth. *Developmental Biology* 107(2), 355–363. ISSN: 0012-1606.

Calboli, F. C. F., Kennington, W. J., and Partridge, L. (2003). Qtl Mapping Reveals a Striking Coincidence in the Positions of Genomic Regions Associated with Adaptive Variation in Body Size in Parallel Clines of Drosophila Melanogaster on Different Continents. *Evolution* 57(11), 2653–2658. ISSN: 1558-5646.

Carreira, V. P., Mensch, J., and Fanara, J. J. (Mar. 2009). Body size in Drosophila: genetic architecture, allometries and sexual dimorphism. *Heredity* 102(3), 246–256. ISSN: 0018-067X, 1365-2540.

Carreira, V. P., Soto, I. M., Mensch, J., and Fanara, J. J. (2011). Genetic basis of wing morphogenesis in Drosophila: sexual dimorphism and non-allometric effects of shape variation. *BMC Developmental Biology* 11(1), 32. ISSN: 1471-213X.

Carreira, V. P., Imberti, M. A., Mensch, J., and Fanara, J. J. (July 2013). Gene-by-Temperature Interactions and Candidate Plasticity Genes for Morphological Traits in Drosophila melanogaster. *PLoS ONE* 8(7). Ed. by T. Flatt, e70851. ISSN: 1932-6203.

Celis, J. F. de and Bray, S. (Sept. 1997). Feed-back mechanisms affecting Notch activation at the dorsoventral boundary in the *Drosophila* wing. *Development* 124(17), 3241–3251. ISSN: 0950-1991, 1477-9129.

Chan, Y. F., Marks, M. E., Jones, F. C., Villarreal, G., Shapiro, M. D., Brady, S. D., Southwick, A. M., Absher, D. M., Grimwood, J., Schmutz, J., Myers, R. M., Petrov, D., Jónsson, B., Schluter, D., Bell, M. A., and Kingsley, D. M. (Jan. 2010). Adaptive Evolution of Pelvic Reduction in Sticklebacks by Recurrent Deletion of a Pitx1 Enhancer. *Science* 327(5963), 302–305. ISSN: 0036-8075, 1095-9203.

Chandler, C. H., Chari, S., and Dworkin, I. (June 2013). Does your gene need a background check? How genetic background impacts the analysis of mutations, genes, and evolution. *Trends in Genetics* 29(6), 358–366. ISSN: 01689525.

Chandler, C. H., Chari, S., Kowalski, A., Choi, L., Tack, D., DeNieu, M., Pitchers, W., Sonnenschein, A., Marvin, L., Hummel, K., Marier, C., Victory, A., Porter, C., Mammel, A., Holms, J., Sivaratnam, G., and Dworkin, I. (Nov. 2017). How well do you know your mutation? Complex effects of genetic background on expressivity, complementation, and ordering of allelic effects. *PLOS Genetics* 13(11). Ed. by T. F. C. Mackay, e1007075. ISSN: 1553-7404.

Chen, S.-A. A., Kern, A. F., Ang, R. M. L., Xie, Y., and Fraser, H. B. (Apr. 2023). Gene-by-environment interactions are pervasive among natural genetic variants. *Cell Genomics* 3(4), 100273. ISSN: 2666979X.

Chevin, L.-M. and Hospital, F. (Nov. 2008). Selective Sweep at a Quantitative Trait Locus in the Presence of Background Genetic Variation. *Genetics* 180(3), 1645–1660. ISSN: 1943-2631.

Collyer, M. L. and Adams, D. C. (July 2018). RRPP: An R package for fitting linear models to high-dimensional data using residual randomization. *Methods in Ecology and Evolution* 9(7). Ed. by R. Freckleton, 1772–1779. ISSN: 2041-210X, 2041-210X.

Colosimo, P. F., Hosemann, K. E., Balabhadra, S., Villarreal, G., Dickson, M., Grimwood, J., Schmutz, J., Myers, R. M., Schluter, D., and Kingsley, D. M. (Mar. 2005).

Widespread Parallel Evolution in Sticklebacks by Repeated Fixation of Ectodysplasin Alleles. *Science* 307(5717), 1928–1933. ISSN: 0036-8075, 1095-9203.

Colosimo, P. F., Peichel, C. L., Nereng, K., Blackman, B. K., Shapiro, M. D., Schluter, D., and Kingsley, D. M. (Mar. 2004). The Genetic Architecture of Parallel Armor Plate Reduction in Threespine Sticklebacks. *PLOS Biology* 2(5), e109. ISSN: 1545-7885.

CONVERGE consortium (July 2015). Sparse whole-genome sequencing identifies two loci for major depressive disorder. *Nature* 523(7562), 588–591. ISSN: 0028-0836, 1476-4687.

Coop, G. and Ralph, P. (Sept. 2012). Patterns of Neutral Diversity Under General Models of Selective Sweeps. *Genetics* 192(1), 205–224. ISSN: 1943-2631.

Coyle, S. M., Huntingford, F. A., and Peichel, C. L. (July 2007). Parallel Evolution of Pitx1 Underlies Pelvic Reduction in Scottish Threespine Stickleback (Gasterosteus aculeatus). *Journal of Heredity* 98(6), 581–586. ISSN: 0022-1503, 1465-7333.

Daub, J. T., Hofer, T., Cutivet, E., Dupanloup, I., Quintana-Murci, L., Robinson-Rechavi, M., and Excoffier, L. (2013). Evidence for Polygenic Adaptation to Pathogens in the Human Genome. *Molecular Biology and Evolution* 30(7), 1544–1558. ISSN: 1537-1719, 0737-4038.

Debat, V., Debelle, A., and Dworkin, I. (Nov. 2009). PLASTICITY, CANALIZATION, AND DEVELOPMENTAL STABILITY OF THE *DROSOPHILA* WING: JOINT EFFECTS OF MUTATIONS AND DEVELOPMENTAL TEMPERATURE. *Evolution* 63(11), 2864–2876. ISSN: 00143820, 15585646.

Dembeck, L. M., Huang, W., Magwire, M. M., Lawrence, F., Lyman, R. F., and Mackay, T. F. C. (May 2015). Genetic Architecture of Abdominal Pigmentation in Drosophila melanogaster. *PLOS Genetics* 11(5). Ed. by C. D. Jones, e1005163. ISSN: 1553-7404.

Diaz de la Loza, M. and Thompson, B. (Apr. 2017). Forces shaping the Drosophila wing. *Mechanisms of Development* 144, 23–32. ISSN: 09254773.

Dillon, M. E. (Jan. 2006). Into thin air: Physiology and evolution of alpine insects. *Integrative and Comparative Biology* 46(1), 49–61. ISSN: 1540-7063, 1557-7023.

Dittmar, E. L., Oakley, C. G., Conner, J. K., Gould, B. A., and Schemske, D. W. (Apr. 2016). Factors influencing the effect size distribution of adaptive substitutions. *Proceedings of the Royal Society B: Biological Sciences* 283(1828), 20153065. ISSN: 0962-8452, 1471-2954.

Dobens, A. C. and Dobens, L. L. (Aug. 2013). FijiWings: An Open Source Toolkit for Semiautomated Morphometric Analysis of Insect Wings. *G3 Genes|Genomes|Genetics* 3(8), 1443–1449. ISSN: 2160-1836.

Dobzhansky, T. (Apr. 1929). The influence of the quantity and quality of chromosomal material on the size of the cells in drosophila melanogaster. *Wilhelm Roux' Archiv fur Entwicklungsmechanik der Organismen* 115(3), 363–379. ISSN: 0043-5546.

Duchen, P., Živković, D., Hutter, S., Stephan, W., and Laurent, S. (Jan. 2013). Demographic Inference Reveals African and European Admixture in the North American *Drosophila melanogaster* Population. *Genetics* 193(1), 291–301. ISSN: 1943-2631.

Dworkin, I. (Apr. 2006). Epidermal Growth Factor Receptor and Transforming Growth Factor- Signaling Contributes to Variation for Wing Shape in Drosophila melanogaster. *Genetics* 173(3), 1417–1431. ISSN: 0016-6731.

Dworkin, I., Palsson, A., and Gibson, G. (Apr. 2005). Replication of an *Egfr* -Wing Shape Association in a Wild-Caught Cohort of *Drosophila melanogaster*. *Genetics* 169(4), 2115–2125. ISSN: 0016-6731, 1943-2631.

Etournay, R., Popović, M., Merkel, M., Nandi, A., Blasse, C., Aigouy, B., Brandl, H., Myers, G., Salbreux, G., Jülicher, F., and Eaton, S. (June 2015). Interplay of cell dynamics and epithelial tension during morphogenesis of the Drosophila pupal wing. *eLife* 4, e07090. ISSN: 2050-084X.

Fabian, D. K., Lack, J. B., Mathur, V., Schlötterer, C., Schmidt, P. S., Pool, J. E., and Flatt, T. (Apr. 2015). Spatially varying selection shapes life history clines among populations of *Drosophila melanogaster* from sub-Saharan Africa. *Journal of Evolutionary Biology* 28(4), 826–840. ISSN: 1010061X.

Fatumo, S., Carstensen, T., Nashiru, O., Gurdasani, D., Sandhu, M., and Kaleebu, P. (Apr. 2019). Complimentary Methods for Multivariate Genome-Wide Association Study Identify New Susceptibility Genes for Blood Cell Traits. *Frontiers in Genetics* 10, 334. ISSN: 1664-8021.

Félix, M.-A. and Barkoulas, M. (Aug. 2015). Pervasive robustness in biological systems. *Nature Reviews Genetics* 16(8), 483–496. ISSN: 1471-0056, 1471-0064.

Fisher, R. (1930). *The Genetical Theory of Natural Selection*. Clarendon Press, Oxford.

Fritsche, L. G. et al. (Feb. 2016). A large genome-wide association study of age-related macular degeneration highlights contributions of rare and common variants. *Nature Genetics* 48(2), 134–143. ISSN: 1061-4036, 1546-1718.

Fuhrmann, N., Prakash, C., and Kaiser, T. S. (Feb. 2023). Polygenic adaptation from standing genetic variation allows rapid ecotype formation. *eLife* 12, e82824. ISSN: 2050-084X.

Garcia-Bellido, A. and Merriam, J. (1971). Parameters of the wing imaginal disc development ofDrosophila melanogaster. *Developmental biology* 24(1), 61–87. ISSN: 0012-1606.

Gilchrist, A. S. and Partridge, L. (Feb. 2001). The contrasting genetic architecture of wing size and shape in Drosophila melanogaster. *Heredity* 86(2), 144–152. ISSN: 0018-067X, 1365-2540.

Gompel, N. and Prud'homme, B. (Aug. 2009). The causes of repeated genetic evolution. *Developmental Biology* 332(1), 36–47. ISSN: 00121606.

Gordon, S. P., Reznick, D. N., Kinnison, M. T., Bryant, M. J., Weese, D. J., Räsänen, K., Millar, N. P., and Hendry, A. P. (July 2009). Adaptive Changes in Life History and Survival following a New Guppy Introduction. *The American Naturalist* 174(1), 34–45. ISSN: 0003-0147, 1537-5323.

Gouy, A., Daub, J. T., and Excoffier, L. (2017). Detecting gene subnetworks under selection in biological pathways. *Nucleic Acids Research* 45(16), e149–e149. ISSN: 0305-1048, 1362-4962.

Green, R. M., Fish, J. L., Young, N. M., Smith, F. J., Roberts, B., Dolan, K., Choi, I., Leach, C. L., Gordon, P., Cheverud, J. M., Roseman, C. C., Williams, T. J., Marcucio, R. S., and Hallgrímsson, B. (Dec. 2017). Developmental nonlinearity drives phenotypic robustness. *Nature Communications* 8(1), 1970. ISSN: 2041-1723.

Greene, C. S., Penrod, N. M., Williams, S. M., and Moore, J. H. (June 2009). Failure to Replicate a Genetic Association May Provide Important Clues About Genetic Architecture. *PLoS ONE* 4(6). Ed. by T. I. A. Sorensen, e5639. ISSN: 1932-6203.

Groth, B. R., Huang, Y., Monette, M. J., and Pool, J. E. (Aug. 2018). Directional selection reduces developmental canalization against genetic and environmental perturbations in Drosophila wings: BRIEF COMMUNICATION. *Evolution* 72(8), 1708–1715. ISSN: 00143820.

Hayward, L. K. and Sella, G. (Oct. 2019). *Polygenic adaptation after a sudden change in environment*. preprint. Evolutionary Biology.

Hoekstra, H. E. (Sept. 2006). Genetics, development and evolution of adaptive pigmentation in vertebrates. *Heredity* 97(3), 222–234. ISSN: 0018-067X, 1365-2540.

Höllinger, I., Pennings, P. S., and Hermisson, J. (Mar. 2019). Polygenic adaptation: From sweeps to subtle frequency shifts. *PLOS Genetics* 15(3). Ed. by J. C. Fay, e1008035. ISSN: 1553-7404.

Houle, D., Bolstad, G. H., Linde, K. van der, and Hansen, T. F. (Aug. 2017). Mutation predicts 40 million years of fly wing evolution. *Nature* 548(7668), 447–450. ISSN: 0028-0836, 1476-4687.

Houle, D. and Fierst, J. (2013). Properties of Spontaneous Mutational Variance and Covariance for Wing Size and Shape in Drosophila Melanogaster. *Evolution* 67(4), 1116–1130. ISSN: 1558-5646.

Houle, D., Mezey, J., Galpern, P., and Carter, A. (Dec. 2003). Automated measurement of Drosophila wings. *BMC Evolutionary Biology* 3(1), 25. ISSN: 1471-2148.

Huang, W. et al. (July 2014). Natural variation in genome architecture among 205 Drosophila melanogaster Genetic Reference Panel lines. *Genome Research* 24(7), 1193–1208. ISSN: 1088-9051.

Hubbard, J. K., Uy, J. A. C., Hauber, M. E., Hoekstra, H. E., and Safran, R. J. (May 2010). Vertebrate pigmentation: from underlying genes to adaptive function. *Trends in Genetics* 26(5), 231–239. ISSN: 01689525.

Ioannidis, J. P. A., Tarone, R., and McLaughlin, J. K. (July 2011). The False-positive to False-negative Ratio in Epidemiologic Studies: *Epidemiology* 22(4), 450–456. ISSN: 1044-3983.

Jain, K. and Stephan, W. (May 2017). Rapid Adaptation of a Polygenic Trait After a Sudden Environmental Shift. *Genetics* 206(1), 389–406. ISSN: 1943-2631.

Johannesson, K., Johannesson, B., and Rolán-Alvarez, E. (Dec. 1993). MORPHOLOGICAL DIFFERENTIATION AND GENETIC COHESIVENESS OVER A MICROENVIRONMENTAL GRADIENT IN THE MARINE SNAIL LITTORINA SAXATILIS. *Evolution* 47(6). _eprint: https://academic.oup.com/evolut/article-pdf/47/6/1770/48062910/evolut 1787. ISSN: 0014-3820.

Jong, G. de and Bochdanovits, Z. (Dec. 2003). Latitudinal clines inDrosophila melanogaster: Body size, allozyme frequencies, inversion frequencies, and the insulin-signalling pathway. *Journal of Genetics* 82(3), 207–223. ISSN: 0022-1333, 0973-7731.

Kaiser, T. S., Neumann, D., and Heckel, D. G. (2011). Timing the tides: Genetic control of diurnal and lunar emergence times is correlated in the marine midge Clunio marinus. *BMC Genetics* 12(1), 49. ISSN: 1471-2156.

Kaiser, T. S., Haeseler, A. von, Tessmar-Raible, K., and Heckel, D. G. (Mar. 2021). Timing strains of the marine insect *Clunio marinus* diverged and persist with gene flow. *Molecular Ecology* 30(5), 1264–1280. ISSN: 0962-1083, 1365-294X.

Karasov, T., Messer, P. W., and Petrov, D. A. (June 2010). Evidence that Adaptation in Drosophila Is Not Limited by Mutation at Single Sites. *PLoS Genetics* 6(6). Ed. by H. S. Malik, e1000924. ISSN: 1553-7404.

Kardos, M. and Luikart, G. (May 2021). The Genetic Architecture of Fitness Drives Population Viability during Rapid Environmental Change. *The American Naturalist* 197(5), 511–525. ISSN: 0003-0147, 1537-5323.

Katsuyama, T., Sugawara, T., Tatsumi, M., Oshima, Y., Gehring, W. J., Aigaki, T., and Kurata, S. (Nov. 2005). Involvement of *winged eye* encoding a chromatin-associated

bromo-adjacent homology domain protein in disc specification. *Proceedings of the National Academy of Sciences* 102(44), 15918–15923. ISSN: 0027-8424, 1091-6490.

Kelly, J. K. and Hughes, K. A. (Mar. 2019). Pervasive Linked Selection and Intermediate-Frequency Alleles Are Implicated in an Evolve-and-Resequencing Experiment of *Drosophila simulans*. *Genetics* 211(3), 943–961. ISSN: 0016-6731, 1943-2631.

Kennington, W. J., Hoffmann, A. A., and Partridge, L. (Sept. 2007). Mapping Regions Within Cosmopolitan Inversion In(3R)Payne Associated With Natural Variation in Body Size in Drosophila melanogaster. *Genetics* 177(1), 549–556. ISSN: 0016-6731.

Kimura, M. (Feb. 1968). Evolutionary Rate at the Molecular Level. *Nature* 217(5129), 624–626. ISSN: 0028-0836, 1476-4687.

King, E. G. and Long, A. D. (June 2017). The Beavis Effect in Next-Generation Mapping Panels in *Drosophila melanogaster*. *G3 Genes|Genomes|Genetics* 7(6), 1643–1652. ISSN: 2160-1836.

King, E. G., Merkes, C. M., McNeil, C. L., Hoofer, S. R., Sen, S., Broman, K. W., Long, A. D., and Macdonald, S. J. (Aug. 2012a). Genetic dissection of a model complex trait using the Drosophila Synthetic Population Resource. *Genome Research* 22(8), 1558–1566. ISSN: 1088-9051.

King, E. G., Macdonald, S. J., and Long, A. D. (July 2012b). Properties and Power of the Drosophila Synthetic Population Resource for the Routine Dissection of Complex Traits. *Genetics* 191(3), 935–949. ISSN: 0016-6731, 1943-2631.

Klingenberg, C. P. (June 2016). Size, shape, and form: concepts of allometry in geometric morphometrics. *Development Genes and Evolution* 226(3), 113–137. ISSN: 0949-944X, 1432-041X.

Klingenberg, C. P. (Mar. 2022). Methods for studying allometry in geometric morphometrics: a comparison of performance. *Evolutionary Ecology*. ISSN: 0269-7653, 1573-8477.

Koch, E. L., Morales, H. E., Larsson, J., Westram, A. M., Faria, R., Lemmon, A. R., Lemmon, E. M., Johannesson, K., and Butlin, R. K. (June 2021). Genetic variation for adaptive traits is associated with polymorphic inversions in *Littorina saxatilis*. *Evolution Letters* 5(3), 196–213. ISSN: 2056-3744.

Koch, E. L., Ravinet, M., Westram, A. M., Johannesson, K., and Butlin, R. K. (Sept. 2022). Genetic architecture of repeated phenotypic divergence in *Littorina saxatilis* ecotype evolution. *Evolution*, evo.14602. ISSN: 0014-3820, 1558-5646.

Kofler, Orozco-terWengel, P., De Maio, N., Pandey, R. V., Nolte, V., Futschik, A., Kosiol, C., and Schlötterer, C. (2019a). PoPoolation: A Toolbox for Population Genetic

Analysis of Next Generation Sequencing Data from Pooled Individuals. *PLoS ONE* 6(1) (). Ed. by M. Kayser, e15925. ISSN: 1932-6203.

Kofler, Pandey, R. V., and Schlotterer, C. (2019b). PoPoolation2: identifying differentiation between populations using sequencing of pooled DNA samples (Pool-Seq). *Bioinformatics* 27(24) (), 3435–3436. ISSN: 1367-4803, 1460-2059.

Lack, J. B., Cardeno, C. M., Crepeau, M. W., Taylor, W., Corbett-Detig, R. B., Stevens, K. A., Langley, C. H., and Pool, J. E. (Apr. 2015). The *Drosophila* Genome Nexus: A Population Genomic Resource of 623 *Drosophila melanogaster* Genomes, Including 197 from a Single Ancestral Range Population. *Genetics* 199(4), 1229–1241. ISSN: 1943-2631.

Lack, J. B., Monette, M. J., Johanning, E. J., Sprengelmeyer, Q. D., and Pool, J. E. (2016a). Decanalization of wing development accompanied the evolution of large wings in high-altitude *Drosophila*. *Proceedings of the National Academy of Sciences* 113(4), 1014–1019. ISSN: 0027-8424, 1091-6490.

Lack, J. B., Yassin, A., Sprengelmeyer, Q. D., Johanning, E. J., David, J. R., and Pool, J. E. (2016b). Life history evolution and cellular mechanisms associated with increased size in high-altitude Drosophila. *Ecology and Evolution* 6(16), 5893–5906. ISSN: 2045-7758.

Lamichhaney, S., Han, F., Berglund, J., Wang, C., Almén, M. S., Webster, M. T., Grant, B. R., Grant, P. R., and Andersson, L. (2016). A beak size locus in Darwin’s finches facilitated character displacement during a drought. *Science* 352(6284). _eprint: https://www.science.org/doi/pdf/10.1126/science.aad8786, 470–474.

Land, J. V. t., Putten, P. V., Zwaan, Kamping, and Delden, W. V. (Mar. 1999). Latitudinal variation in wild populations of *Drosophila melanogaster* : heritabilities and reaction norms. *Journal of Evolutionary Biology* 12(2), 222–232. ISSN: 1010-061X, 1420-9101.

Li, H., Handsaker, B., Wysoker, A., Fennell, T., Ruan, J., Homer, N., Marth, G., Abecasis, G., Durbin, R., and 1000 Genome Project Data Processing Subgroup (Aug. 2009). The Sequence Alignment/Map format and SAMtools. *Bioinformatics* 25(16), 2078–2079. ISSN: 1367-4803, 1460-2059.

Li, H. and Durbin, R. (Mar. 2010). Fast and accurate long-read alignment with Burrows–Wheeler transform. *Bioinformatics* 26(5), 589–595. ISSN: 1460-2059, 1367-4803.

MacPherson, A. and Nuismer, S. L. (Feb. 2017). The probability of parallel genetic evolution from standing genetic variation. *Journal of Evolutionary Biology* 30(2), 326–337. ISSN: 1010-061X, 1420-9101.

Madeira, F., Pearce, M., Tivey, A. R. N., Basutkar, P., Lee, J., Edbali, O., Madhusoodanan, N., Kolesnikov, A., and Lopez, R. (July 2022). Search and sequence analysis tools services from EMBL-EBI in 2022. *Nucleic Acids Research* 50(W1), W276–W279. ISSN: 0305-1048, 1362-4962.

Marigorta, U. M., Rodríguez, J. A., Gibson, G., and Navarro, A. (July 2018). Replicability and Prediction: Lessons and Challenges from GWAS. *Trends in Genetics* 34(7), 504–517. ISSN: 01689525.

Marquez, E. J. and Houle, D. (Mar. 2015). *Dimensionality and the statistical power of multivariate genome-wide association studies*. preprint. Genomics.

Marriage, T. N., King, E. G., Long, A. D., and Macdonald, S. J. (Sept. 2014). Fine-Mapping Nicotine Resistance Loci in *Drosophila* Using a Multiparent Advanced Generation Inter-Cross Population. *Genetics* 198(1), 45–57. ISSN: 0016-6731, 1943-2631.

Martin, A. and Orgogozo, V. (2013). The Loci of Repeated Evolution: A Catalog of Genetic Hotspots of Phenotypic Variation. *Evolution* 67(5), 1235–1250. ISSN: 1558-5646.

Martin, A. and Reed, R. D. (Nov. 2014). Wnt signaling underlies evolution and development of the butterfly wing pattern symmetry systems. *Developmental Biology* 395(2), 367–378. ISSN: 00121606.

Martín, F. A., Herrera, S. C., and Morata, G. (Nov. 2009). Cell competition, growth and size control in the *Drosophila* wing imaginal disc. *Development* 136(22), 3747–3756. ISSN: 1477-9129, 0950-1991.

Matamoro-Vidal, A., Salazar-Ciudad, I., and Houle, D. (Sept. 2015). Making quantitative morphological variation from basic developmental processes: where are we? The case of the Drosophila wing. *Developmental dynamics : an official publication of the American Association of Anatomists* 244(9), 1058–1073. ISSN: 1058-8388.

Matamoro-Vidal, A., Huang, Y., Salazar-Ciudad, I., Shimmi, O., and Houle, D. (July 2018). Quantitative Morphological Variation in the Developing *Drosophila* Wing. *G3 Genes|Genomes|Genetics* 8(7), 2399–2409. ISSN: 2160-1836.

McGuigan, K. (Mar. 2006). Studying phenotypic evolution using multivariate quantitative genetics: EVOLUTIONARY QUANTITATIVE GENETICS. *Molecular Ecology* 15(4), 883–896. ISSN: 09621083, 1365294X.

Melo, D., Garcia, G., Hubbe, A., Assis, A. P., and Marroig, G. (Nov. 2016). EvolQG - An R package for evolutionary quantitative genetics. *F1000Research* 4, 925. ISSN: 2046-1402.

Melo, D., Marroig, G., and Wolf, J. B. (July 2019). Genomic Perspective on Multivariate Variation, Pleiotropy, and Evolution. *Journal of Heredity* 110(4), 479–493. ISSN: 0022-1503, 1465-7333.

Micchelli, C. A., Rulifson, E. J., and Blair, S. S. (Apr. 1997). The function and regulation of *cut* expression on the wing margin of *Drosophila* : Notch, Wingless and a dominant negative role for Delta and Serrate. *Development* 124(8), 1485–1495. ISSN: 0950-1991, 1477-9129.

Miller, C. T., Glazer, A. M., Summers, B. R., Blackman, B. K., Norman, A. R., Shapiro, M. D., Cole, B. L., Peichel, C. L., Schluter, D., and Kingsley, D. M. (May 2014). Modular Skeletal Evolution in Sticklebacks Is Controlled by Additive and Clustered Quantitative Trait Loci. *Genetics* 197(1), 405–420. ISSN: 1943-2631.

Neufeld, T. P., Cruz, A. F. A. de la, Johnston, L. A., and Edgar, B. A. (June 1998). Coordination of Growth and Cell Division in the Drosophila Wing. *Cell* 93(7), 1183–1193. ISSN: 00928674.

O'Brown, N. M., Summers, B. R., Jones, F. C., Brady, S. D., and Kingsley, D. M. (Jan. 2015). A recurrent regulatory change underlying altered expression and Wnt response of the stickleback armor plates gene EDA. *eLife* 4, e05290. ISSN: 2050-084X.

Oldham, S. and Hafen, E. (Feb. 2003). Insulin/IGF and target of rapamycin signaling: a TOR de force in growth control. *Trends in Cell Biology* 13(2), 79–85. ISSN: 09628924.

Orgogozo, V., Morizot, B., and Martin, A. (May 2015). The differential view of genotype phenotype relationships. *Frontiers in Genetics* 6. ISSN: 1664-8021.

Orr, H. A. (Aug. 1998). THE POPULATION GENETICS OF ADAPTATION: THE DISTRIBUTION OF FACTORS FIXED DURING ADAPTIVE EVOLUTION. *Evolution* 52(4), 935–949. ISSN: 00143820.

Orr, H. A. (Feb. 2005). The genetic theory of adaptation: a brief history. *Nature Reviews Genetics* 6(2), 119–127. ISSN: 1471-0056, 1471-0064.

Orteu, A. and Jiggins, C. D. (Aug. 2020). The genomics of coloration provides insights into adaptive evolution. *Nature Reviews Genetics* 21(8), 461–475. ISSN: 1471-0056, 1471-0064.

Paaby, A. B., Blacket, M. J., Hoffmann, A. A., and Schmidt, P. S. (2010). Identification of a candidate adaptive polymorphism for Drosophila life history by parallel independent clines on two continents. *Molecular Ecology* 19(4), 760–774. ISSN: 1365-294X.

Palsson, A., Dodgson, J., Dworkin, I., and Gibson, G. (2005). Tests for the replication of an association between Egfr and natural variation in Drosophila melanogaster wing morphology. *BMC Genetics* 6(1), 44. ISSN: 14712156.

Palsson, A. and Gibson, G. (July 2004). Association Between Nucleotide Variation in Egfr and Wing Shape in Drosophila melanogaster. *Genetics* 167(3), 1187–1198. ISSN: 1943-2631.

Pan, D. (Apr. 2007). Hippo signaling in organ size control. *Genes & Development* 21(8), 886–897. ISSN: 0890-9369.

Pan, Y., Alégot, H., Rauskolb, C., and Irvine, K. D. (Oct. 2018). The dynamics of Hippo signaling during *Drosophila* wing development. *Development* 145(20), dev165712. ISSN: 0950-1991, 1477-9129.

Parks, A. L. et al. (Mar. 2004). Systematic generation of high-resolution deletion coverage of the Drosophila melanogaster genome. *Nature Genetics* 36(3), 288–292. ISSN: 1061-4036, 1546-1718.

Partridge, L., Langelan, R., Fowler, K., Zwaan, B., and French, V. (Aug. 1999). Correlated responses to selection on body size in *Drosophila melanogaster*. *Genetical Research* 74(1), 43–54. ISSN: 0016-6723, 1469-5073.

Pearson, K. and Davin, A. G. (1924). ON THE BIOMETRIC CONSTANTS OF THE HUMAN SKULL. *Biometrika* 16, 328–363.

Perkins, L. A. et al. (Nov. 2015). The Transgenic RNAi Project at Harvard Medical School: Resources and Validation. *Genetics* 201(3), 843–852. ISSN: 1943-2631.

Pesevski, M. and Dworkin, I. (2020). Genetic and environmental canalization are not associated among altitudinally varying populations of Drosophila melanogaster. *Evolution* 74(8). _eprint: https://onlinelibrary.wiley.com/doi/pdf/10.1111/evo.14039, 1755–1771. ISSN: 1558-5646.

Pesevski, M. and Dworkin, I. (July 2021). *The influence of adaptation to life at high-altitude on condition dependent sexual shape and size dimorphism in Drosophila melanogaster*. preprint. Evolutionary Biology.

Pitchers, W., Nye, J., Márquez, E. J., Kowalski, A., Dworkin, I., and Houle, D. (Apr. 2019). A Multivariate Genome-Wide Association Study of Wing Shape in *Drosophila melanogaster*. *Genetics* 211(4), 1429–1447. ISSN: 0016-6731, 1943-2631.

Pitchers, W., Pool, J. E., and Dworkin, I. (Feb. 2013). Altitudinal Clinal Variation in Wing Size and Shape in African Drosophila Melanogaster: One Cline or Many? *Evolution* 67(2), 438–452. ISSN: 1558-5646.

Pool, J. E., Braun, D. T., and Lack, J. B. (Oct. 2016). Parallel Evolution of Cold Tolerance Within *Drosophila melanogaster*. *Molecular Biology and Evolution*, msw232. ISSN: 0737-4038, 1537-1719.

Porter, H. F. and O'Reilly, P. F. (Apr. 2017). Multivariate simulation framework reveals performance of multi-trait GWAS methods. *Scientific Reports* 7(1), 38837. ISSN: 2045-2322.

Pritchard, J. K. and Di Rienzo, A. (Oct. 2010). Adaptation – not by sweeps alone. *Nature Reviews Genetics* 11(10), 665–667. ISSN: 1471-0056, 1471-0064.

Quinlan, A. R. and Hall, I. M. (Mar. 2010). BEDTools: a flexible suite of utilities for comparing genomic features. *Bioinformatics* 26(6), 841–842. ISSN: 1460-2059, 1367-4803.

Ray, R. P., Nakata, T., Henningsson, P., and Bomphrey, R. J. (Apr. 2016). Enhanced flight performance by genetic manipulation of wing shape in Drosophila. *Nature Communications* 7(1), 10851. ISSN: 2041-1723.

Reddiex, A. J. and Chenoweth, S. F. (Oct. 2021). Integrating genomics and multivariate evolutionary quantitative genetics: a case study of constraints on sexual selection in *Drosophila serrata*. *Proceedings of the Royal Society B: Biological Sciences* 288(1960), 20211785. ISSN: 0962-8452, 1471-2954.

Resino, J., Salama-Cohen, P., and García-Bellido, A. (May 2002). Determining the role of patterned cell proliferation in the shape and size of the *Drosophila* wing. *Proceedings of the National Academy of Sciences* 99(11), 7502–7507. ISSN: 0027-8424, 1091-6490.

Reznick, D. and Endler, J. A. (1982). The Impact of Predation on Life History Evolution in Trinidadian Guppies (Poecilia reticulata). 36(1), 160–177.

Rockman, M. V. (Jan. 2012). THE QTN PROGRAM AND THE ALLELES THAT MATTER FOR EVOLUTION: ALL THAT'S GOLD DOES NOT GLITTER. *Evolution* 66(1), 1–17. ISSN: 00143820.

Rohlf, F. J. and Corti, M. (Dec. 2000). Use of Two-Block Partial Least-Squares to Study Covariation in Shape. *Systematic Biology* 49(4). Ed. by R. Olmstead, 740–753. ISSN: 1076-836X, 1063-5157.

Rohlf, F. J. and Slice, D. (Mar. 1990). Extensions of the Procrustes Method for the Optimal Superimposition of Landmarks. *Systematic Zoology* 39(1), 40. ISSN: 00397989.

Ryder, E. et al. (Sept. 2007). The DrosDel Deletion Collection: A Drosophila Genomewide Chromosomal Deficiency Resource. *Genetics* 177(1), 615–629. ISSN: 1943-2631.

Schluter, D. (Oct. 1996). Adaptive Radiation Along Genetic Lines of Least Resistance. *Evolution* 50(5), 1766. ISSN: 00143820.

Schluter, D., Marchinko, K. B., Arnegard, M. E., Zhang, H., Brady, S. D., Jones, F. C., Bell, M. A., and Kingsley, D. M. (Jan. 2021). Fitness maps to a large-effect locus in introduced stickleback populations. *Proceedings of the National Academy of Sciences* 118(3), e1914889118. ISSN: 0027-8424, 1091-6490.

Shriner, D. (2012). Moving toward System Genetics through Multiple Trait Analysis in Genome-Wide Association Studies. *Frontiers in Genetics* 3. ISSN: 1664-8021.

Spitzer, K., Pelizzola, M., and Futschik, A. (Mar. 2020). Modifying the Chi-square and the CMH test for population genetic inference: Adapting to overdispersion. *The Annals of Applied Statistics* 14(1). ISSN: 1932-6157.

Sprengelmeyer, Q. D., Lack, J. B., Braun, D. T., Monette, M. J., and Pool, J. E. (Mar. 2022). The evolution of larger size in high-altitude *Drosophila melanogaster* has a variable genetic architecture. *G3 Genes|Genomes|Genetics* 12(3). Ed. by R. Anholt, jkab454. ISSN: 2160-1836.

Sprengelmeyer, Q. D., Mansourian, S., Lange, J. D., Matute, D. R., Cooper, B. S., Jirle, E. V., Stensmyr, M. C., and Pool, J. E. (Mar. 2020). Recurrent Collection of Drosophila melanogaster from Wild African Environments and Genomic Insights into Species History. *Molecular Biology and Evolution* 37(3). Ed. by A. Larracuente, 627–638. ISSN: 0737-4038, 1537-1719.

Steiner, C. C., Weber, J. N., and Hoekstra, H. E. (Aug. 2007). Adaptive Variation in Beach Mice Produced by Two Interacting Pigmentation Genes. *PLoS Biology* 5(9). Ed. by M. A. Noor, e219. ISSN: 1545-7885.

Stephens, M. (July 2013). A Unified Framework for Association Analysis with Multiple Related Phenotypes. *PLoS ONE* 8(7). Ed. by F. Emmert-Streib, e65245. ISSN: 1932-6203.

Stern, D. L. and Orgogozo, V. (Sept. 2008). THE LOCI OF EVOLUTION: HOW PREDICTABLE IS GENETIC EVOLUTION? *Evolution* 62(9), 2155–2177. ISSN: 00143820, 15585646.

Stetter, M. G., Thornton, K., and Ross-Ibarra, J. (Nov. 2018). Genetic architecture and selective sweeps after polygenic adaptation to distant trait optima. *PLOS Genetics* 14(11). Ed. by R. D. Hernandez, e1007794. ISSN: 1553-7404.

Tam, V., Patel, N., Turcotte, M., Bossé, Y., Paré, G., and Meyre, D. (May 2019). Benefits and limitations of genome-wide association studies. *Nature Reviews Genetics*, 1. ISSN: 1471-0064.

Tomioka, K. and Matsumoto, A. (Feb. 2015). Circadian molecular clockworks in non-model insects. *Current Opinion in Insect Science* 7, 58–64. ISSN: 22145745.

Travisano, M. and Shaw, R. G. (Feb. 2013). LOST IN THE MAP. *Evolution* 67(2), 305–314. ISSN: 00143820.

Tripathi, B. K. and Irvine, K. D. (Apr. 2022). The wing imaginal disc. *Genetics* 220(4). Ed. by C. Thummel, iyac020. ISSN: 1943-2631.

Trotta, V., Calboli, F. C., Ziosi, M., and Cavicchi, S. (2007). Fitness variation in response to artificial selection for reduced cell area, cell number and wing area in natural populations of Drosophila melanogaster. *BMC Evolutionary Biology* 7(Suppl 2), S10. ISSN: 14712148.

Uller, T., Moczek, A. P., Watson, R. A., Brakefield, P. M., and Laland, K. N. (Aug. 2018). Developmental Bias and Evolution: A Regulatory Network Perspective. *Genetics* 209(4), 949–966. ISSN: 0016-6731, 1943-2631.

Visscher, P. M., Wray, N. R., Zhang, Q., Sklar, P., McCarthy, M. I., Brown, M. A., and Yang, J. (July 2017). 10 Years of GWAS Discovery: Biology, Function, and Translation. *The American Journal of Human Genetics* 101(1), 5–22. ISSN: 00029297.

Visser, J. A. G. M., Hermisson, J., Wagner, G. P., Meyers, L. A., Bagheri-Chaichian, H., Blanchard, J. L., Chao, L., Cheverud, J. M., Elena, S. F., Fontana, W., Gibson, G., Hansen, T. F., Krakauer, D., Lewontin, R. C., Ofria, C., Rice, S. H., Dassow, G. v., Wagner, A., and Whitlock, M. C. (Sept. 2003). PERSPECTIVE: EVOLUTION AND DETECTION OF GENETIC ROBUSTNESS. *Evolution* 57(9), 1959–1972. ISSN: 0014-3820, 1558-5646.

Vonesch, S. C., Lamparter, D., Mackay, T. F. C., Bergmann, S., and Hafen, E. (Jan. 2016). Genome-Wide Analysis Reveals Novel Regulators of Growth in Drosophila melanogaster. *PLOS Genetics* 12(1). Ed. by G. S. Barsh, e1005616. ISSN: 1553-7404.

Wahlund, S. (1928). ZUSAMMENSETZUNG VON POPULATIONEN UND KORRELATIONSERSCHEINUNGEN VOM STANDPUNKT DER VERERBUNGSLEHRE AUS BETRACHTET. *Hereditas* 11(1), 65–106.

Weber, K., Johnson, N., Champlin, D., and Patty, A. (Mar. 2005). Many P-Element Insertions Affect Wing Shape in Drosophila melanogaster. *Genetics* 169(3), 1461–1475. ISSN: 1943-2631.

Weigmann, K., Cohen, S. M., and Lehner, C. F. (Sept. 1997). Cell cycle progression, growth and patterning in imaginal discs despite inhibition of cell division after inactivation of *Drosophila* Cdc2 kinase. *Development* 124(18), 3555–3563. ISSN: 0950-1991, 1477-9129.

Westram, A. M., Faria, R., Johannesson, K., and Butlin, R. (Aug. 2021). Using replicate hybrid zones to understand the genomic basis of adaptive divergence. *Molecular Ecology* 30(15), 3797–3814. ISSN: 0962-1083, 1365-294X.

Whiting, J. R., Paris, J. R., Parsons, P. J., Matthews, S., Reynoso, Y., Hughes, K. A., Reznick, D., and Fraser, B. A. (Apr. 2022). On the genetic architecture of rapidly adapting and convergent life history traits in guppies. *Heredity* 128(4), 250–260. ISSN: 0018-067X, 1365-2540.

Wittkopp, P. J., Carroll, S. B., and Kopp, A. (Sept. 2003). Evolution in black and white: genetic control of pigment patterns in Drosophila. *Trends in Genetics* 19(9), 495–504. ISSN: 01689525.

Wray, N. R., Wijmenga, C., Sullivan, P. F., Yang, J., and Visscher, P. M. (June 2018). Common Disease Is More Complex Than Implied by the Core Gene Omnigenic Model. *Cell* 173(7), 1573–1580. ISSN: 00928674.

Wright, S. (Jan. 1934). Physiological and Evolutionary Theories of Dominance. *The American Naturalist* 68(714), 24–53. ISSN: 0003-0147, 1537-5323.

Xu, S. (2003). Theoretical Basis of the Beavis Effect.

Yeaman, S. (May 2013). Genomic rearrangements and the evolution of clusters of locally adaptive loci. *Proceedings of the National Academy of Sciences* 110(19). ISSN: 0027-8424, 1091-6490.

Yeaman, S. (Oct. 2015). Local Adaptation by Alleles of Small Effect. *The American Naturalist* 186(S1), S74–S89. ISSN: 0003-0147, 1537-5323.

Yengo, L. et al. (Oct. 2022). A saturated map of common genetic variants associated with human height. *Nature* 610(7933), 704–712. ISSN: 0028-0836, 1476-4687.

Zhang, W., Reeves, G. R., and Tautz, D. (Mar. 2021). Testing Implications of the Omnigenic Model for the Genetic Analysis of Loci Identified through Genome-wide Association. *Current Biology* 31(5), 1092–1098.e6. ISSN: 09609822.

Zhao, B., Tumaneng, K., and Guan, K.-L. (Aug. 2011). The Hippo pathway in organ size control, tissue regeneration and stem cell self-renewal. *Nature Cell Biology* 13(8), 877–883. ISSN: 1465-7392, 1476-4679.

Zwaan, B. J., Azevedo, R. B. R., James, A. C., 't Land, J. van, and Partridge, L. (Mar. 2000). Cellular basis of wing size variation in Drosophila melanogaster: a comparison of latitudinal clines on two continents. *Heredity* 84(3), 338–347. ISSN: 0018-067X, 1365-2540.